RF Project 2267
Report 8

THE OHIO STATE UNIVERSITY

RESEARCH FOUNDATION

1314 KINNEAR ROAD COLUMBUS, OHIO 4321

STRESS CORROSION CRACKING OF TITANIUM ALLOYS

E. L. Owen, F. H. Beck and M. G. Fontana
Department of Metallurgical Engineering

NATIONAL AERONAUTICS & SPACE ADMINISTRATION
Washington, D.C. 20546

Grant No. NGL 36-008-051

RF Project 2267

Report No. 8

SEMIANNUAL

REPORT

By

THE OHIO STATE UNIVERSITY
RESEARCH FOUNDATION

1314 KINNEAR RD.
COLUMBUS, OHIO 43212

To NATIONAL AERONAUTICS AND SPACE ADMINISTRATION

Washington, D.C. 20546

Grant No. NGL 36-008-051

On STRESS CORROSION CRACKING OF TITANIUM ALLOYS

For the period 1 January 1970 - 30 June 1970

Submitted by F. H. Beck and M. G. Fontana

Department of Metallurgical Engineering

Date December, 1970

FOREWORD

This report covers work through June 31, 1970 on the initiation of stress corrosion cracks in Ti-6Al-4V alloy by acid environments. Of particular interest was the selectivity of corrosion attack and hydride formation in the alloy when exposed near the corrosion potential in a simulated stress corrosion crack crevice environment (aqueous HCl solution of low pH). The mode of attack was found to be stress dependent and hydride formation resulted from the corrosion process.

This report is based on the Ph.D. dissertation of Mr. E. L. Owen. Work was performed at The Ohio State University under NASA Grant No. NGL 36-008-051.

TABLE OF CONTENTS

Section		Page
I	INTRODUCTION	1
II	LITERATURE SURVEY	2
	The Titanium-Hydrogen System	2
	The Hydride Phase	8
	The Electrochemical Introduction of Hydrogen	12
	Diffusion of Hydrogen in Titanium	13
	Hydrogen Embrittlement of Titanium Alloys	14
	The Role of Hydrogen in Titanium Stress-Corrosion Cracking Theories	15
III	EXPERIMENTAL PROCEDURE	23
	Material	23
	Specimens	23
	Hydrogen Charging	24
	Neodymium Hydrogen Detector	30
	Foil Preparation	31
	Electron Transmission Microscopy	31
IV	RESULTS	31
	Electrochemical Dependence of SCC	31
	Polarization Behavior	32
	Hydrogen Charging Experiments	37
	Hydride Precipitation	58
	Electron Transmission Microscopy	58

Section		Page
V	DISCUSSION	82
	Initiation of SCC	82
	Propagation of SCC	83
VI	CONCLUSIONS	96
VII	PROPOSED FUTURE WORK	97
Appendix A	- Metallographic Polishing Techniques for Titanium	99
Appendix B	- The Window Technique	101
REFERENCES		103

LIST OF FIGURES

Figure		Page
1	Isobar for Adsorption of Hydrogen by Titanium	3
2	The Titanium-Hydrogen Equilibrium Diagram	5
3	Solubility of Hydrogen in Titanium	6
4	Room Temperature Solubility of Hydrogen in the Titanium-Aluminum System	7
5	Effect of Hydrogen on the Density of High Purity Titanium-Hydrogen Alloys	9
6	Plot Showing Relationship Between Crack Velocity and Potential for Ti-8Al-1Mo-1V in 0.6M Halide Solutions	18
7	Proposed Distribution of Hydrides About an Advancing Stress Corrosion Crack	21
8	Microstructure of As-Received Ti-6Al-4V Cold-Rolled Sheet	25
9	Microstructure of Annealed Ti-6Al-4V Sheet	26
10	a. Double Notch Specimens b. Cell for Charging while Stressing	27 27
11	Load-Elongation Curve for an Annealed Transverse Ti-6Al-4V Specimen	28
12	a. Experimental Set-up for Electrolytic Charging b. Set-up for Electrolytic Polishing of Foil Specimens	29 29
13	Electrochemical Dependence of Failure Stress on Applied Potential for Three-Point Bend Specimens in 0.6M KBr	33
14	Fracture Appearance of Ti-8Al-1Mo-1V Sheet Specimen Broken in 0.6M KBr at -500 mV (SCE)	34
15	Fracture Appearance of Ti-8Al-1Mo-1V Specimen Broken in 0.6M KBr at +850 mV (SCE)	35
16	Polarization Curve for Annealed Ti-6Al-4V in Deareated 5N HCl	36

LIST OF FIGURES (continued)

Figure		Page
17	Hydrogen Concentration as a Function of Electrochemical Potential and Time in Ti-6Al-4V Alloy at Room Temperature	38
18	Current Density as a Function of Time for a Typical Potentiostatic Hydrogen Charging Experiment for Ti-6Al-4V in 5N HCl	39
19	Ti-6Al-4V Specimen Charged at -742 mV (SCE) for $\frac{1}{2}$ Hour Specimen Has Thin Film of Nd on Surface	40
20	a. Nd Specimen Showing Hydrogen Distribution after Charging at -742 mV (SCE) for $\frac{1}{2}$ Hour	41
	b. Same	41
21	Nd Specimen Showing Distribution of Hydrogen after Charging at -742 mV (SCE) for 1 Hour	42
22	Nd Specimen Showing Hydrogen Distribution after Charging at -742 mV (SCE) for 4 Hours	43
23	Appearance of Ti-6Al-4V Surface after $\frac{1}{2}$ Hour Exposure at -742 mV (SCE) in 5N HCl	45
24	a. Surface of Ti-6Al-4V after Exposure at -742 mV (SCE) for 4 Hours in 5N HCl	46
	b. Same	46
25	Attack of Alpha Grains after Exposure for 4 Hours at -742 mV (SCE) in 5N HCl	47
26	a. Surface Appearance after Exposure at -500 mV (SCE) for 1 Hour in 5N HCl	49
	b. Same	49
27	Surface Appearance after Exposure for 10 Hours at the Corrosion Potential in 5N HCl	50
28	Surface Appearance after Exposure for 4 Hours at -1500 mV (SCE) in 5N HCl	51

LIST OF FIGURES (continued)

Figure		Page
29	a. Appearance of Surface of Specimen Stressed to 80% of the Yield During Exposure at -742 mV (SCE) for 2 Hours in 5N HCl	52
	b. Same	52
30	a. Pits Associated with Notch Tip Region on Specimen Broken at -850 mV in $\frac{1}{2}$ Hour in 5N HCL. Loaded to 95% of Failure Stress. Oblique Illumination	53
	b. Schematic Representation of (a)	53
31	Notch Tip Region of Specimen Exposed to 5N HCl at -850 mV for $\frac{1}{2}$ Hour. Loaded to 50% of Failure Stress. Oblique Illumination	54
32	Notch Tip Region of Specimen Loaded to 95% of Fracture Stress and Exposed at -850 mV (SCE) for 1 minute	55
33	Appearance of Hydrides in Ti-6Al-4V after 2 Hours at -850 mV in 5N HCl	56
34	Transmission Micrograph Showing Typical Strain Free Microstructure of Annealed Ti-6Al-4V	57
35	Appearance of Elongated Beta Lying in Alpha Grain Boundary	59
36	Appearance of Subgrains in Ti-6Al-4V after Anneal at 1500°F for 18 Hours	60
37	Subgrain Boundary in Ti-6Al-4V	62
38	Dislocation Pairs on Active Prism Slip Plane in Ti-6Al-4V Alloy. Specimen Given 5% Plastic Strain	63
39	Prism Slip in Ti-6Al-4V. Specimen Given 10% Plastic Strain	64
40	Basal Slip in Ti-6Al-4V Specimen Strained 5%	65
41	Spontaneous Hydrides on Prism Planes. Both Charged at -850 mV for 1 Hour	66
42	Spontaneous Hydrides about Beta Particles after Charging at -850 mV for 1 Hour	67

LIST OF FIGURES (continued)

Figure		Page
43	Basketweave Appearance of Hydrides a. Charged at -1500 mV for $\frac{1}{2}$ Hour b. Charged at -1042 mV for $\frac{1}{2}$ Hour	68
44	Spontaneous Hydrides in Dark Field Using $(\bar{1}1\bar{1})_\gamma$ Reflection	69
45	a. Diffraction Pattern From Hydrides Shown in Fig. 44 b. Indexed Pattern Showing Habit Plane Trace	70 70
46	Trace Analysis Solution for Figs. 44 and 45	71
47	Strain-Induced Hydrides in Dark Field Using $(\bar{1}\bar{1}0)_\gamma$ Reflection	72
48	Indexed Diffraction Pattern Obtained from Hydrides in Fig. 47	73
49	Trace Analysis Solution for Figs. 47 and 48	74
50	Strain-Induced Hydrides in Specimen Charged for 1 Hour at -850 mV in 5N HCl	76
51	Strain-Induced Hydrides in Specimen Charged 1 Hour at -850 mV in 5N HCl	77
52	Strain-Induced Hydrides During Dissolution in Electron Beam. Specimen Charged $\frac{1}{2}$ Hour at -850 mV and Strained 5%	78
53	Strain-Induced Hydrides Showing Contrast Effects and Interface Dislocations. Specimen Charged at -850 mV for 1 Hour in 5N HCl and Deformed 5% in Tension	79
54	Strain-Induced Hydrides in Specimen Charged at -850 mV for 1 Hour and Deformed 5% in Tension	80
55	Strain-Induced Hydrides Lying on Active Slip Planes. Specimen Charged at -850 mV for 1 Hour and Deformed 5% in Tension	81
56	Potential pH Diagram for Titanium which includes a Stable Hydride Phase	84

LIST OF FIGURES (continued)

Figure		Page
57	Model for SCC Initiation a. Emergent Slip Step b. Complete Rapid Repassivation c. Repassivation Leading to a Pitting Mechanism	85
58	The "Window" Technique of Electropolishing	102

I. INTRODUCTION

Titanium, discovered in 1790, was first called menchanite, but in 1795 received its present name based upon the Greek gods, the Titans. Perhaps, it is this name which has resulted in the common misconception that titanium is the wonder metal. More likely, this reputation has probably resulted from two engineering properties which titanium exhibits--a high strength-to-weight ratio and excellent corrosion resistance to most environments. The widespread use of titanium has been limited primarily by its price which is a result of the high processing costs required to reduce its ore which is a very stable oxide.

Titanium is presently used primarily in jet engines and aircraft frames but it is finding increased applications in spacecrafts. The use of titanium in spacecrafts coupled with its increased use, especially in the SST, has resulted in the present world-wide research effort.

The fact that titanium exhibits excellent corrosion resistance to most environments belies the fact that it will "stress-corrode" or exhibit reduced fracture toughness in many of the seemingly less aggressive environments such as distilled water, sea water and impure methanol. The active-passive behavior of titanium is undoubtedly responsible for this susceptibility as in other metals which depend upon a thin oxide or protective film for their corrosion resistance. It is, therefore, the very film which gives titanium its corrosion resistance which is partially responsible for its susceptibility to stress-corrosion.

That titanium exhibits hydrogen embrittlement is well documented and the similarities which exist between this type of failure and stress corrosion have led to the belief by many that SCC is a form of hydrogen uptake as a result of the corrosion processes. For this to be verified, several important observations will need to be made. First, it must be established that nascent hydrogen will diffuse to and concentrate at the crack tip region. Second, it must be established that the hydrogen can be picked up and concentrate rapidly enough in this region of interest such that it can keep up with the advancing crack. Third, it must be established that the crack does not propagate by electrochemical dissolution. Lastly, it must be determined whether this form of hydrogen embrittlement results from the precipitation of the hydride phase or from a more general deterioration of mechanical properties.

The present investigation is concerned primarily with this question of hydrogen embrittlement as related to stress-corrosion cracking. The basis of this investigation is to study the pickup of hydrogen from aqueous environments at room temperature. The environments and potentials were chosen to simulate the processes occurring at an active crack tip. In addition, the spontaneous and strain induced hydrides which precipitate in super-saturated alpha titanium were studied by transmission electron microscopy.

II. LITERATURE SURVEY

The titanium-hydrogen system has been investigated by numerous investigators for many years. The first investigation generally accepted as reliable was reported by Kirschfeld and Sieverts[1] in 1929. Most of the current information, however, has been obtained since 1954. It was in 1954 that service failures of jet-engine parts were attributed to hydrogen contamination of the titanium alloy used in the engine. This led to a considerable amount of research devoted to the problem of hydrogen embrittlement of titanium alloys. As a result of this research we now have a reasonable understanding of hydrogen embrittlement and through alloying and design we have been able to essentially eliminate this problem.

Of more current interest is the possibility of hydrogen contamination, in one form or another, being responsible for stress-corrosion cracking of titanium alloys. This possibility has rejuvenated considerable interest in the titanium-hydrogen system. The interest has shifted somewhat, however, from the atomic specie of hydrogen to the hydride as the bad actor. The possibility of the hydride being responsible for stress corrosion is, at this time, extremely controversial and wide open. There are many good arguments for and against this possibility and it is only the difficulty in analyzing for hydrogen and in looking at the actual crack tip region which is impeding progress in this area of investigation.

THE TITANIUM-HYDROGEN SYSTEM

Titanium is commonly referred to as an exothermic occluder with respect to hydrogen. This means that the amount of atomic hydrogen absorbed by the metal decreases as the temperature increases. This occurs because the system forms a "pseudo-metallic hydride"[2] which was referred to by McQuillan[3,4,5,6] as the gamma phase. To explain the nature of exothermic occlusion, Cotterill[7] writes, "Generally speaking, the solubility of hydrogen in titanium increases, since solution is an endothermic process. However, the total amount of hydrogen absorbed decreases as the temperature increases due to the exothermic nature of hydride formation." Figure 1 shows an isobar for the absorption of hydrogen by titanium which illustrates this exothermic occlusion.

In titanium, hydrogen is not entirely ionized to a proton nor is it converted to negatively charged ions. Rather, the hydrogen enters in an excited or partially ionized state and forms an intermediate bond*

*In the limiting cases, hydrogen ionizes to a negatively charged ion giving rise to a chemical compound with ionic bonds or to a positively charged ion (proton), which enters the metal with no disruption, owing to its size.

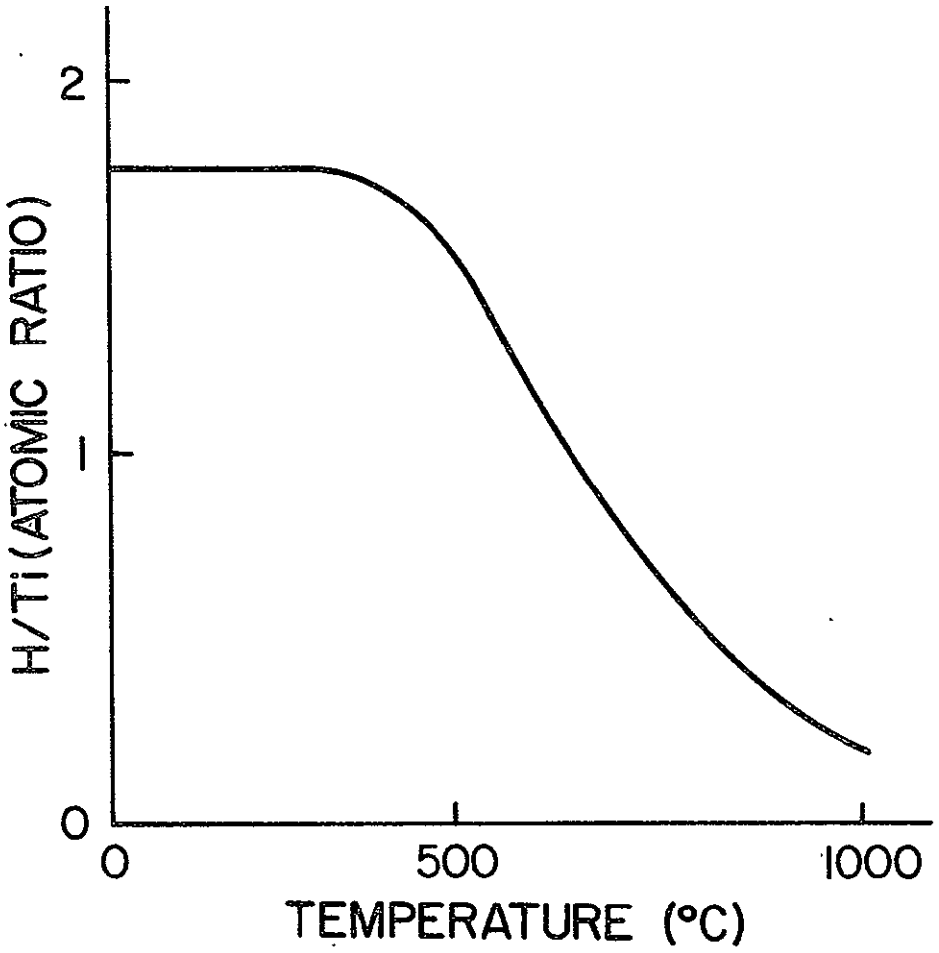

Fig. 1 - Isobar for the Absorption of Hydrogen by Titanium (Ref. 8)

with the titanium atoms.[8] The hydrogen atoms occupy interstitial sites as evidenced by the small lattice parameter increase in alpha titanium as the hydrogen content is increased.

The gamma phase in the titanium-hydrogen system is commonly based on the stoichiometric composition, TiH_2. However, under normal conditions, this compound only exists in the presence of excess metal atoms in the system.[8] The composition range, normally reported for the hydride, is from 60 to 66 at.% hydrogen ($TiH_{1.5-2}$). It can be seen in Fig. 1 that the ratio of hydrogen atoms to titanium atoms is approximately 1.75, at low temperatures. This corresponds to the commonly reported composition, $TiH_{1.75}$.

Several investigators[3,9] have proposed phase diagrams for the titanium-hydrogen binary system but perhaps the most commonly accepted diagram is that presented by Lenning, Craighead and Jaffee.[10] Figure 2 shows this phase diagram. This equilibrium diagram applies to the pure components at one atmosphere pressure of hydrogen. As can be seen from this diagram, hydrogen stabilizes the beta phase down to 325°C at approximately 44 at.% hydrogen, which is the eutectoid composition. It is for this reason that hydrogen is referred to as a beta stabilizer. The solubility of hydrogen in the beta phase at the eutectoid temperature is approximately five times larger than in the alpha phase.

Figure 3 shows the low temperature portion of the phase diagram in the titanium rich end as determined by Koster, Bangert and Ewert.[11] This portion of the diagram was established using internal-friction studies. McQuillan[12] proposed the following equation to express the solubility of hydrogen in alpha titanium:

$$\log C = 6.829 - \frac{1.95 \times 10^3}{T}$$

where C is the concentration of hydrogen in ppm (by weight) and T is the absolute temperature. At room temperature the solubility of hydrogen in alpha titanium is very low. From the diagram in Fig. 3 it is 1 to 2 ppm and from the above equation it is 1.95 ppm.

The phase diagrams shown in Figs. 2 and 3 represent the limiting case for pure titanium which is extremely difficult to obtain in the laboratory and impossible from a commercial standpoint. Therefore, of more interest is the effect of alloying additions on the behavior of hydrogen in the alloys. For example, certain beta stabilizers such as molybdenum, increase the solubility of hydrogen in beta titanium at room temperature. This is shown by the fact that in predominately alpha alloys, a small amount of molybdenum containing beta phase increases the hydrogen tolerance as measured by impact properties.[13] That is, it increases the alloys resistance to impact hydrogen embrittlement. Other beta stabilizers such as iron, manganese, vanadium and columbium result in a beta phase of lower hydrogen solubility.[13] Beta stabilized with vanadium has the lowest apparent hydrogen solubility.

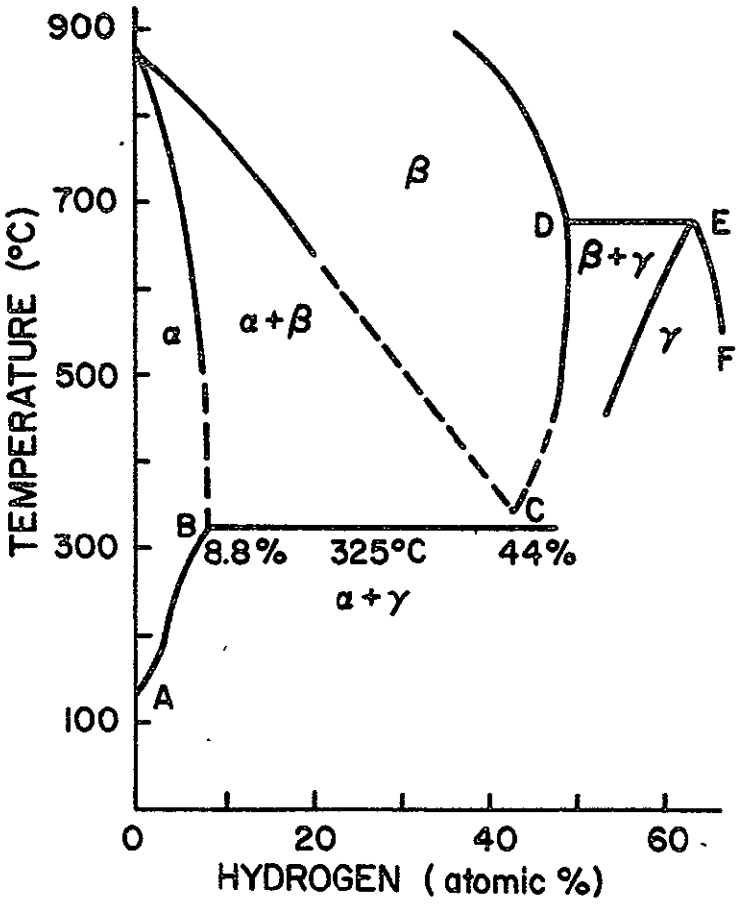

Fig. 2 - The Titanium-Hydrogen Equilibrium Diagram (Ref. 10)

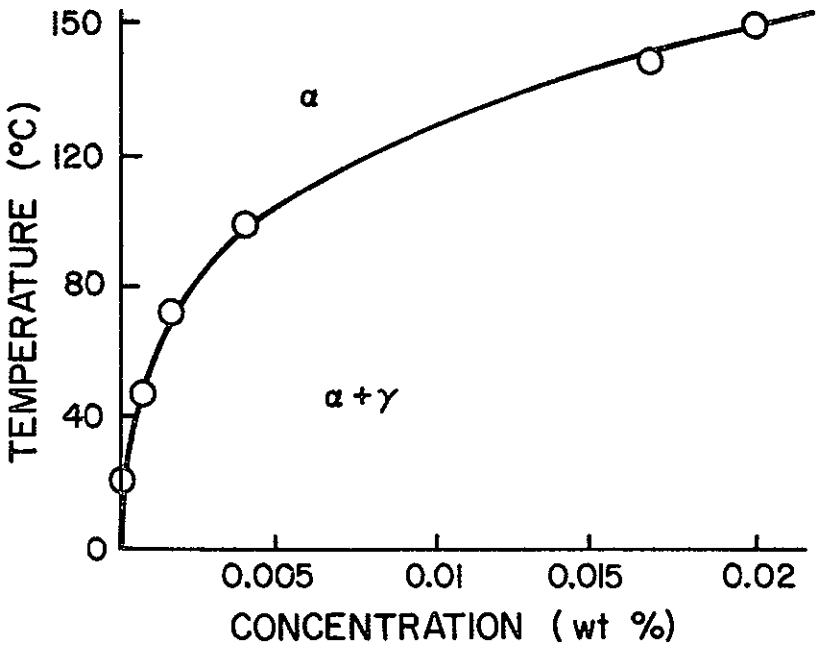

Fig. 3 - Solubility of Hydrogen in α-Titanium (Ref. 11)

The alpha stabilizers such as aluminum, tin, nitrogen and oxygen have been investigated more thoroughly. Aluminum increases the hydrogen solubility in alpha titanium markedly near room temperature and decreases it at elevated temperatures.[14]

A partial ternary diagram for the titanium-aluminum-hydrogen system was established by Berger, Williams and Jaffee[15] and is shown in Fig. 4. From this diagram it can be seen that the solubility of hydrogen in alpha titanium is increased several times by the addition of aluminum. More recent work by Sanderson and Scully[16] has verified this result. They found that hydrogen pickup during chemical polishing increases as the aluminum content of the alloy increases. This result may, however, not be due to the increased content of aluminum but rather to the increased volume of the ordered Ti_3Al phase as suggested by workers at Battelle Memorial Institute.[17] They have found that the rate of hydrogen absorption at 650°C in Ti-20Al alloy is doubled by allowing the second phase, Ti_3Al, to precipitate. They, therefore, suggest that it is the increase in volume fraction of the second phase, Ti_3Al, which accounts for the increase in hydrogen absorption rates as the aluminum content is increased.

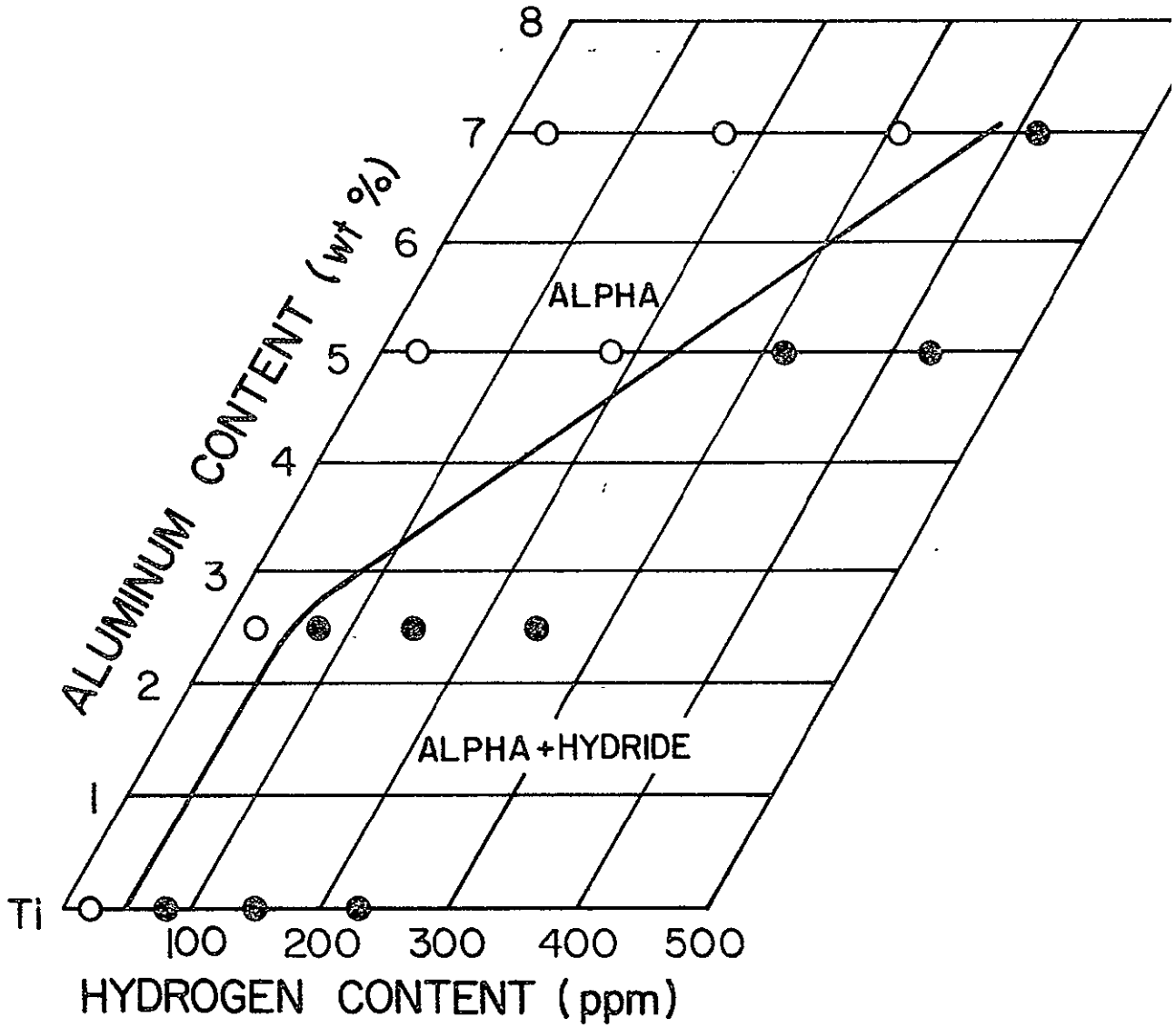

Fig. 4 - Room-Temperature Solubility of Hydrogen in the Titanium-Aluminum System as Determined by Microstructural Examination (Ref. 15)

The neutral hydrogen atoms with a radius of 0.41 Å fit very well in the tetrahedral holes of the BCC beta phase which have a radius of 0.44 Å. This good fit accounts for the high solubility of hydrogen in beta titanium. The alpha titanium lattice contains tetrahedral holes with a radius of 0.34 Å and octahedral holes with a radius of 0.62 Å. The misfit between the hydrogen atoms and the tetrahedral holes in the alpha titanium is 20%, which is too large to allow an appreciable number of hydrogen atoms to occupy these holes. Hence, the hydrogen atoms could be accommodated in the octahedral holes which are much larger than the hydrogen atoms. The increase in free energy due to the larger vibrational freedom of the hydrogen atoms in the octahedral holes limits the solubility of hydrogen in these holes.[8] This, of course, holds for the neutral hydrogen atom but it is not known in exactly what form the hydrogen is present in the titanium. As mentioned previously, it is believed to be in a partially ionized state. Hagg,[18] however, calculated the radius of occluded hydrogen to be 0.46 Å, which is larger than the reported neutral radius and, hence, accommodation would be more difficult in the tetrahedral holes. Some investigators believe that the hydrogen initially enters octahedral holes, then shift into tetrahedral sites.[19]

Additions of aluminum decrease the size of both holes as well as both the "c" and "a" parameters of the hexagonal titanium lattice. Thus, if the hydrogen did indeed occupy the tetrahedral holes, increasing the aluminum content would decrease the hydrogen solubility. This is the opposite of what is actually observed as shown in Fig. 4. As mentioned previously, investigators[15,16] found that increasing the aluminum content increased the hydrogen solubility. This could be explained by the presence of the ordered second phase, Ti_3Al, or by the fact that the hydrogen atoms do occupy the octahedral holes and decreasing the size of these holes would increase the solubility of the hydrogen. This latter possibility can be discounted by the fact that the hydrogen, when it enters titanium, expands the lattice. This would tend to support the idea that the hydrogen atoms do, in fact, occupy the smaller tetrahedral holes. Because of this lattice expansion and the light weight of hydrogen, a reduction in the density is anticipated. Figure 5 shows a plot of density versus hydrogen content for high-purity titanium - hydrogen alloys.

THE HYDRIDE PHASE

The gamma phase, as previously mentioned, is an interstitial compound and is referred to as a "pseudo-metallic hydride". The composition of this phase is not fixed and can exist over a relatively wide range of compositions as can be inferred from the incomplete phase diagram shown in Fig. 2. According to Hägg[21] the range of composition over which the hydride phase exists is between 47.4 at.% and 64.2 at.%. McQuillan[12] reports that the highest concentration of hydrogen in the gamma phase corresponds to $TiH_{1.73}$ and according to others[10] the lower

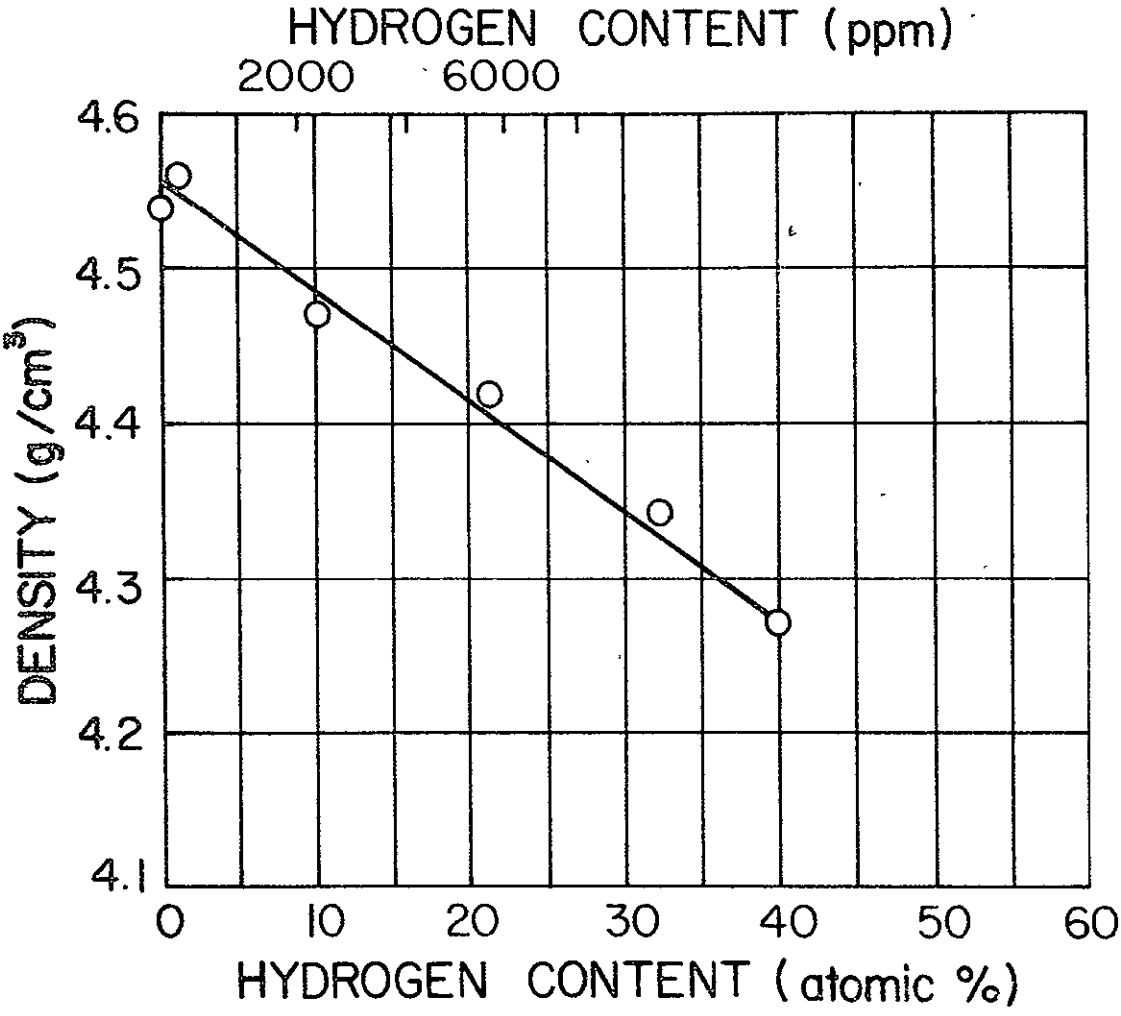

Fig. 5 - Effect of Hydrogen on the Density of High-Purity Titanium-Hydrogen Alloys (Ref. 20)

limit of hydrogen concentration in this phase is 50 at.%. Yakel[22] completely saturated alpha titanium with hydrogen and determined that the concentration corresponds to $TiH_{1.99}$. This is close to the ideal stoichiometric composition of TiH_2 which may, in fact, not be attainable.

There have been several different crystal structures reported for the gamma phase. In 1931, Hägg[21] determined by x-ray diffraction that the hydride phase had a face-centered cubic lattice. The lattice parameters were determined to be from 4.397 Å at 50 at.% to 4.460 Å at 62.4 at.% hydrogen. Other investigators,[21,22] using neutron diffraction, reported in 1956 that the hydride exhibited a tetragonal structure. Jaffee[22] determined that the lattice parameters for the body-centered-tetragonal gamma phase were a = 3.12 Å and c = 4.18 Å. The basic bravais lattice is, however, body-centered-tetragonal.

A second-order phase transformation in which the energy and volume change continuously has been reported by Sidhu et. al.[23] for the gamma phase. They determined that as the composition of the gamma phase approaches TiH_2, the cubic unit cell distorts to a face-centered-tetragonal cell. They report that the FCC structure of the hydride is of the CaF_2 type. This structure would place the titanium atoms in a FCC arrangement in the unit cell with the eight hydrogen atoms occupying the tetrahedral holes.

The same second-order transformation was reported by Yakel[22] when he reported that the structure of the gamma phase is BCT below 310°K and FCC above that temperature. Recent work by J. D. Boyd[25] has indicated yet another lattice structure for the hydride phase. He reports that strain induced hydrides have a body-centered cubic structure with a = 3.3 Å. He reports that these hydrides are nonequilibrium intermediate precipitates that have a lower activation energy for nucleation than the gamma phase.

The orientation relationships between the gamma phase and the alpha titanium lattice in the Ti-8Al-1Mo-1V alloy are given in Table 1 along with the habit planes for each. Orientations (1), (2) and (3) were observed for spontaneously nucleated hydrides at elevated temperatures, whereas (4) and (5) were observed for strain induced hydrides at room temperature. Orientation (4) was indexed as FCT with "a" = 4.7Å and "c" = 3.3Å, whereas, (5) was indexed as BCC with "a" = 3.3Å. Note that orientations (1), (2), (3) and (4) have close-packed $[1\bar{2}10]_\alpha$ directions parallel to the close-packed $[1\bar{1}0]_\gamma$ direction. Orientation (5) is the nonequilibrium intermediate precipitates which were observed by Boyd.[25]

In addition to the crystallographic orientations for the hydride precipitate, the hydrides also exhibit stress orientation. Louthan[27] determined that hydride precipitation in titanium super-saturated with hydrogen occurs on the habit planes oriented most nearly perpendicular to the stress axis. The level of stress required for this stress orientation was below the yield stress (i. e., at least 30,000 psi were required for stress orientation).

Table 1 - Orientation Relationships between the Alpha Titanium Lattice and the Gamma Phase in the Ti-8Al-1Mo-1V Alloy

	Orientation Relationship	Habit Plane	Ref.
(1)	$\{0001\}_\alpha \parallel \{001\}_\gamma$, $\langle 1\bar{2}10\rangle_\alpha \parallel \langle 1\bar{1}0\rangle_\gamma$	$(\bar{1}010)_\alpha \parallel (\bar{1}00)_\gamma$	26
(2)	$\{0001\}_\alpha \parallel \{112\}_\gamma$, $\langle 1\bar{2}10\rangle_\alpha \parallel \langle 1\bar{1}0\rangle_\gamma$	$(1\bar{1}00)_\alpha \parallel (3\bar{1}\bar{1})_\gamma$	26
(3)	$\{0001\}_\alpha \parallel \{110\}_\gamma$, $\langle 1\bar{2}10\rangle_\alpha \parallel \langle 1\bar{1}0\rangle_\gamma$	$(0\bar{1}10)_\alpha \parallel (1\bar{1}\bar{1})_\gamma$	26
(4)	$\{0001\}_\alpha \parallel \{111\}_\gamma$, $\langle 1\bar{2}10\rangle_\alpha \parallel \langle 1\bar{1}0\rangle_\gamma$	$(\bar{1}100)_\alpha \parallel (3\bar{1}\bar{1})_\gamma$	26
(5)	$\{0001\}_\alpha \parallel (011)_\gamma$, $[\bar{1}\bar{1}20]_\alpha \parallel [1\bar{1}1]$	$(1\bar{1}00)_\alpha \parallel (21\bar{1})$	17

This stress orientation occurs because of the volume expansion of the lattice accompanying the precipitation. The most energetically favored habit planes would be those oriented such that the volume expansion of the plate-like hydride would act to relieve some of the tensile stress in the lattice.[27] The texture of cold-rolled alpha titanium is such that the majority of the grains have the $[10\bar{1}0]_\alpha$ direction parallel to the rolling direction and the (0001) plane rotated 40° about this direction from the rolling plane.[28] This texture allows the majority of the hydride habit planes $\{10\bar{1}0\}$ to be oriented perpendicular or nearly perpendicular to the longitudinal or rolling direction. Hence, when a longitudinal stress of sufficient magnitude is applied during the precipitation, the hydrides will form on these $\{10\bar{1}0\}$ planes and help to relieve the tensile stress. Similiarly, for a transverse stress the $\{10\bar{1}1\}$ planes would be favored. In this instance, the $\{10\bar{1}1\}$ planes would not be perpendicular to the stress axis but would contribute 86% of the volume expansion to the stress relief.[28]

The application of stresses also helps to overcome the large driving force required for the spontaneous nucleation of the hydride precipitate as demonstrated by J. D. Boyd.[25] He has shown that in the Ti-8Al-1Mo-1V alloy a supersaturation of 800 ppm hydrogen is required for spontaneous nucleation in unstressed specimens, whereas only 200 ppm are required if a small amount of plastic strain is introduced into the lattice. Table 1 showed the orientation relationships for these spontaneous and strain-induced hydrides.

THE ELECTROCHEMICAL INTRODUCTION OF HYDROGEN

It is believed that hydrogen enters the metal from solution containing hydrogen ions by way of the adsorbed specie. The overall reaction for the reduction of the hydrogen ions may be written:

$$2H^+ + 2e^- \rightarrow H_2 \qquad (1)$$

There are, however, several steps involved in this reaction. These could be written

$$H^+ + M + e^- \rightarrow M - H_{ads} \qquad (2)$$

$$M - H_{ads} + M - H_{ads} \rightarrow H_2 + 2M \qquad (3)$$

$$M - H_{ads} + H^+ + e^- \rightarrow H_2 + M \qquad (4)$$

Equation (2) is the commonly written discharge reaction where the hydrogen ion combines with a metal site, M, to form the adsorbed specie. Equation (3) is the recombination reaction, one of two possible evolution reactions, which yields hydrogen gas. Equation (4) is the electrochemical desorption reaction, the second evolution reaction, also yielding hydrogen gas. Since the hydrogen ions seldom combine in the solution as written in the overall reaction (1), the rate controlling step is either the discharge reaction (2) or one of the two evolution reactions. For titanium, the rate controlling step is the electrochemical desorption as represented by Eq. (3).[29] The discharge reaction is "fast" and, hence, the available surface sites for adsorption are normally occupied. The occlusion of hydrogen occurs from the adsorbed hydrogen on the surface. This may be represented as

$$M - H_{ads} = M - H_{abs}$$

This reversible reaction creates a diffusion gradient so that the absorbed hydrogen diffuses into the lattice. Any factor which would affect this equilibrium would therefore affect the rate of hydrogen absorption. For example, increasing the hydrogen ion concentration will increase the rate of hydrogen pickup. Also, changing the surface by either the formation of an oxide layer or a hydride layer will affect the absorption rate. Gulbransen and Andrew[30] show that oxide films retard the occlusion of hydrogen in zirconium. Room temperature oxide films were the most resistant.

The formation of a hydride layer on the surface of α - titanium alloys has been reported[31,32] during immersion in hydrofluoric, hydrochloric, sulphuric and phosphoric acids. An immersion of only a few

seconds is required in concentrated hydrofluoric acid.[31] Otsuka[32] reports that this hydride layer retards corrosion of titanium. It is believed that this hydride layer inhibits the pickup of hydrogen by titanium alloys.[10]

DIFFUSION OF HYDROGEN IN TITANIUM

Wasilewski and Kehl[33] have measured the diffusion rates of hydrogen in both alpha and beta titanium. The expressions for the diffusion coefficients are

$$D_\alpha = 1.8 \times 10^{-2} \exp\left(\frac{-12{,}380 \pm 680}{RT}\right)$$

$$D_\beta = 1.95 \times 10^{-3} \exp\left(\frac{-6{,}640 \pm 500}{RT}\right)$$

The larger diffusion coefficient in the beta titanium is understandable from the fact that the body-centered cubic beta structure is more "open" than the close-packed alpha titanium lattice. The interstitial space assuming a hard sphere model, in the BCC lattice amounts to 32% of the total volume of the structure versus about 26% in the alpha titanium lattice. The diffusion coefficient of hydrogen in alpha titanium at room temperature is about 2×10^{-11} cm^2/sec from the above equation.

Occluded hydrogen is affected by the stress field in an elastic solid. It has been shown[34] that an elastic tensile stress decreases the chemical potential of an interstitial solute and an elastic compressive stress increases it. The stress may be externally applied or may exist internally as around a dislocation. Thus, if we were to consider an edge dislocation with a compressive elastic stress field above the slip plane and a tensile field below, the hydrogen will tend to segregate to the tensile region where it will help relieve the tensile stresses. In this manner, the dislocations with tensile elastic stress fields will accumulate atmospheres of hydrogen. The hydrogen will thus become essentially immobile.

Troiano[35] states that hydrogen will diffuse to points of maximum triaxiality such as is present at the root of a notch or crack. This is, of course, the basis for many of the theories which hold the hydrogen ion responsible for stress corrosion cracking.

HYDROGEN EMBRITTLEMENT OF TITANIUM ALLOYS

Hydrogen, in sufficient quantities in titanium alloys, can lead to embrittlement. This embrittlement is commonly divided into two categories, impact embrittlement and low-strain-rate embrittlement, based upon the loading rate at which each type appears. Both types appear to be related to the precipitation of the hydride phase.

Impact embrittlement appears to be most common in alpha alloys and is characterized by a transition from ductile to brittle behavior as the temperature is lowered. There are four variables which affect this type of embrittlement: hydrogen content, strain rate, stress concentration and temperature.[36] The transition temperature is increased by increasing the hydrogen concentration, increasing the loading rate and introducing stress raisers such as notches into the samples. Embrittlement is most pronounced in notched impact tests which accounts for this type of embrittlement being called impact embrittlement.

Low-strain-rate embrittlement, on the other hand, is most common in alpha-beta alloys and is more severe as the strain rate is decreased. Also, there appears to be a definite temperature range over which embrittlement occurs. This temperature range, at low strain rates, appears to be from 75 to -100°F.[37] This type of embrittlement can occur with very low amounts of plastic strain.[37] Residual stresses from fabrication or assembly may be sufficient to cause embrittlement and cracking.[39] This type of failure is also called "delayed cracking" because the failure does not commonly occur until the part has been in service for a period of time.

These two types of hydrogen embrittlement appear quite dissimilar; however, it is highly probable that they are actually quite similar and influenced by the same basic factor, a decrease in solid solubility in both alpha and beta titanium with temperature.[37] According to Williams,[37] "if precipitation occurs on cooling to room temperature, impact embrittlement occurs. If, on the other hand, precipitation does not occur on cooling to room temperature, a supersaturated solid solution is formed that is susceptible to precipitation (or hydrogen segregation) under the action of strain, and low-strain-rate embrittlement is observed." Since this low-strain-rate embrittlement requires an activation process for the precipitation of the hydride phase, lowering the temperature will decrease the ease of precipitation and embrittlement will disappear. At higher temperatures the solubility of hydrogen in the titanium increases and again embrittlement will disappear. This, then, accounts for the temperature range in which low-strain-rate embrittlement occurs.

Since hydrogen embrittlement is dependent upon the hydride phase, alloying is one of the most effective methods of increasing the resistance to this type of embrittlement. For example, impact embrittlement is decreased by alloying with elements which increase the hydrogen

solubility. Aluminum increases an alloy's apparent hydrogen solubility as shown in Fig. 4. It is believed, however, that the effect of aluminum is to increase the activation energy for hydride nucleation rather than to increase the equilibrium solubility of hydrogen in the alpha phase.[25] The addition of 7% aluminum to titanium raises the level of hydrogen required for embrittlement in impact testing from 50 ppm to more than 300 ppm.[37] Also, small amounts of beta-stabilizing elements will also increase the alloys resistance to impact embrittlement.

Low-strain-rate embrittlement is best controlled by increasing the amount of beta phase in the alloys. Molybdenum was determined to be the most effective alloying element.[37] Both oxygen and aluminum are detrimental to an alloy's resistance to low-strain-rate embrittlement. Boyd[25] has studied the precipitation of strain-induced hydrides and has obtained good evidence to show that hydride formation in a Ti-8Al-1Mo-1V alloy is responsible for low-strain-rate embrittlement. Aluminum apparently increases an alloy's resistance to impact embrittlement by making hydride precipitation more difficult, but in doing so renders an alloy more susceptible to low-strain-rate embrittlement.

Hydrogen present in titanium alloys at levels insufficient to cause "embrittlement" has a marked effect upon the mechanical properties. Hydrogen can result in a noticeable increase in strength with no loss in ductility when present in alpha and alpha-beta titanium alloys.[13] Hydrogen appears to have little effect on the tensile properties of all beta alloys.[13] Hydrogen appears to decrease the notch sensitivity to stress rupture in these low hydrogen levels.[38] In addition, impact properties of titanium alloys are unaffected.[37]

THE ROLE OF HYDROGEN IN TITANIUM STRESS-CORROSION CRACKING THEORIES

Before the hydrogen theories of stress corrosion cracking are discussed, it would be beneficial to review the critical observations as related to stress corrosion cracking in titanium. Most of these observations and, indeed, most of the research concerning stress corrosion cracking are concerned with the propagation of stress corrosion cracks. The initiation stage, being more difficult to study, has not received as much attention.

There are many factors which control an alloys susceptibility to stress corrosion cracking. Among these are: (1) environment, (2) stress, (3) electrochemical potential, (4) metallurgical structure, and (5) alloy content.

There are numerous environments which have been found to lower the notched fracture toughness of titanium alloys. Some of these are hot salt, nitrogen tetroxide, methanol and salt water (3.5% NaCl at room

temperature). This survey is concerned primarily with the salt water environments. Beck[39] has determined that "stress corrosion cracking" of Ti-8Al-1Mo-1V alloy in aqueous environments at room temperature is specific to three anions; chloride, bromide and iodide. Fontana et al.[40] demonstrated this same specificity of aqueous environments by observing similar cracking behavior in 0.6M NaCl, KBr and KI solutions. The cation apparently has little or no effect upon the cracking behavior.[39]

As the name suggests, stress corrosion cracking is dependent upon the action of a tensile stress. Initial work[41,42] in the area of titanium stress corrosion indicated that for cracking to occur, specimens must be notched and in a state of plane strain and, in some cases precracked by fatigue. These are the most severe conditions that can be imposed upon a specimen. The parameter commonly used to evaluate a specimen's susceptibility to stress corrosion is the reduction in fracture toughness. It is more accurately a measure of the susceptibility to propagation of pre-existing cracks and, as such, is an important parameter. It does not, however, consider the initiation of a crack and, as such, may not be a true indication of an alloy's susceptibility to stress corrosion in the classic sense. More recently, Fontana et al.[40] have demonstrated that such severe stress-raisers are not required. He found that both initiation and propagation occurred on smooth three-point bend specimens of Ti-8-1-1 sheet in aqueous room temperature environments.

The primary slip systems for alpha titanium alloys are:

(1) $\{10\bar{1}0\}$ 1/3 $\langle 11\bar{2}0\rangle$

(2) $\{10\bar{1}1\}$ 1/3 $\langle 11\bar{2}0\rangle$

(3) $\{0001\}$ 1/3 $\langle 11\bar{2}0\rangle$

The prism slip system (1) is preferred owing to the lower than ideal c/a ratio; however, all three can be operative in the alpha phase and have been observed. Churchman[43] has shown that the critical resolved shear stress for the three systems are close in impure titanium. This would allow a $[11\bar{2}0]$ dislocation to glide in three planes, the slip planes, and would lead to a cellular dislocation array.[44] The addition of aluminum to titanium acts to restrict cross-slip and renders the prism planes the preferred slip planes.[44]

Stress corrosion cracking of the alpha phase of titanium alloys in 3.5% NaCl is transgranular in nature. Blackburn and Williams[45] have shown the alpha phase of Ti-8-1-1 to fail by cleavage fracture on the $\{10\bar{1}8\}$ or $\{10\bar{1}7\}$ planes. These planes are rotated 12 to 14° from the basal plane about $[1\bar{2}10]$. They also observed that the macroscopic crack front propagates discontinuously. However, owing to the extensive branching of the crack and the continuity of the current-time plots, they conclude that cracking is continuous.

Beck[39] reports that the velocity of crack propagation is controlled by the imposed potential. The more noble the potential, the greater the velocity. Figure 6 shows a plot of this electrochemical dependence of the crack velocity. Beck[39] also reports that there are two potential regions in which protection occurs, a cathodic region below -1000 mV (SCE) and an anodic region above about 0 mV (SCE) in KBr. In addition, he reports "pitting corrosion" at potentials above about +1000 mV (SCE) in KBr.

The metallurgical structure and alloy content will determine an alloys susceptibility to SCC. The alloys listed below have been shown[46,47,48,49] to be susceptible to reduced fracture toughness in salt water:

Ti - 0.317 O
Ti - 8Mn
Ti - 2.5Al-1Mo-10Sn-5Zr
Ti - 3Al-11Cr-13V
Ti - 4Al-4Mn
Ti - 5Al-2.5Sn
Ti - 6Al-2.5Sn
Ti - 6Al-4V
Ti - 6Al-3Cb-2Sn
Ti - 6Al-4V-1Sn
Ti - 6Al-4V-2Co
Ti - 6Al-6V-2.5Sn
Ti - 7Al-2Cb-1Ta
Ti - 7Al-3Cb
Ti - 7Al-3Mo
Ti - 7Al-3Cb-2Sn
Ti - 8Al-1Mo-1V
Ti - 8Al-3Cb-2Sn

These are primarily alpha and alpha-beta alloys. As a general rule, the alpha alloys are susceptible while some alpha-beta alloys are and some are not susceptible.

The most commonly used alpha stabilizer is aluminum. However, increasing the aluminum content increases an alloys susceptibility to both low-strain-rate hydrogen embrittlement and stress corrosion.[42,47,49,50] There is a nonsusceptible-to-susceptible type transformation between five and six percent aluminum. Seagle et al.[50] suggest that this susceptibility of higher aluminum alloys is indirectly related to the formation of Ti_3Al. This is an ordered phase which forms by exposures in the temperature range 900-1500° F depending upon the aluminum content. Ti_3Al is commonly present as small dispersed coherent regions of long range order.[45]

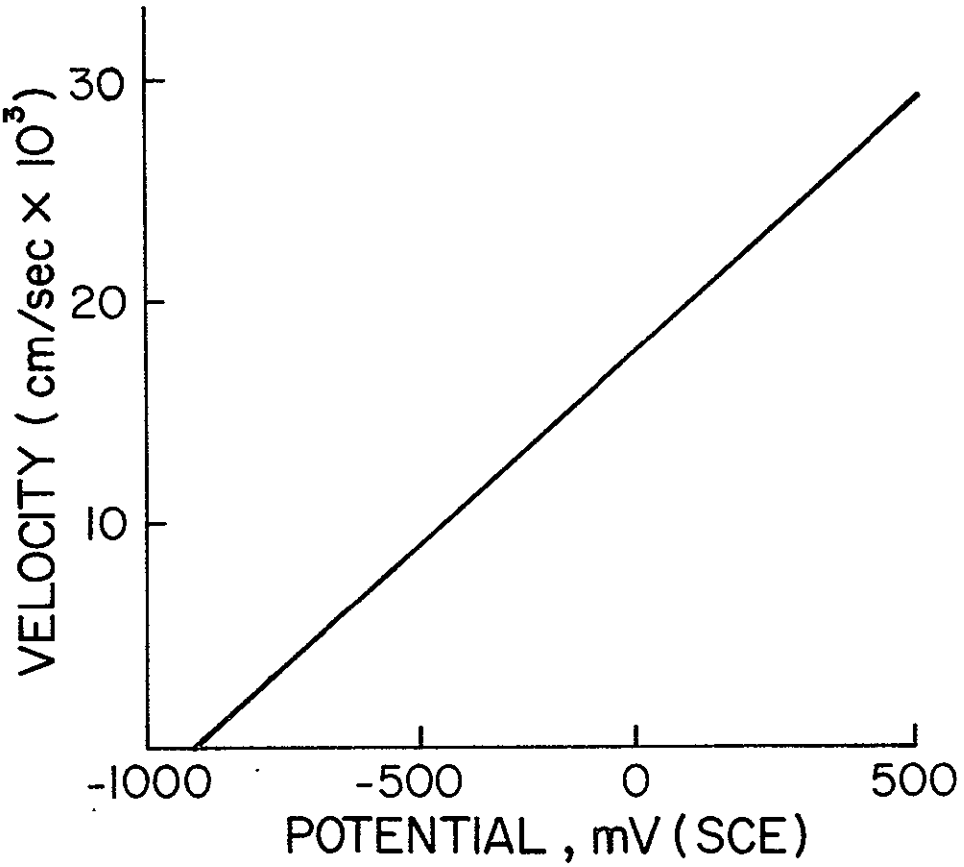

Fig. 6 - Plot Showing Relationship between Crack Velocity and Potential for Ti-8Al-1Mo-1V in 0.6M Halide Solutions (Ref. 39)

In addition to the formation of the α_2 phase (Ti_3Al), there is a transition from cellular to coplaner dislocation arrays at an aluminum content of approximately 5 wt.% Al.[45] Also, dislocation tangling becomes more difficult and the thickness of the slip bands decreases as the aluminum content increases.[45] Transgranular stress corrosion cracking is generally associated with coplanar dislocation arrays which correspond to wide slip steps.[51]

The effect of heat treatment on an alloy's susceptibility is very significant. Many susceptible alloys can be rendered nonsusceptible by the use of the proper heat treatment.[45,50,52,53] Lane et. al.[54] show there is a correlation between microstructure and the susceptibility of several titanium-aluminum alloys. They determined that microstructures containing long coarse alpha platelets were most susceptible. Workers at Reactive Metals[47] have determined that there is a temperature range between 900 and 1500°F which gives maximum susceptibility in Ti-8-1-1. This corresponds to the temperature range for Ti_3Al formation.

Hydrogen is another alloying element which must be considered. Hydrogen is not commonly thought of in these terms, but it is present in most commercial alloys at levels approaching 100 ppm. As was stated previously, the equilibrium hydrogen solubility in pure titanium is between 1 and 2 ppm. We, therefore, have an alloy which is supersaturated in hydrogen as it comes from the mill. Hydrogen, in sufficient quantities, will lead to low-strain-rate embrittlement as previously mentioned. In Ti-8-1-1, 200 ppm hydrogen are required to precipitate the hydride which can presumably lead to hydrogen embrittlement.[25] Thus we need introduce only approximately 100 ppm hydrogen locally at or near a notch or stress raiser to set up conditions which could lead to a low-strain-rate embrittlement.

The possibility of hydrogen being responsible for stress corrosion cracking has become a very controversial issue. There are several proposed mechanisms which include hydrogen as the bad actor. These hydrogen and/or hydride theories seem to fit the observed behavior as well or better than other proposed mechanisms. In addition to the salt water environments, many researchers believe hydrogen to be responsible in the hot salt, methanol and nitrogen tetroxide environments. It is doubtful, however, that any one mechanism will be operative in all the environments in which titanium alloys exhibit susceptibility. Other proposed theories include electrochemical dissolution, the repeated formation and rupture of a brittle oxide film, the stress sorption theories and chloride ion theories.

Work by Rideout et al.[55] indicates that the absorption of hydrogen during the corrosion process could promote cracking. They find that the crack propagates in rapid bursts in the hot salt environment and also that hydrogen segregates to the crack areas. Their work also demonstrates the need for moisture before cracking can occur. This seems to fit the mechanism proposed by Sanderson et al.,[56] in which the hydride is presumed to form ahead of the crack tip.

Sanderson, Powell and Scully[56] postulate that during repassivation in aqueous environments, hydrogen is discharged at the tip of the crack and enters the metal and hydride formation occurs. The hydride continuously forms ahead of the crack tip and cracking proceeds either continuously or in rapid bursts.

Mackay et al.[57] introduced tritium by cathodic charging and using electron microautoardiography determined the distribution of tritium in several alloys. In the alpha alloy, Ti-5Al-2.5Sn, the tritium was evenly distributed throughout. In the alpha-beta alloy, Ti-6Al-4V, the tritium was also evenly distributed after charging at 80 mA/in.^{2}. Using a higher current density of 0.4 A/in.^{2} they observed that the tritium formed clusters at the alpha-beta interfaces, alpha-alpha boundaries and in the alpha phase. No filaments were observed in the beta phase. They next introduced 40 to 50 ppm tritium from the gas phase at 725°C.[58] In this case, the charging at elevated temperature and air quenching produced extensive cracking in the alpha alloy. The fracture was intergranular. In the alpha-beta alloys, Ti-8-1-1 and Ti-6-4, the tritium was observed to be concentrated in the beta phase. It, therefore, appears that the method in which hydrogen is introduced or, better, the temperature at which the hydrogen is introduced, will drastically affect the distribution of the hydrogen in the microstructure.

Sanderson and Scully[59] have reported that hydrides formed in foil specimens of Ti-5Al-2.5Sn when they were bent in an acidified chloride solution. These hydrides formed along the bend in the foil. These same workers[16] have observed that the size of the hydride formed in this alloy increased as the aluminum content increased. Precipitation occurred on the same planes and in the same directions. In the highest aluminum alloy, Ti-8.64Al, the hydrides were plates as compared to the needle-like precipitates observed in the lower alloys.

J. D. Boyd et al.[17,25,26,60] have done a considerable amount of research on the mechanism of aqueous salt stress corrosion cracking. As mentioned earlier, they have determined that up to 600 ppm hydrogen can be introduced by elevated temperature gas charing with no hydride nucleation and no apparent microstructural changes in Ti-8-1-1. Specimens charged with 800 ppm hydrogen, however, contained a large amount of the hydride phase. These were referred to as spontaneously nucleated hydrides and were present as rather large platelets lying on the $\{10\bar{1}0\}_\alpha$ habit planes.

They found that this large nucleation energy barrier, a supersaturation of 800 ppm, could be considerably reduced to 200 ppm by introducting a small amount of plastic deformation. These strain-induced hydrides are present on the active slip bands and lie along the entire length of each slip band. These hydrides are much thinner than the spontaneously nucleated hydrides. The orientation relationships of both of these hydrides are given in Table 1.

These same workers have also determined that the propagation of stress corrosion cracks in titanium alloys in aqueous environments occurs by the nucleation of cleavage microcracks in some of the alpha grains near the main crack. Evidence of cleavage in titanium alloys has only been found when the Ti_3Al phase is present in the alpha grains.

The mechanism for SCC they propose is the most complete hydride theory available and appears to fit most of the observations of the cracking behavior in aqueous environments. Their proposed model assumes the reduction of hydrogen ions at or near the crack tip which gives rise to an area of high hydrogen concentration around the crack tip. Strain induced hydrides would nucleate and grow rapidly along the active slip planes. The hydrogen concentrations required for this would be at least 200 ppm as defined by the concentrations required for strain induced hydrides. Figure 7 is a representation of this model. Note that they assume the hydrogen reduction to occur at a distance of one micron behind the crack tip. This assumption is from the analysis of Beck[39]

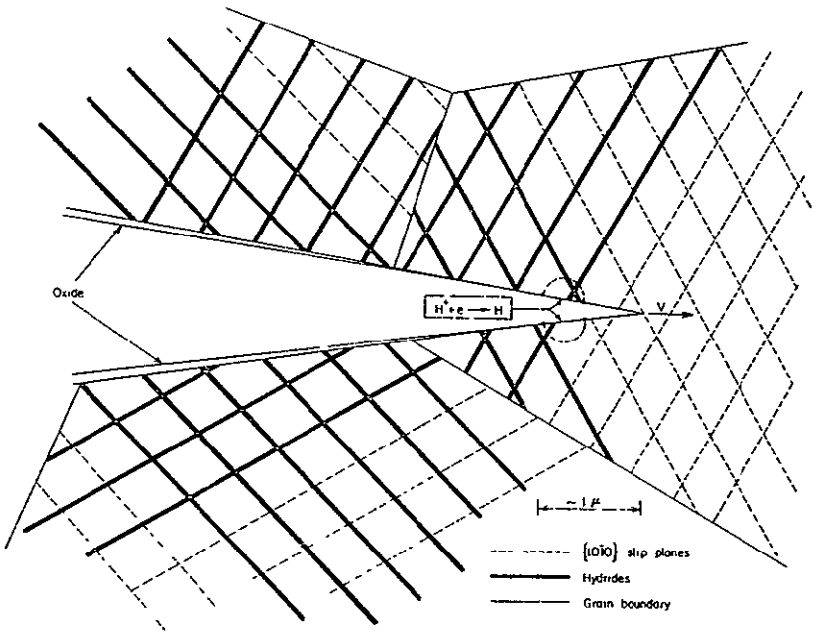

Fig. 7 - Proposed Distribution of Hydrides about an Advancing Stress Corrosion Crack (Ref. 17)

continuum electrochemical mass-transport-kinetic model. They suggest that these strain-induced hydrides effectively block the active slip planes and prevent the emergence of glide dislocations. Since cross-slip is difficult, a dislocation pile-up occurs, and dislocation movement is prevented. This limits the plastic zone and the stress concentration at the crack tip would be much greater than it would be if the hydrides were not present. "The tensile stresses resulting from this dislocation pile-up would be a maximum across a plane normal to the $(10\bar{1}0)$ slip plane and this is consistent with the observed (0001) cleavage plane".

This model is for the propagation of stress corrosion cracks and/or low-strain-rate embrittlement and, as such, does not consider the initiation phase of cracking. The basic argument against such a model is that the hydrogen buildup in the area around the crack tip may not achieve the desired supersaturation for hydride nucleation before the crack has moved. That is, the crack may outrun this ability for any fixed area to buildup enough supersaturation.

Tiller and Schrieffer[61] have proposed a "hydrogen pump" which is active at the crack tip. They propose that since a specimen under tensile stress exhibits stress enhancement in the vicinity of a crack tip, the local volume per atom must change, which leads to a redistribution of the free electrons in the metal. "This redistribution of free electrons creates a macropotential change in the metal which varies with position around the crack tip and extends to the outer limits of the stress field." They calculate that the crack tip region will be significantly cathodic from this redistribution of electrons. This then leads to the rapid migration of H^+ ions into the tip region where they discharge and migrate into the regions of high tensile stress within the metal.

This "hydrogen pump" model could then better explain the pickup of hydrogen at the crack tip and, if it is correct, could fit very conveniently into the previous model of Boyd et al.[17,28,60]

Mauney and Starke[62] have further refined the model of Boyd et al. to explain the rather unusual $(10\bar{1}8)$ or $(10\bar{1}7)$ fracture planes for the stress corrosion cracks. Their model has the hydride nucleating on the $(10\bar{1}0)$ and $10\bar{1}1)$ planes, the predominant slip planes, which blocks slip on these planes. This allows the not so predominant $\{11\bar{2}2\}$ $1/3\langle 11\bar{2}3\rangle$ system to come operative. The titanium hydrides form on planes which would cause dislocation pile-ups of the $\langle 11\bar{2}3\rangle$ type and would allow the application of Stroh's theory of fracture.[63]

Stroh determined that the cleavage plane was the plane with the maximum tensile stress across it, and, as such, is oriented such that it makes an angle of 70.5° with the pileup's slip plane. The angle between the pile-up's slip plane and the $\{1017\}$ and the $\{1018\}$ plane is 70.76° and 69.14°, respectively. Thus, Mauney and Starke[62] have perhaps determined the reason for the rather unusual cleavage plane in susceptible titanium alloys cracked in aqueous environments.

Most theories for the initiation of stress-corrosion cracks do not include hydrogen as an integral part in the mechanism. It is assumed, in most theories, that the hydrogen does not enter into the mechanism until the initiation step is complete. The initiation step is quite commonly thought of as a pitting type of attack which establishes a notch and a low pH within this notch. Once this has occurred, the conditions exist for a hydrogen embrittlement type fracture.

III. EXPERIMENTAL PROCEDURE

MATERIAL

The Ti-6Al-4V alloy used in this investigation was supplied in the form of cold rolled 0.005-in. thick sheet. Chemical analysis of this material is given in Table 2. The microstructure of the as-received material is shown in Fig. 8.

This material was given a vacuum anneal at 1500°F for 18 hours followed by furnace cooling. The vacuum was maintained at 10^{-7} mmHg. The microstructure of the annealed material is shown in Fig. 9.

SPECIMENS

There were basically four different types of specimens used in this investigation. The first type of specimen is for optical metallography and is simply a 1/2" × 1-1/2" × 0.005" sheet specimen which was spot welded to a wire of the Ti-6Al-4V alloy. This type of specimen also was used for the neodymium hydrogen detector method employed in this investigation. Immediately prior to cathodic charging these specimens were "activated" by immersion in the chemical thinning solution which is described later under foil preparation. The second specimen type is for examination of the surface after cathodic charging. These specimens are of the same size as the first type but were mechanically polished (see Appendix A) and then spot welded to a Ti-6-4 wire. These specimens were not "activated" as this treatment destroys the polish. The third type of specimen is intended for electron transmission microscopy. These specimens are 1/2" × 1-1/2" but are chemically thinned to 0.001 in. in thickness. These specimens are spot welded to a Ti-6-4 wire and activated prior to the cathodic treatment. The last type of specimen is a double-notched sheet specimen used for the stressing experiments.

The double-notched specimens were employed in order to study the effect of stress upon the pickup of hydrogen and the precipitation of the hydride phase. Figure 10 shows the specimen dimensions and the cell in which the specimen was charged. Specimens were chemically thinned in the center to from 0.001 in. to 0.003 in. depending upon whether transmission foils were required or not. The ends were not thinned to facilitate griping of the specimen. After thinning the specimens were notched and electropolished.

The notch sensitivity ratio, the ratio of stress at fracture in notched specimens to the stress at fracture of unnotched specimens, was determined to be 0.7 for these specimens. Both specimens were transverse such that the rolling direction was perpendicular to the loading direction. The load-elongation curve for the unnotched specimen is shown in

Table 2. Chemical Analysis of As-Received Ti-6Al-4V Used in this Investigation

	ppm	wt.%
Al	-	6.95
V	-	4.20
Mg	20	
Mn	100	
Sn	100	
Pb	20	
Fe	2000	
Ni	40	
Cu	150	
Na	2000	
Cl	100	
W	200	
Ca	200	
Mo	150	
Ta	2000	
Zr	200	
C	-	
N	-	
O	-	
H	-	

Fig.11 . The notched specimen failed to reach the yield point before fracture. All tensile tests were performed on a table model Instron Testing Machine.

HYDROGEN CHARGING

The specimens were electrolytically charged with hydrogen potentiostatically. A Wenking research potentiostat was used for potential control. In addition, the potential was monitored with a Hewlett Packard 3440A digital voltmeter. Figure 12a shows the experimental set-up.

The environment used in this investigation was 5N HCL which was deareated by bubbling high-purity nitrogen through the cell. The pH of the 5N HCl environment is approximately -0.7.

Prior to charging, most of the specimens to be treated in the 5N HCl were activated by immersion in a solution of 75 parts water, 22 parts nitric acid and 3 parts hydrofluoric acid. This treatment shifted the corrosion potential from +100 mV(± 50) SCE for the passive surface to -620 mV(± 30) SCE on the active surface. Once activated, the surface tended not to repassivate in this 5N HCl environment.

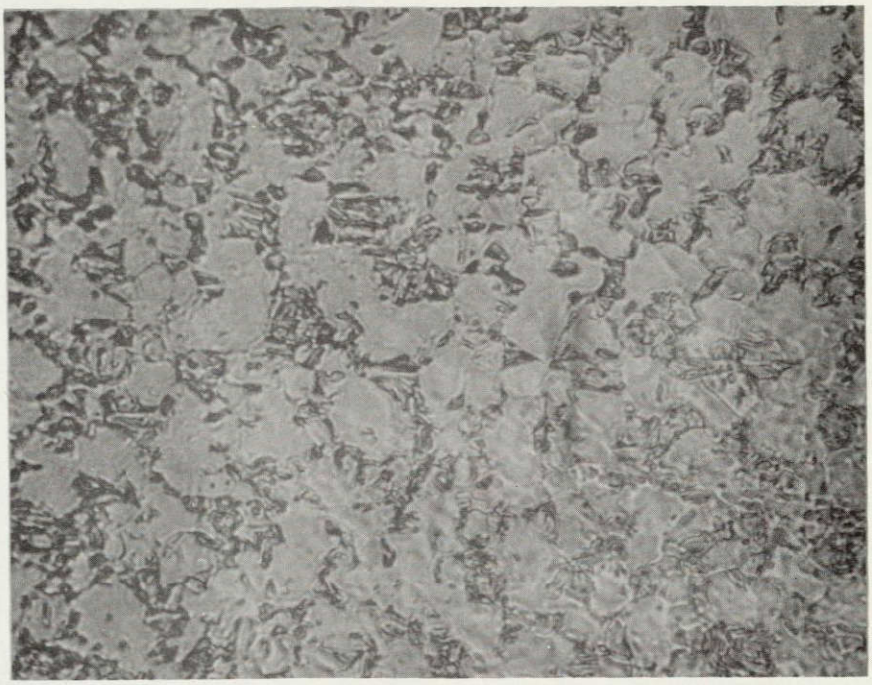

Fig. 8 - Microstructure of As-Received Ti-6Al-4V Cold-Rolled Sheet (750 X). Etch: 1½% HF, 3½% HNO_3, 95% H_2O

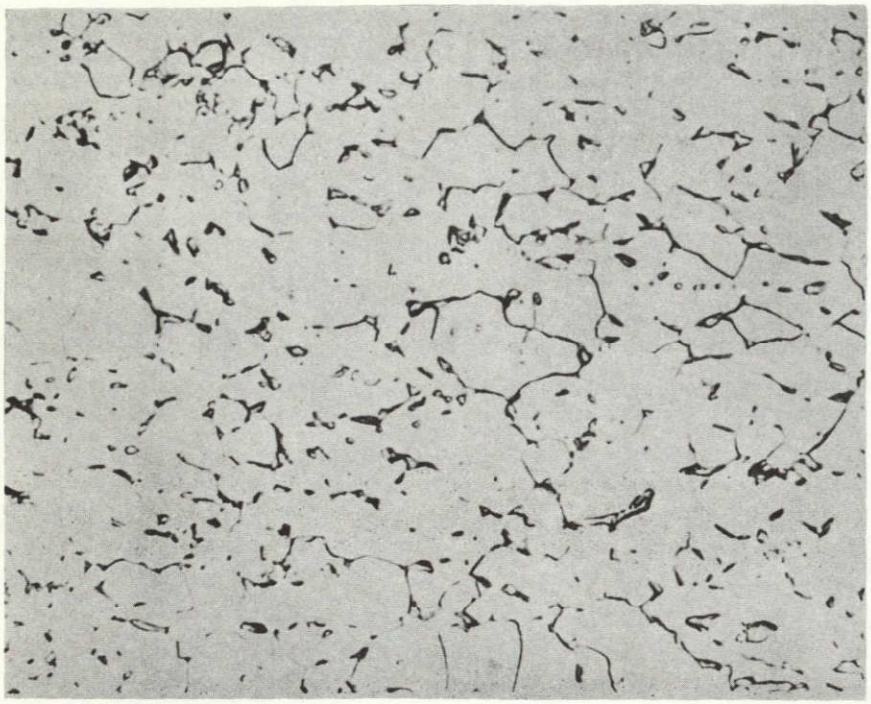

Fig. 9 - Microstructure of Annealed Ti-6Al-4V Sheet (750 X).
Etch: 1½% HF, 3½% HNO_3, 95% H_2O

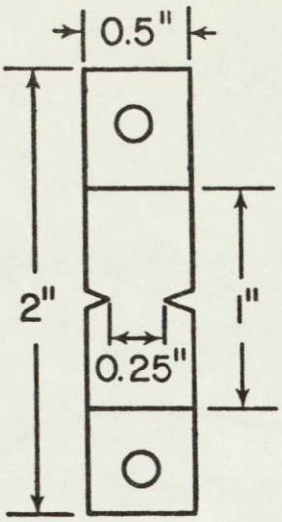

a

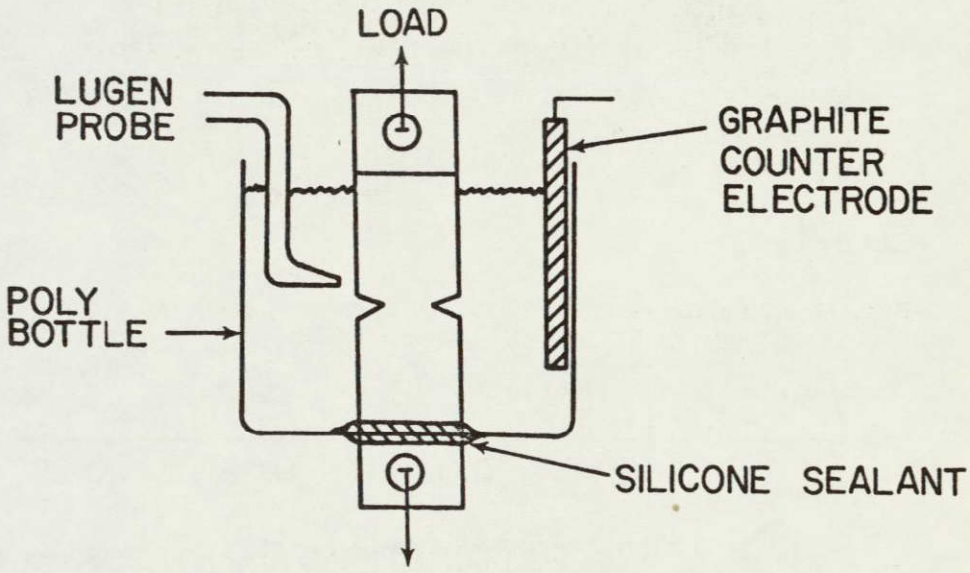

b

Fig. 10 - a. Double Notch Specimens
b. Cell for Charging while Stressing

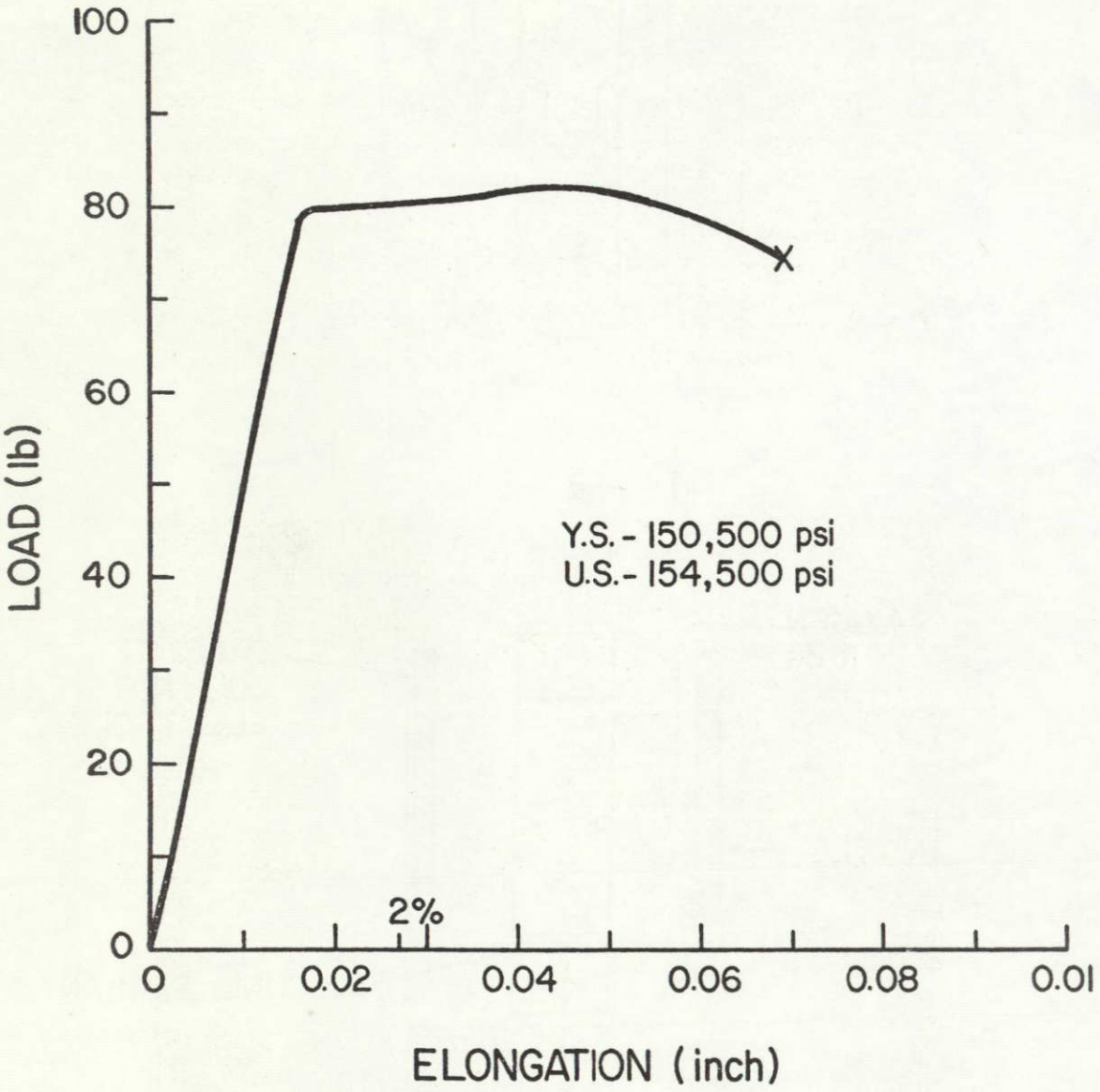

Fig. 11 - Load - Elongation Curve for an Annealed Transverse Ti-6Al-4V Specimen

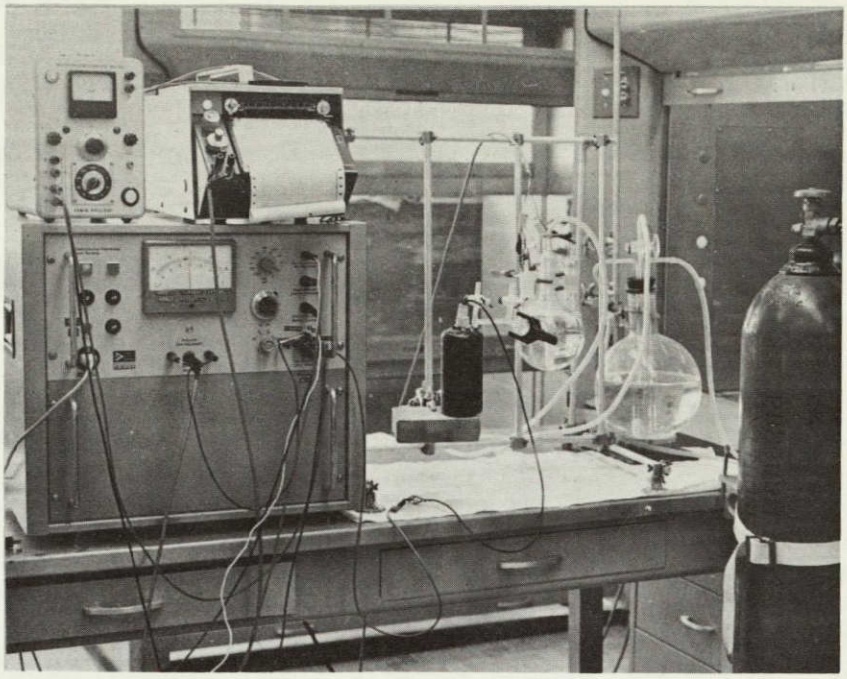

a

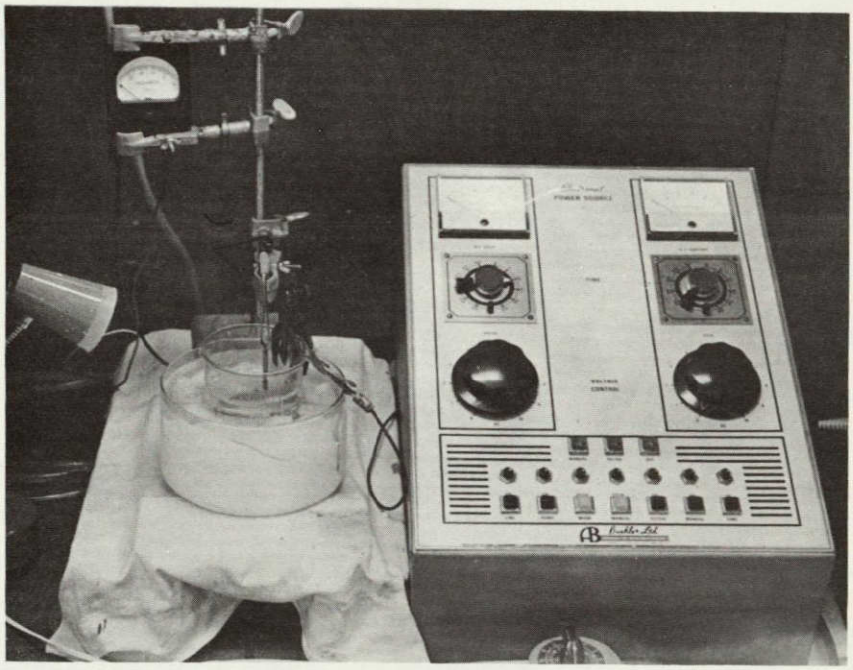

d

Fig. 12 - a. Experimental Set-up for Electrolytic Charging.
b. Set-up for Electrolytic Polishing of Foil Specimens.

The specimens which were not activated were the polished specimens and the stressed specimens. For these specimens the desired potential was set and the current was monitored with a Brown potentiometer recorder.

NEODYMIUM HYDROGEN DETECTOR

The neodymium hydrogen detector is a relatively new technique which was first reported by Toy and Phillips[64]. The experimental technique employed in this investigation is based upon their original technique.

The specimens were first electrolytically charged with hydrogen and electropolished by the methods previously described. The specimens were then etched with a solution of 3-1/2 parts nitric acid, 1-1/2 parts hydrofluoric acid and 95 parts water. Next, the specimens were placed in a Kinney Model SC3 vacuum evaporator and 0.1g of neodymium was vapor deposited. The vacuum in the evaporator was 10^{-5} mmHg. The specimen to source distance was three inches. Using a Zeiss surface interferometer, the neodymium film was determined to be approximately 3000 Å thick. This film is optically transparent.

The neodymium was obtained from Research Chemicals Corporation and the chemical analysis is given in Table 3. The neodymium was supplied in the form of chips submersed in mineral oil to protect them from oxidation. This mineral oil must be removed by thoroughly washing the chips in a solvent such as acetone.

Table 3. Analysis of Commercial Neodymium

Impurity	wt.%
Y	0.01
Ca	0.05
Mg	0.005
Si	0.001
Fe	0.005
Pr	0.02
La	0.01
Ce	0.02

After depositing the neodymium the specimens were heated to 300° in the evaporator at 10^{-5} mmHg for one hour. The temperature was monitored from a chromel-alumel thermocouple which was spot welded to a washer which was secured to the heating stage. The heating stage is simply a block of aluminum with two horizontal parallel holes through which quartz tubes are placed. Nichrome wire heating coils are inside these tubes. The power is obtained by tapping from the evaporator leads which are controlled by a variable rheostat.

The specimens were then examined optically. The neodymium reacts with the hydrogen which diffuses from the metal to form a hydride (NdH_2). These hydride reaction nodules appear black in the optical microscope and, as such, map the distribution of hydrogen in the specimen.

FOIL PREPARATION

Foils for transmission electron microscopy were prepared by a two step process. The first step was a chemical thinning using a solution of 75 parts of water, 22 parts nitric acid and 3 parts hydrofluoric acid. The chemical thinning was accomplished by immersion of the specimen in the solution contained in a polyvinyl beaker in an ultrasonic cleaner. This thinning technique removes approximately 0.001 inch per minute and, as such, greatly reduces the time required for a sample preparation. The 0.005-inch sheet specimens are thinned by this technique to 0.001 inch. Specimens may be thinned to foil thickness in this manner but the resulting foils have been found inferior to electropolished foils.

The second step is to electropolish the 0.001-inch thick specimen to foil thickness using the "window" technique (see Appendix B). A Buehler Electromet power source was used to supply the required 25 V dc. The electrolyte used was a mixture of 390 cc methyl alcohol, 350 cc 1 butanol and 60 cc perchloric acid. The electrolyte was maintained at -30°C in a bath of dry ice in acetone. During polishing, the electrolyte was stirred with a magnetic stirrer. This set-up is shown in Fig. 12b.

It was determined that best results were obtained when the current density was maintained between 2 and 4 mA/cm^2. A larger current density gives pitting and a smaller current density gives etching. Between 15 and 35 V dc were required to maintain this current density.

ELECTRON TRANSMISSION MICROSCOPY

Electron transmission microscopy studies of both hydrogen charged and uncharged specimens of Ti-6Al-4V were conducted on a Phillips 300 electron microscope equipped with a goniometer stage. Most examinations were conducted using an accelerating voltage of 10 kV. The foils examined in this investigation were normally at least 2500 Å thick.

IV. RESULTS

ELECTROCHEMICAL DEPENDENCE OF STRESS CORROSION CRACKING

Initial experiments on the Ti-8Al-1Mo-1V alloy, which is an alpha-beta alloy of similar microstructure to the Ti-6Al-4V alloy, established

the electrochemical dependence of the stress corrosion phenomenon. Figure 13 shows this electrochemical dependence of the stress at failure for three point bend specimens. These specimens were broken in 0.6M KBr and the potential was controlled potentiostatically. In addition, these specimens were given a heat treatment to increase their susceptibility. The heat treatment consisted of a solutionizing treatment at 1950°F for one hour, furnace cooled to 1200°F for two hours and water quenched. This treatment gives a microstructure of plate-like alpha which is particularly susceptible to stress corrosion cracking. The load was applied incrementally with 0.1 kg being added every two minutes. The load at failure was then used to calculate the outer fiber stress from the formula[65]

$$S = \frac{3a\ell}{bh^2}$$

where

a = distance between outer supports (in.)
ℓ = load at failure (lb)
h = thickness (in.)
b = specimen width (in.)

Figure 13 demonstrates that there is an electrochemical dependence of failure stress and that there are two regions of susceptibility. These two regions were referred to by Chen[40] as the "stress corrosion region" and the "region of halide-ion attack". The "stress corrosion region" occurs at cathodic potentials between approximately -250 mV and -900 mV (SCE) and the "halide-ion attack region" occurs at potentials above +200 mV (SCE). Figure 14 shows the fracture appearance of a specimen broken at -500 mV (SCE) which is in the region of "stress corrosion". The fracture appears primarily cleavage in nature. Figure 15 shows the fracture appearance of a specimen broken at +850 mV (SCE) which is in the region of "halide-ion attack". This fracture has the appearance of a typical ductile or shear mode of failure.

POLARIZATION BEHAVIOR

The polarization behavior for the annealed Ti-6Al-4V alloy in deaerated 5N HCl was determined potentiostatically and is shown in Fig. 16. The corrosion potential, -650 ± 50 mV (SCE) is quite active in this environment. An oxide coated specimen immersed in this environment will exhibit an initial corrosion potential of approximately +100 mV (SCE). However, the passivating oxide is apparently unstable in the 5N HCl and the potential gradually shifts to the active corrosion potential. Ti-6Al-4V exhibits active-passive behavior in this environment as well as transpassivity due to the chloride ion.

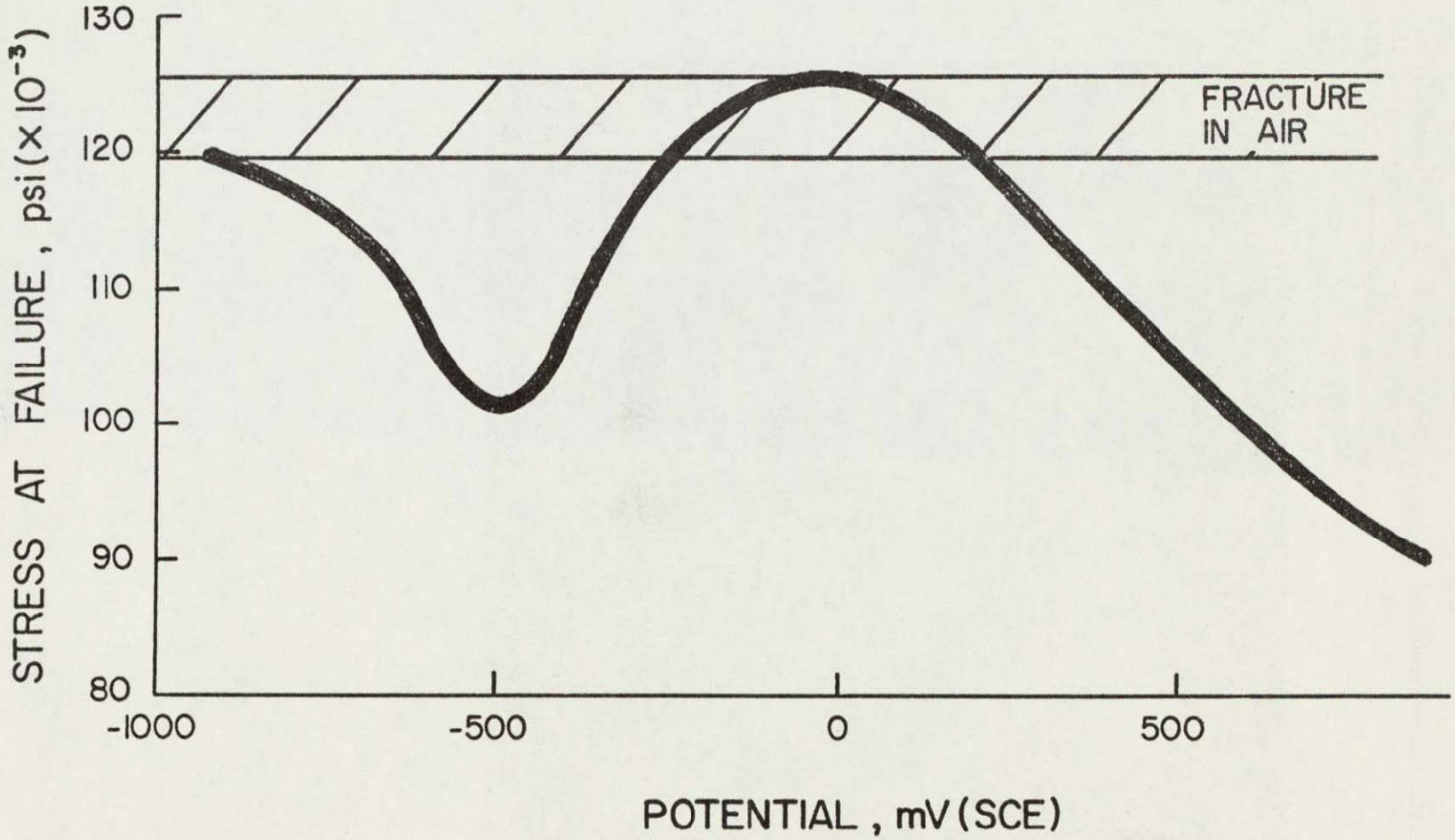

Fig. 13 - Electrochemical Dependence of Failure Stress on Applied Potential for Three - Point Bend Specimens in 0.6M KBr

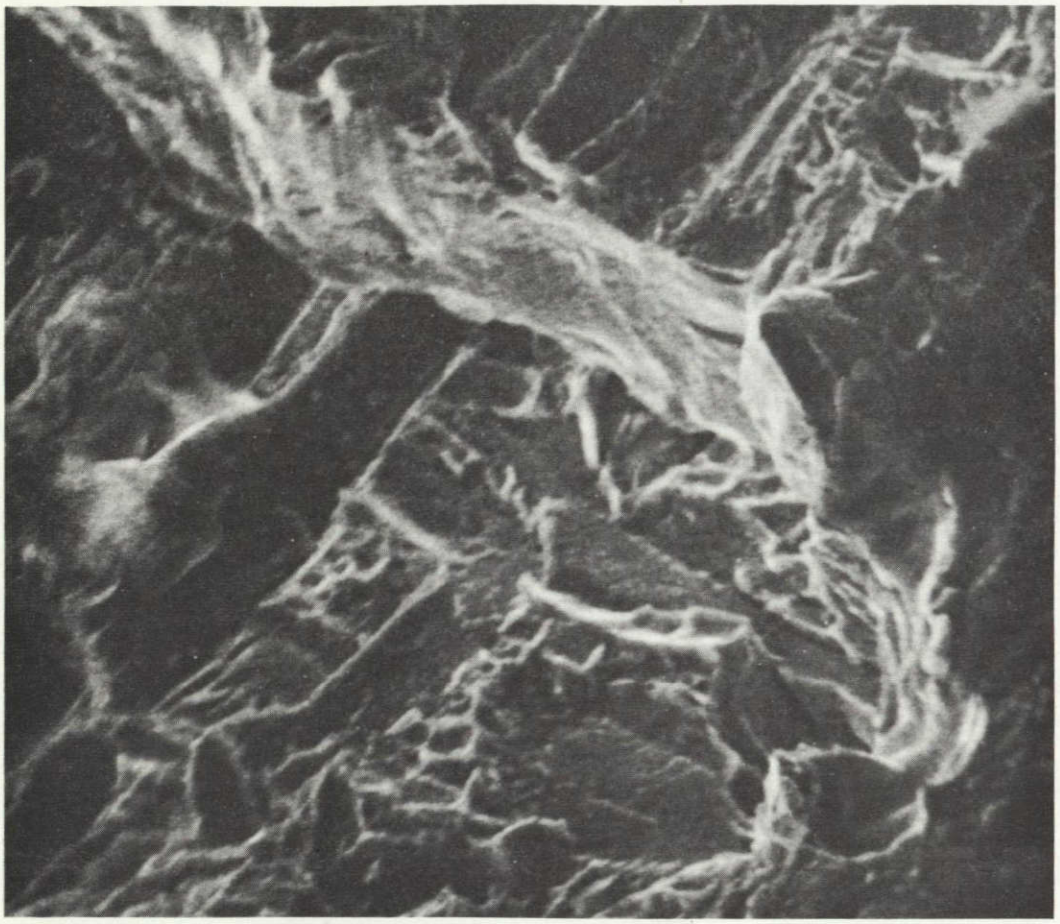

Fig. 14 - Fracture Appearance of Ti-8Al-1Mo-1V Sheet Specimen Broken in 0.6M KBr at -500 mV (SCE). SEM (2000 X)

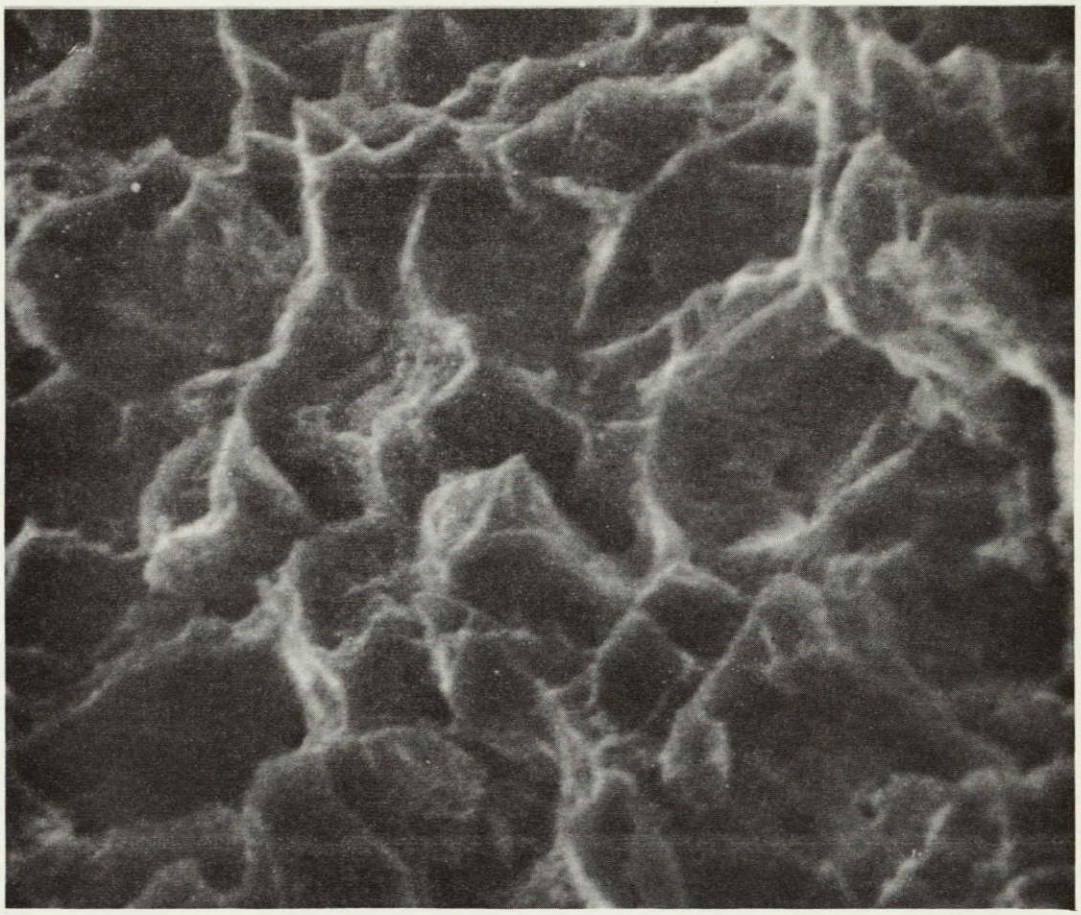

Fig. 15 - Fracture Appearance of Ti-8Al-1Mo-1V Specimen Broken in 0.6M KBr at +850 mV (SCE). SEM (2000 X)

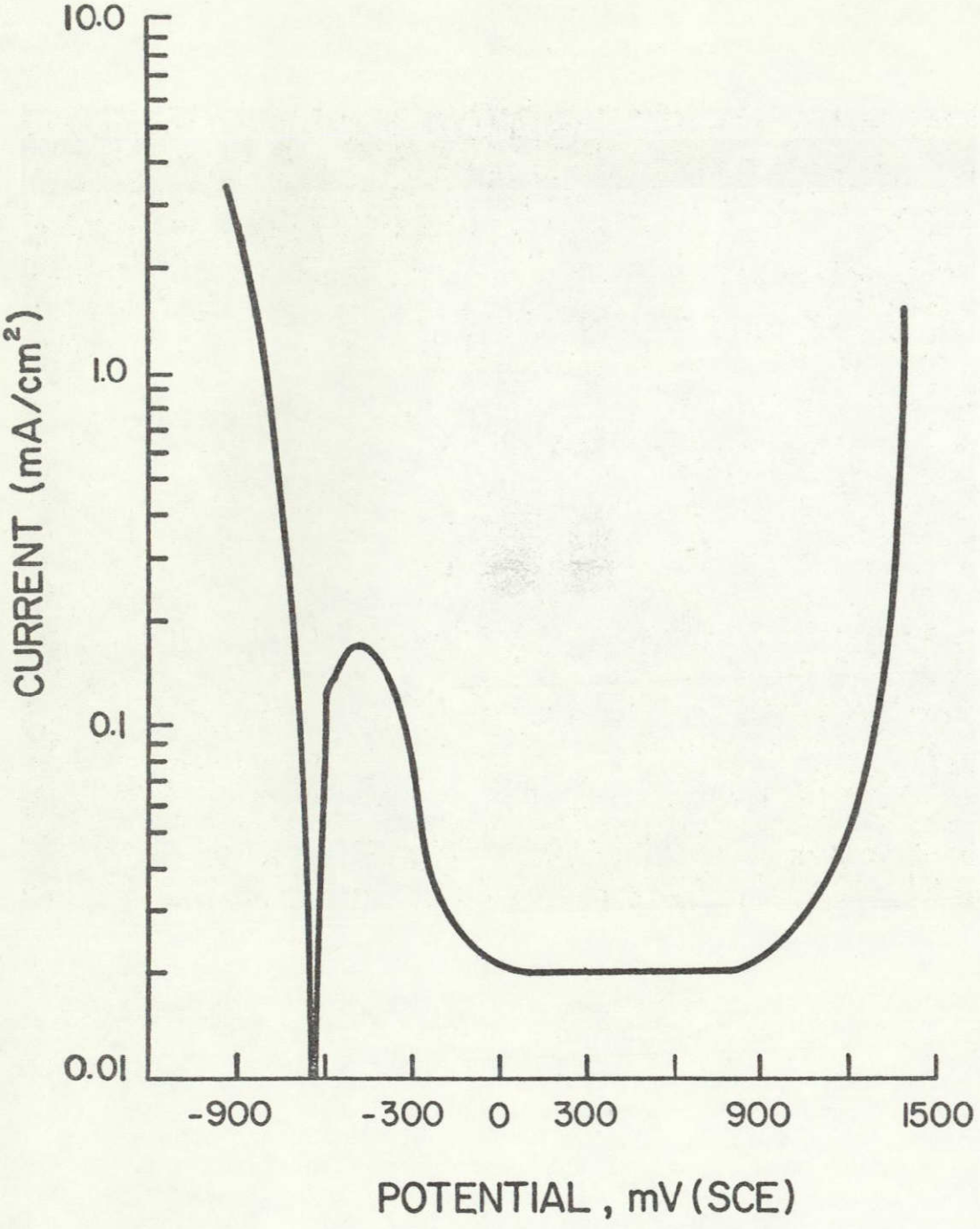

Fig. 16 - Polarization Behavior of Annealed Ti-6Al-4V in Deaerated 5N HCl at Room Temperature

HYDROGEN CHARGING EXPERIMENTS

Cathodic charging of hydrogen was undertaken to determine the behavior introduced at room temperature. All charging experiments were performed on the annealed Ti-6Al-4V sheet material in the 5N HCl environment. Two potentials, -742 mV and -850 mV (SCE) were of primary interest in this investigation. Specimens were charged at these potentials for varying lengths of time up to four hours and the hydrogen concentrations were determined by vacuum fusion analysis. Figure 17 shows the results of these analyses.

The current density corresponding to these potentials varies throughout the time during which the specimens are being charged. For example, at -850 mV, the initial net current density is normally about -0.5 mA/cm^2 but this value increases continuously until, after four hours, the current density is approximately -0.2 mA/cm^2. A plot of current density vs. time is given in Fig. 18 for a typical charging experiment at -850 mV in 5N HCl.

The neodymium hydrogen detector method was used in conjunction with the above hydrogen determinations to determine the location of the hydrogen in the alloys microstructure. Figures 19, 20, 21 and 22 show the results of this technique. Figure 19 shows the microstructure of an annealed Ti-6Al-4V specimen after charging at -742 mV (SCE) for one-half hour, electropolishing, etching and deposition of 3000 Å of neodymium. This illustrates the transparency of the neodymium film to optical microscopy. Figure 20a shows the appearance of this same specimen after heating in vacuum at 300°F for one hour. In this case, the hydrogen that diffused out of the alloy, reacted with the Nd film to form a dark NdH_2 compound in the film on the surface. This micrograph shows that some alpha grains appear quite dark and others light with graduations in between. Individual NdH_2 reaction sites (dark spots) may be seen in some grains. Figure 20b shows an alpha grain containing several pools of beta. This is a higher magnification micrograph of another region of the same specimen as seen in Fig. 8B. Figure 21 shows another specimen which was charged at the same potential for one hour. In this case, the micrograph appears generally darker over the entire surface. Careful examination, particularly in the upper-left hand quadrant, reveals light areas about the beta regions. This would indicate that the hydrogen in these regions had diffused to either the beta grains or the alpha-beta interface. Figure 22 shows the appearance of a specimen charged for four hours at -742 mV. This specimen has the Nd film on the surface and has been heated to 300°F for one hour the same as the other specimens. In this case, there is little evidence of any NdH_2 reaction sites on the alpha grains except in the regions about the beta grains. In addition, some hydride markings are barely visible in some of the alpha grains.

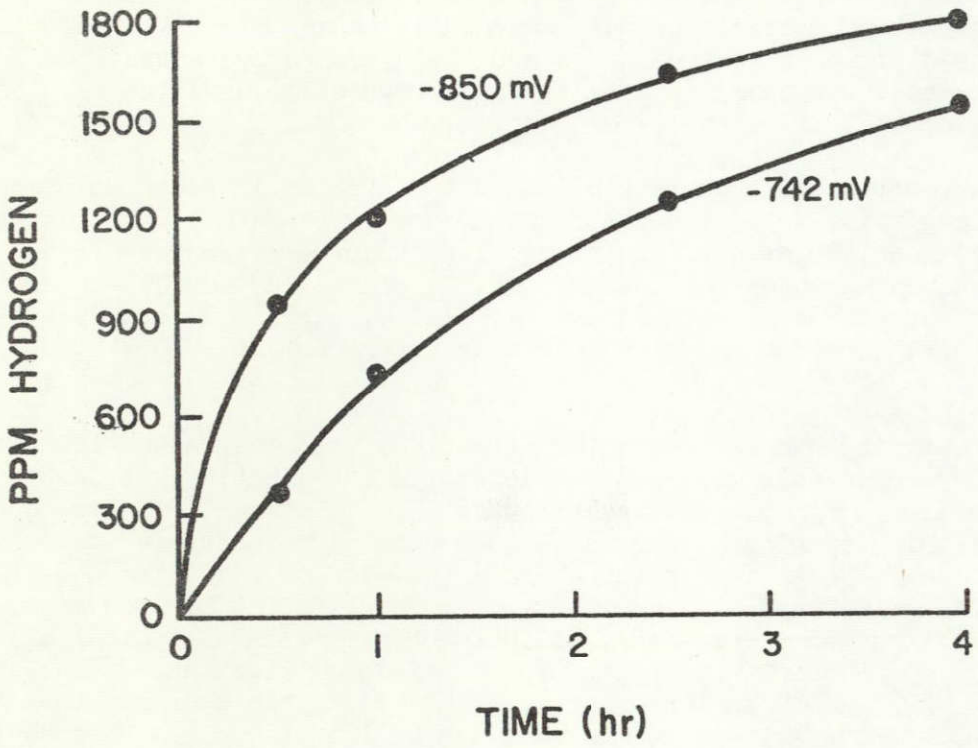

Fig. 17 - Hydrogen Concentration as a Function of Electrochemical Potential and Time in Ti-6Al-4V alloy at Room Temperature

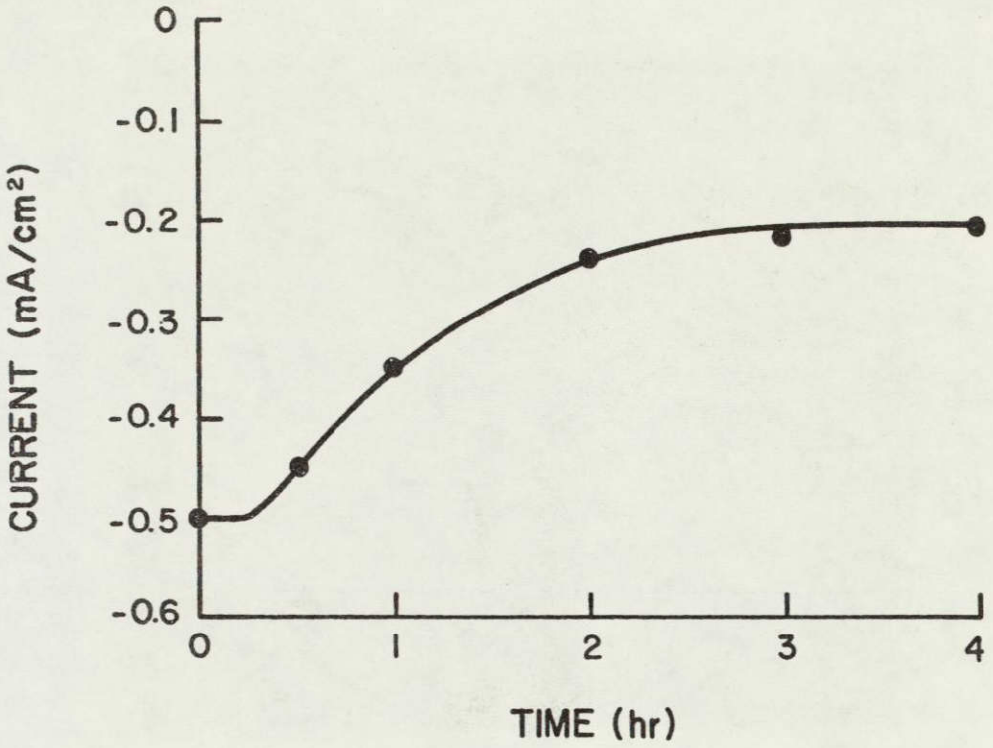

Fig. 18 - Current Density as a Function of Time for a Typical Potentiostatic Hydrogen Charging Experiment for Ti-6Al-4V in 5N HCl

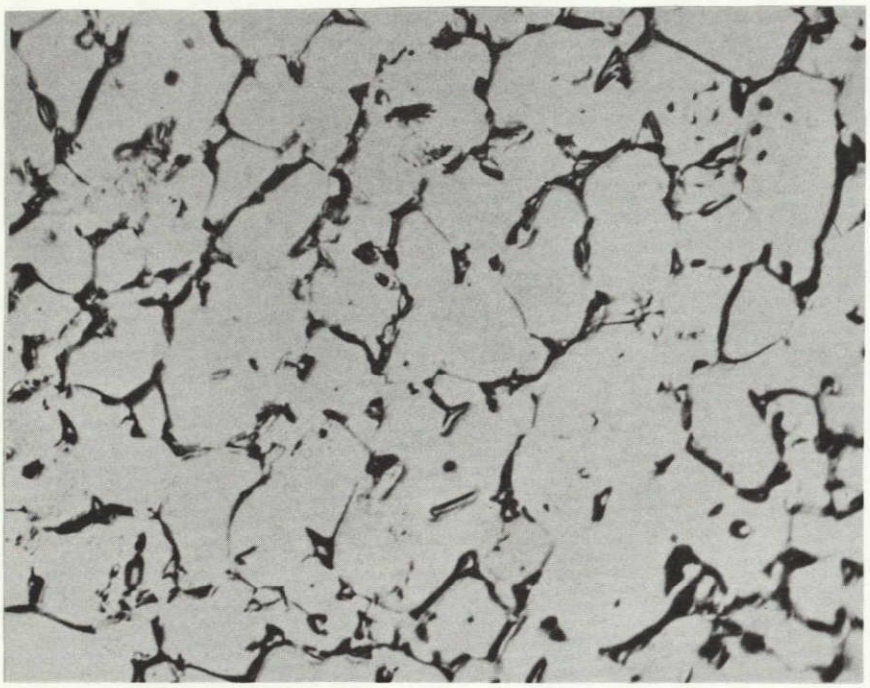

Fig. 19 - Ti-6Al-4V Specimen Charged at -742 mV (SCE) for $\frac{1}{2}$ Hour. Specimen Has Thin Film of Nd on Surface. (1200 X)
Etch: $1\frac{1}{2}\%$ HF, $3\frac{1}{2}\%$ HNO_3, 95% H_2O

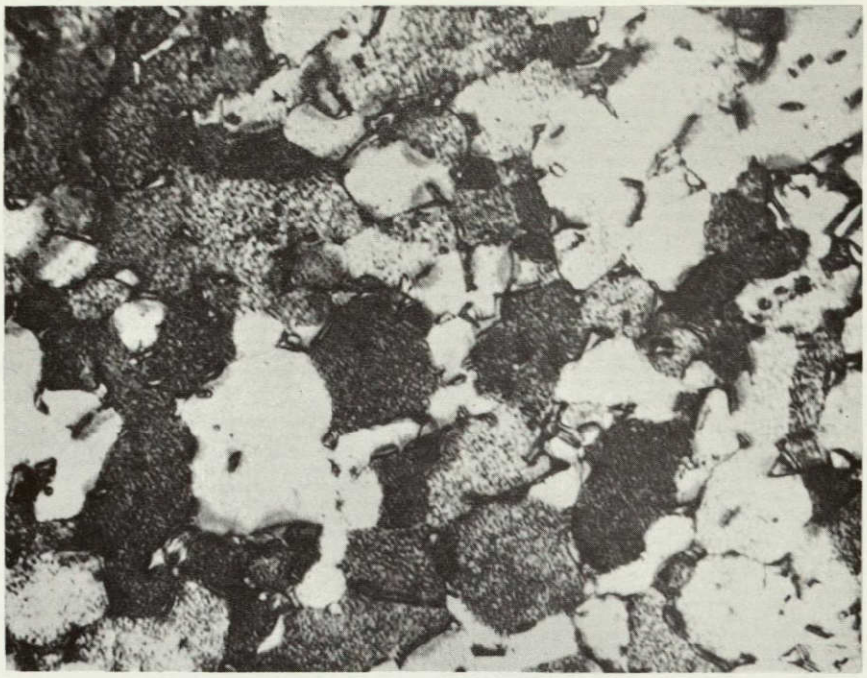

a

b

Fig. 20 - a. Nd Specimen Showing Hydrogen Distribution after Charging at -742 mV (SCE) for $\frac{1}{2}$ Hour. (1000 X)
b. Same (2500 X)

Fig. 21 - Nd Specimen Showing Distribution of Hydrogen after Charging at -742 mV (SCE) for 1 Hour. (1000 X)

Fig. 22 - Nd Specimen Showing Hydrogen Distribution after Charging at -742 mV (SCE) for 4 Hours. (1000 X)

From the neodymium coated specimens the following general observations can be made:

1. Hydrogen is absorbed evenly throughout each individual alpha grain but not throughout the microstructure as evidenced by the fact that some grains appear light and some appear dark.

2. With this technique it is difficult to observe any hydrogen segregation at the alpha-beta interfaces or in the beta grains (see Fig. 20B). This will be discussed later.

3. This technique does not reveal any appreciable partitioning of hydrogen at the alpha-alpha grain boundaries.

4. This technique would be better suited for larger grained specimens.

It was observed in this investigation that hydrogen will segregate to regions of tension. Specimens bent elastically retained their curvature after charging for relatively short periods of time. Also, it was observed that mechanically polished surfaces absorbed hydrogen at much faster rates than unpolished surfaces but this effect was not noted on electropolished surfaces. As an example, a sheet specimen mechanically polished on one surface and charged at -850 mV for two hours in an unstressed condition exhibited considerable curvature after removal from the cell. This curvature was such that the hydrogen, which expands the lattice, was segregated in the polished half of the specimen.

As a consequence of the previously mentioned cathodic charging experiments, it was noted that after charging, the polished surface was destroyed and pits appeared. In order to investigate this phenomenon, specimens were metallographically polished (see Appendix A) and then held at cathodic potentials in 5N HCl for varying times. After this cathodic treatment, the specimens were examined optically and in the scanning electron microscope (SEM). Figure 23 shows the appearance of a polished surface after exposure at -742 mV (SCE) for one-half hour in 5N HCl. Note the initial attack is primarily concentrated in the beta regions. Figure 24a is an SEM photograph of the surface of a specimen held at -742 mV (SCE) for four hours. Figure 24b shows the same surface at a higher magnification. The blocky particles which appear in many of these photographs are particles of diamond polishing compound which were not removed by ultrasonic cleaning. In these figures it can be seen that the beta regions are more severely attacked and also that certain alpha grains appear to have undergone a pitting type of attack. This is illustrated better in Fig. 25 which shows an alpha grain which has many of these micro-pits which resemble tunnels.

Fig. 23 - Appearance of Ti-6Al-4V Surface after $\frac{1}{2}$ Hour Exposure at -742 mV (SCE) in 5N HCl. SEM (2000 X)

a

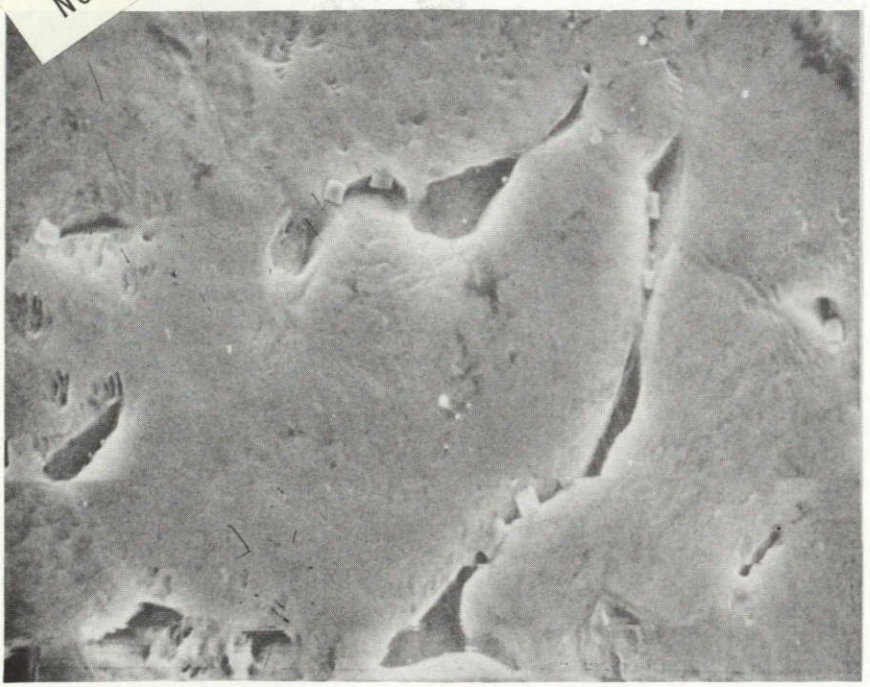

b

Fig. 24 - Surface of Ti-7Al-4V after Exposure at -742 mV (SCE) for 4 Hours in 5N HCl. SEM a) (500 X) b) (2000 X)

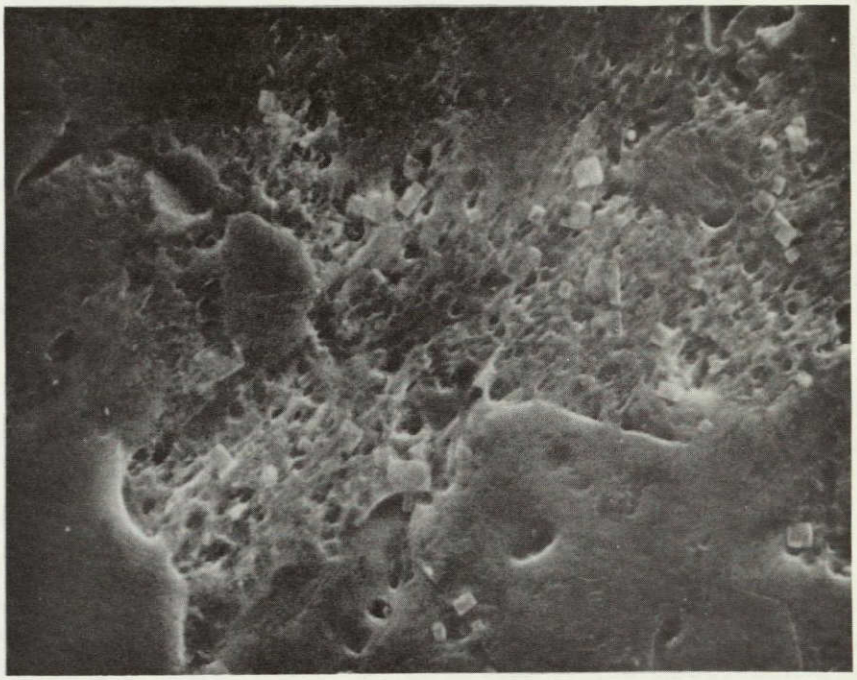

Fig. 25 - Attack of Alpha Grains after Exposure for 4 Hours at -742 mV (SCE) in 5N HCl. SEM (2000 X)

Figures 26a and 26b show the surface appearance after exposure at -500 mV for one hour. In this case the attack of the beta regions appears less severe with most of the attack occurring on the alpha grains. Note, also, numerous small pits which appear quite deep. Figures 27a and 27b show the surface appearance after exposure at the corrosion potential (no applied potential) for 10 hours. Hydrides can be seen in the large alpha grains. These hydrides appear white in the figure and seem associated with the alpha-beta and alpha-alpha grain boundaries. Figure 28 shows the appearance of the surface after exposure at -1500 mV for one hour. The surface, in this case, appears more uniformly attacked all over.

Figures 29a and 29b show the appearance of the tensile surface of a specimen which was stressed to approximately the yield stress by bending during exposure at -742 mV (SCE) for two hours. These figures should be compared with Figs. 23 and 24 which show the surface of an unstressed specimen exposed at this same potential. Note that in the unstressed specimen the beta grains are attacked, whereas the beta grains in the stressed specimens are not. The attack on the stressed specimens appears concentrated at the alpha-beta boundaries. In addition, light colored porous regions are formed in the alpha grains adjacent to these boundaries. The attack in these regions appears to be crystallographic in nature as shown in Fig. 16b. This attack of the alpha is not similar in appearance to the attack shown in Fig. 25. Rather, it is more similiar to the attack of the alpha phase at -500 mV (SCE) shown in Fig. 26b.

Double notched thin sheet specimens of Ti-6Al-4V alloy were used to determine the effect of a tensile stress upon the behavior of the pick-up of hydrogen in this alloy at cathodic potentials. The dimensions of these specimens were given previously. Generally, this technique was found to be unsatisfactory from the standpoint of good reproducibility and the specimen did not lend itself to satisfactory optical metallography owing to the irregular nature of the surface after cathodic charging. Even though few photographs worthy of publication were obtained, the following general observations were made:

1. Cracking appears associated with a localized electrochemical attack in the vicinity of the notch tip. This attack is in the form of pits. This is shown in Figs. 30, 31 and 32. Note in Fig. 33 that the beta phase has been etched.

2. Plastic deformation generally precedes failure. Roughening of the surface occurs and slip lines can be seen in some alpha grains. Figure 34 shows this behavior. This specimen was not exposed to the 5N HCl at cathodic potentials long enough to get pitting.

3. Hydrides are found in the notch tip region before they are found in the bulk of the specimen.

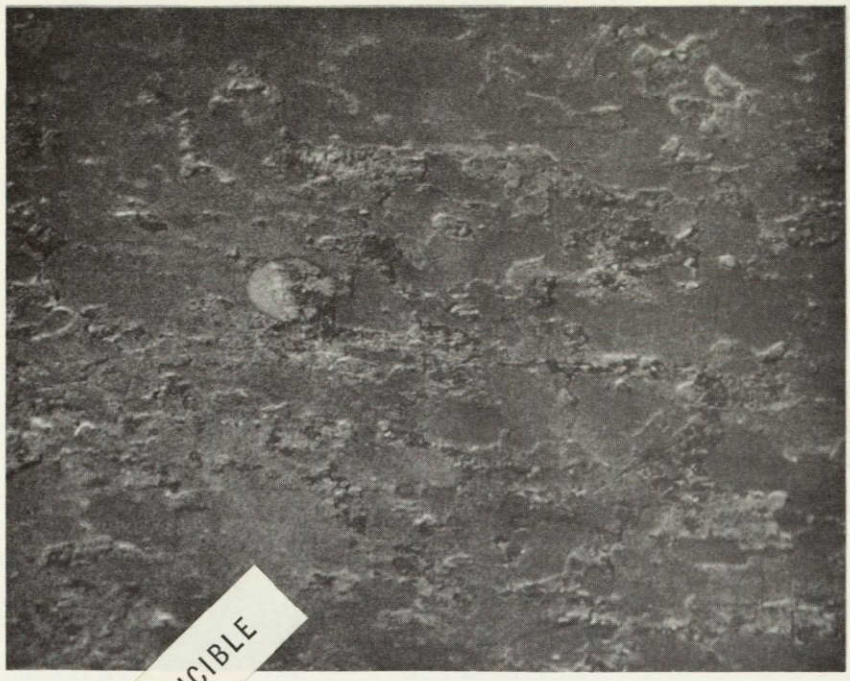

a

b

Fig. 26 - Surface Appearance after Exposure at -500 mV (SCE) for One Hour in 5N HCl. SEM a) (500 X) b) (2000 X)

a

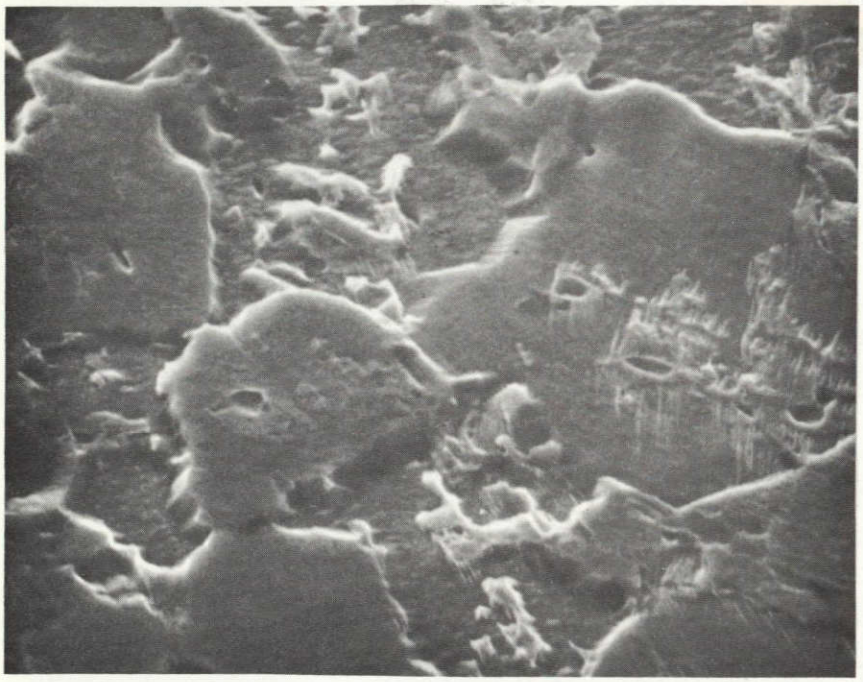

b

Fig. 27 - Surface Appearance after Exposure for 10 Hours at the Corrosion Potential in 5N HCl. SEM a) (500 X) b) (2000 X)

82

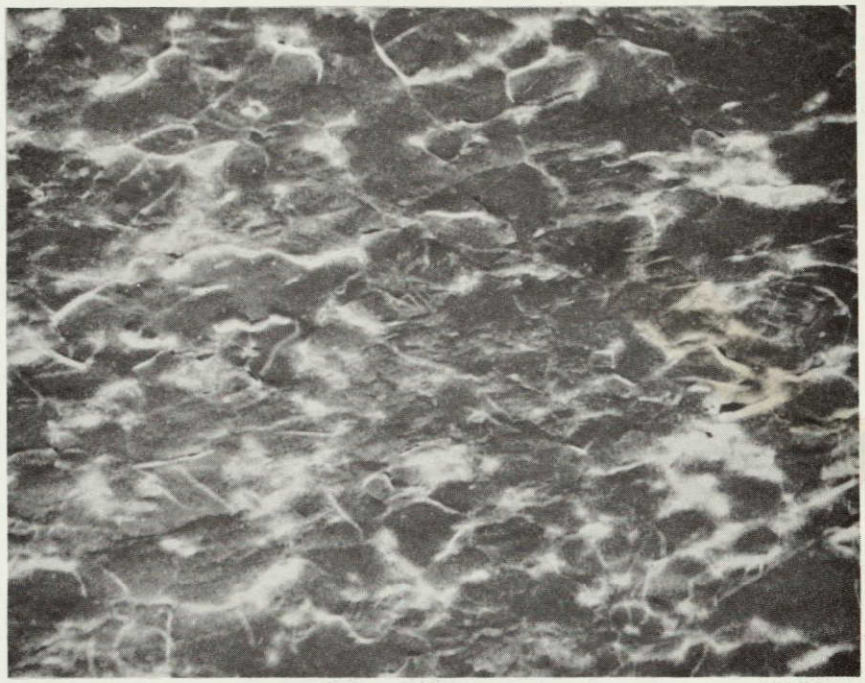

Fig. 28 - Surface Appearance after Exposure for 4 Hours at -1500 mV (SCE) in 5N HCl. SEM (500 X)

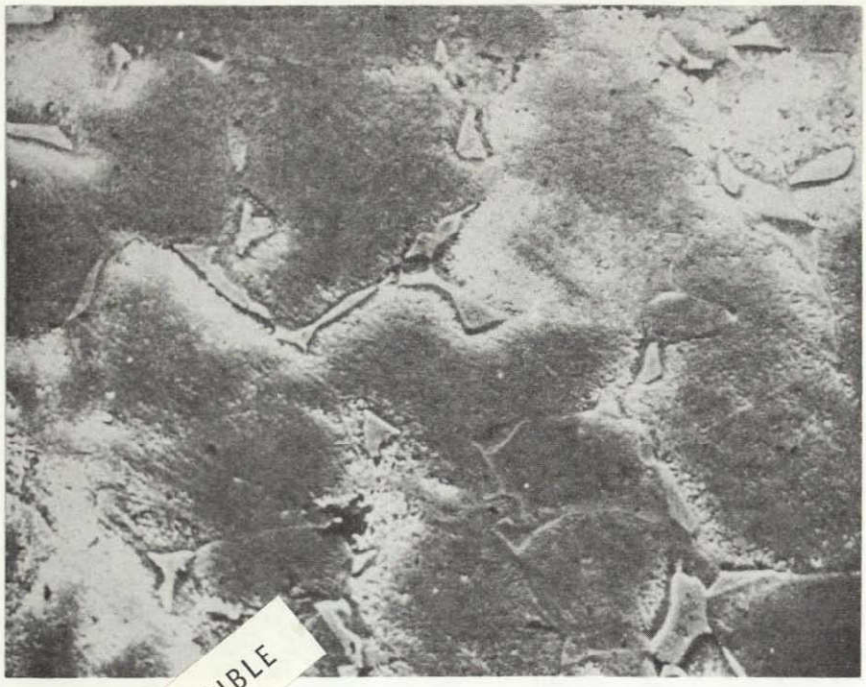

a

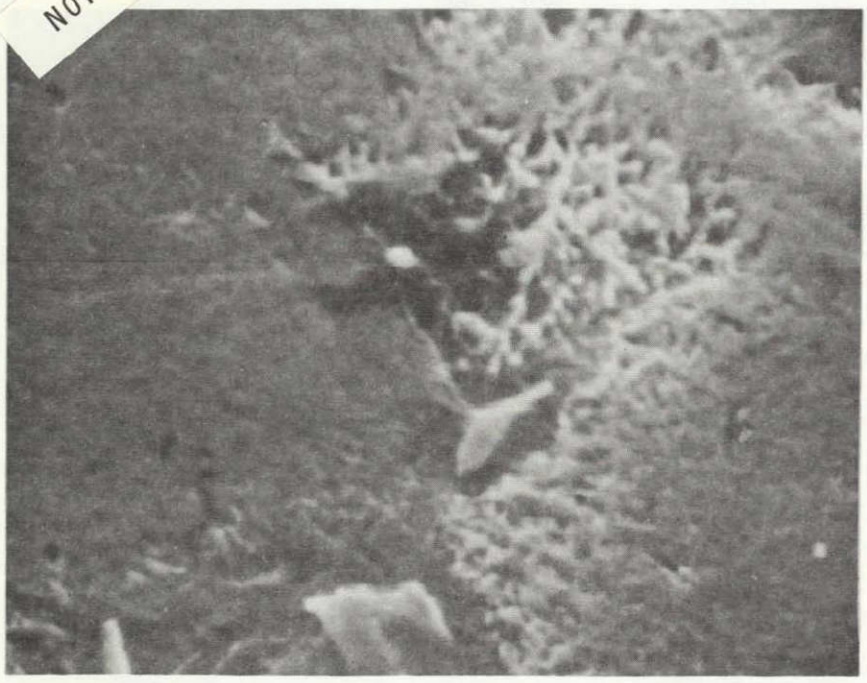

b

Fig. 29 - Appearance of Surface of Specimen Stressed to 80% of the Yield During Exposure at -742 mV (SCE) for 2 Hours in 5N HCl. SEM a) (2000 X) b) (10,000 X)

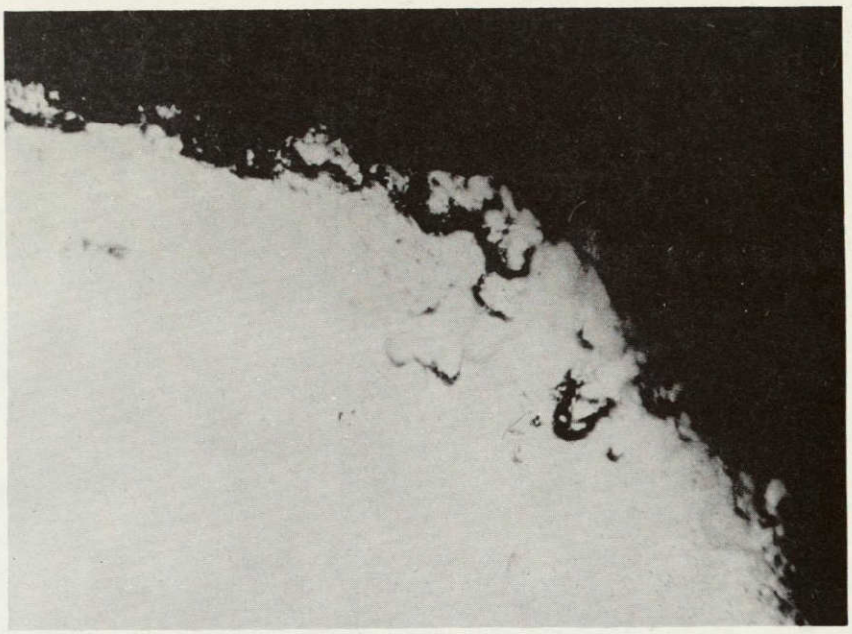

a

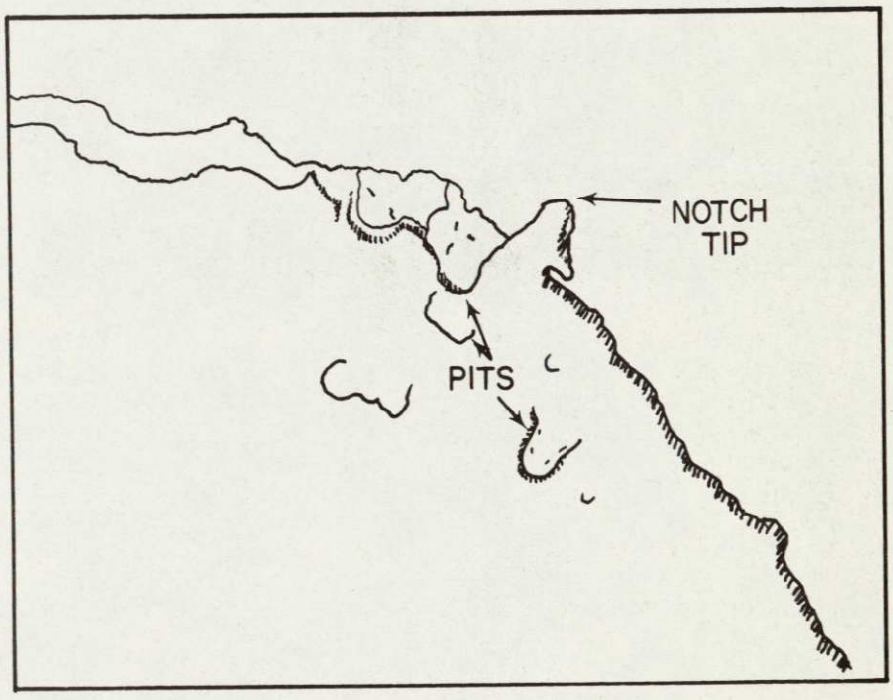

b

Fig. 30 - a. Pits Associated with Notch Tip Region on Specimen Broken at -850 mV in $\frac{1}{2}$ Hour in 5N HCL. Loaded to 95% of Failure Stress. Oblique Illumination (300 X)
b. Schematic Representation of a.

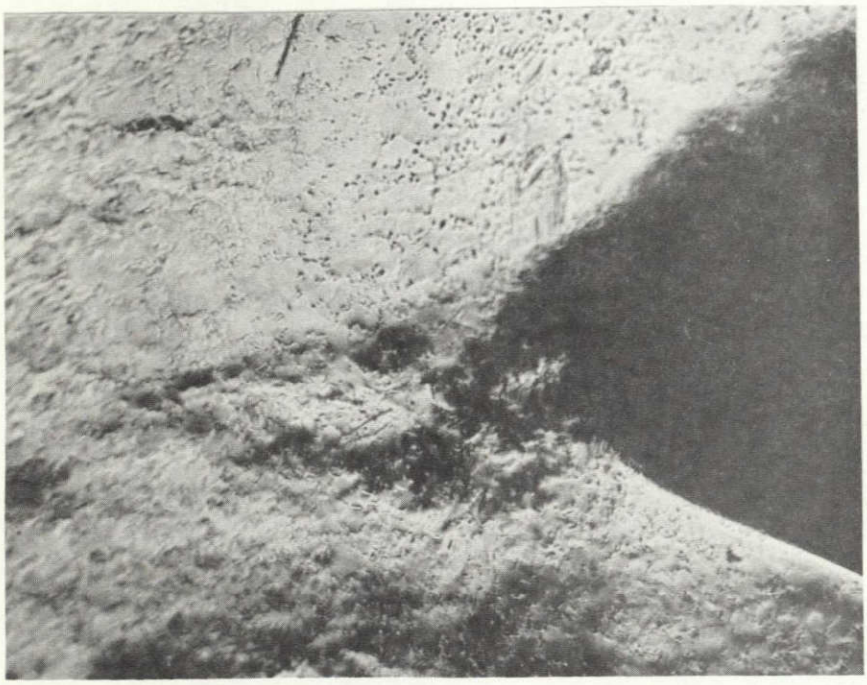

Fig. 31 - Notch Tip Region of Specimen Exposed to 5N HCl at -850 mV for $\frac{1}{2}$ Hour. Loaded to 50% of Failure Stress. Oblique Illumination (300 X)

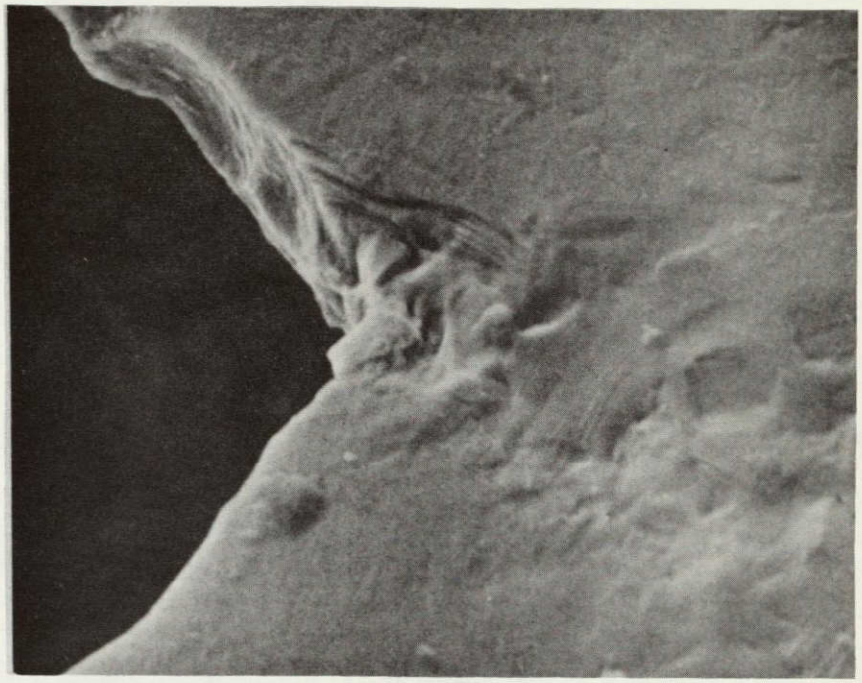

Fig. 32 - Notch Tip Region of Specimen Loaded to 95% of Fracture Stress and Exposed at -850 mV (SCE) for One minute. SEM (500 X)

a

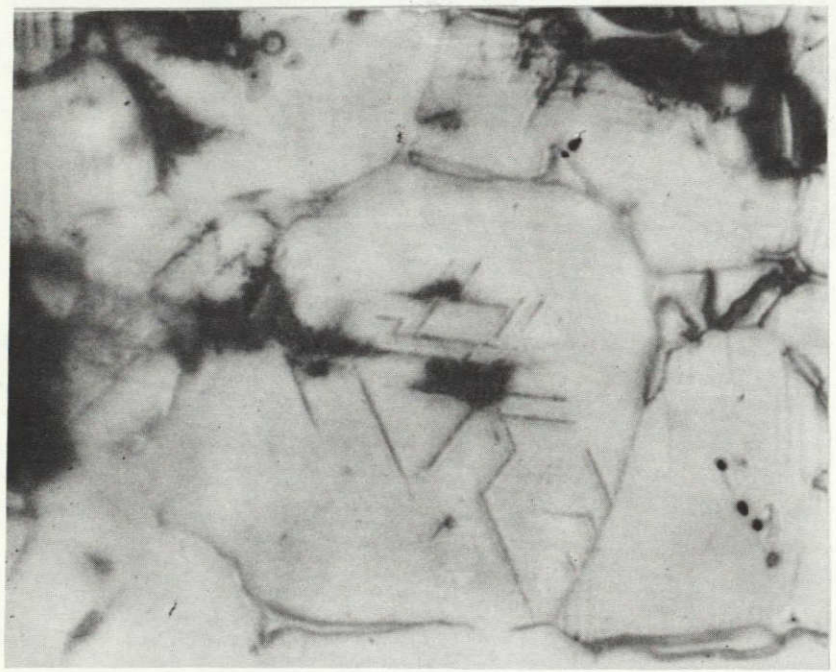

b

Fig. 33 - Appearance of Hydrides in Ti-6Al-4V after 2 Hours at -850 mV in 5N HCl. (2500 X). Etch: 1½% HF, 3½% HNO_3

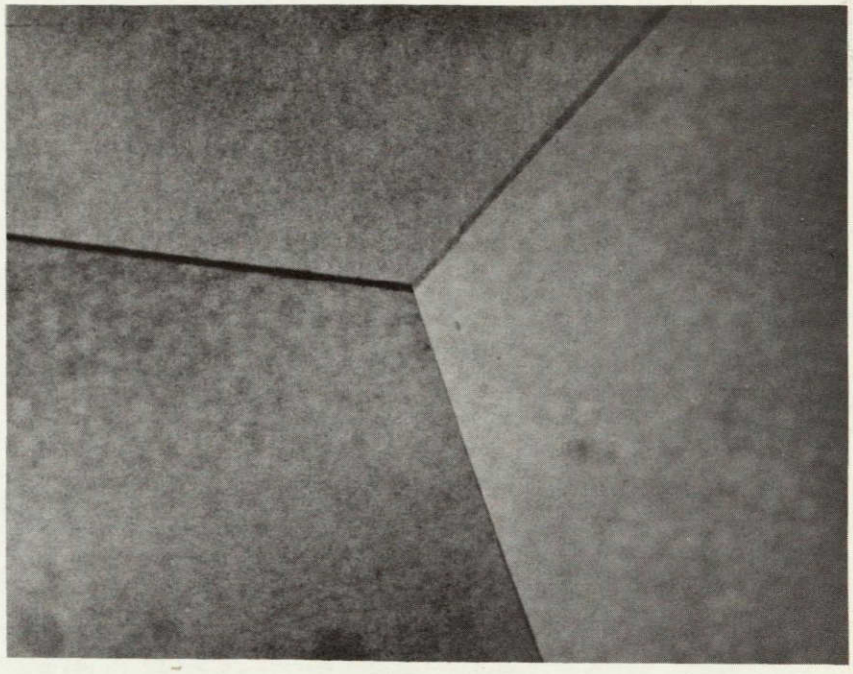

Fig. 34 - Transmission Micrograph Showing Typical Strain Free Microstructure of Annealed Ti-6Al-4V. (60,000 X)

4. Using the neodymium hydrogen detector, the hydrogen concentration in the notch tip region appears greater than in the bulk of the specimen.

HYDRIDE PRECIPITATION

Hydride precipitation was studied by x-ray analysis, optical metallography and electron transmission. X-ray analysis on the GE-XRD diffractometer was used in the initial stages of this investigation; however, this technique was found to be inadequate. It was found that a relatively high volume fraction of the hydride phase was required before a recognizable pattern for this phase could be detected. As an example, specimens placed in 5N HCl at their corrosion potential required 180 hours in this environment before the hydride pattern could be detected. Whereas, optical and electron transmission microscopy revealed the presence of the hydride phase after only 20 hours in the same environment. This difficulty with x-ray diffraction techniques, it was learned later, was experienced by other investigators[66] and is included here for completeness.

Optical metallography was conducted on specimens charged with hydrogen in the 5N HCl environment at the previously mentioned cathodic potentials of interest. Generally it was noted that longer charging times were required before hydrides were observable in the optical microscope than in the electron microscope. This is most likely due to the size (width) of the hydride plate required at the lower magnifications used in optical metallography. Examples of the appearance of the hydride phase in the optical microscope are shown in Figs. 33a and 33b. From these micrographs it appears that the hydride phase nucleates primarily at the alpha-beta boundaries, but some can be seen originating at alpha-alpha boundaries as in Fig. 33b.

ELECTRON TRANSMISSION MICROSCOPY

Transmission electron microscopy was performed on the annealed Ti-6Al-4V alloy and on specimens of this same alloy which were given cathodic treatments in 5N HCl. Figures 34, 35, 36 and 37 show the annealed microstructures prior to any cathodic treatment. Generally, the microstructure consists of large strain-free alpha grains as would be expected in annealed material. The beta grains are much smaller and are typically found at alpha grain boundaries although small spherical pools of beta phase may be found in some alpha grains. Figure 34 is a typical triple-point or junction between three alpha grains. Figure 35 shows a beta grain lying on an alpha grain boundary. The contrast along the alpha-beta interface lies in the alpha grain but the origin of this contrast could not be determined. The regions of beta generally polish faster than the alpha grains which accounts for the fact that the beta appears white in Fig. 35. Figure 36 shows the appearance of one small

Fig. 35 - Appearance of Elongated Beta Lying in Alpha Grain Boundary. TEM (30,000 X)

Fig. 36 - Appearance of Subgrains in Ti-6Al-4V after Anneal at 1500°F for 18 Hours. TEM (21,000 X)

region where recrystallization was incomplete. These regions of subgrains are often seen in the annealed microstructure but are not typical. Figure 37 shows the intricate dislocation network comprising a typical subgrain boundary.

Figure 38 shows dislocation pairs on the prism slip planes in an annealed specimen given 5% plastic deformation. This dislocation structure is characteristic of higher aluminum alloys in which slip is coplanar. Figure 39 shows prism slip on another specimen in which the slip planes are tilted such that they are approximately normal to the photograph. Figure 40 shows basal slip planes edge on. Basal slip was very rare in this investigation. The two dislocation structures most commonly observed in this annealed Ti-6Al-4V were cellular arrays not shown and coplanar arrays. Generally, a grain which exhibited one structure did not exhibit the other. Both were quite common. The formation of the cell structure is generally associated with extensive cross slip and tangling as in lower aluminum alloys.

As was mentioned in the literature survey, J. D. Boyd[25] identified two distinctly different hydrides, an fcc "Spontaneous hydride" and a bcc "strain-induced hydride" in the Ti-8Al-1V alloy. This investigation has identified these two hydrides in the Ti-6Al-4V alloy.

The face-centered-cubic "spontaneous hydride" was the most commonly observed hydride in this investigation. Figures 41 and 42 illustrate the appearance of this hydride. Figure 41 illustrates that the hydrides form on the prism planes as was confirmed by trace analysis.

The stages in the precipitation of this phase are illustrated in Figs. 42 and 43. The spontaneous hydrides appear to nucleate at alpha-beta and alpha-alpha grain boundaries. Figures 42a and 42b show hydrides originating at alpha-beta boundaries. These original hydride plates grow along their habit plane and become relatively thick. New hydride plates appear to nucleate at the hydride matrix interface and these grow until they impinge upon another plate. This progress continues until a basket weave appearance such as is shown in Figs. 43a and 43b occurs.

All of the fcc "spontaneous hydrides" investigated were found to lie on the prism plane of the hcp titanium lattice. Trace analysis was used to determine the orientation relationship $(0001)_\alpha \parallel (110)_\gamma$ $[11\bar{2}0]_\alpha \parallel [1\bar{1}0]_\gamma$. This trace analysis solution is shown in Figs. 44, 45, and 46. From this analysis the habit plane relationship was determined to be $(01\bar{1}0)_\alpha \parallel (1\bar{1}\bar{1})_\gamma$. The lattice constant was determined to be a = 4.5 Å.

"Strain induced hydrides" have been identified in this investigation in the Ti-6Al-4V alloy. These were indexed by electron diffraction as bcc with the lattice parameter "a" = 3.35 Å. These hydrides were found by trace analysis to lie on the prism planes of the hcp titanium lattice. The habit plane relationship was determined to be $(10\bar{1}0)_\alpha \parallel (01\bar{1})_\gamma$. This particular habit plane configuration yields the orientation relationship $(0001)_\alpha \parallel (\bar{1}11)_\gamma$, $[10\bar{1}0]_\alpha \parallel [01\bar{1}]_\gamma$. A trace analysis solution is shown in Figs. 47, 48, 49.

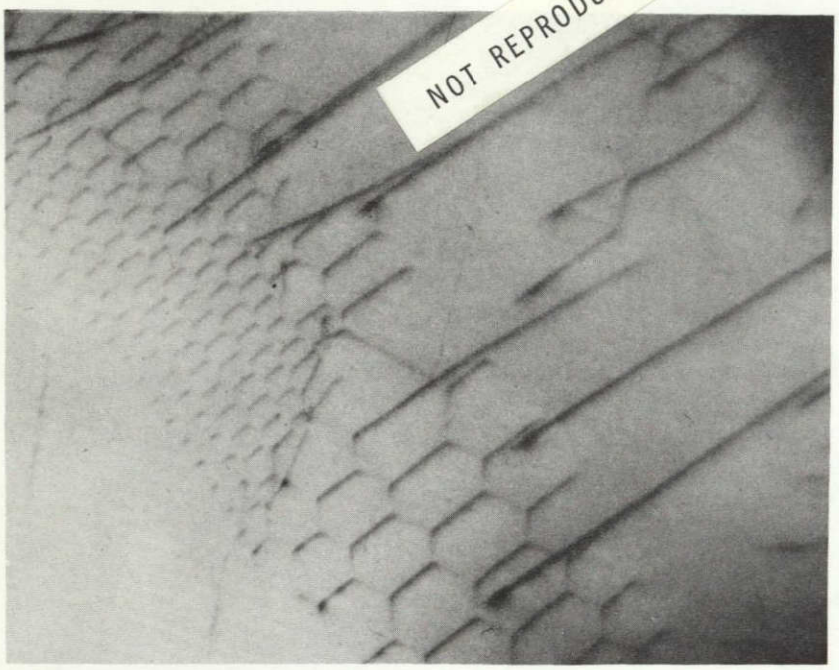

Fig. 37 - Subgrain Boundary in Ti-6Al-4V. TEM (140,000 X)

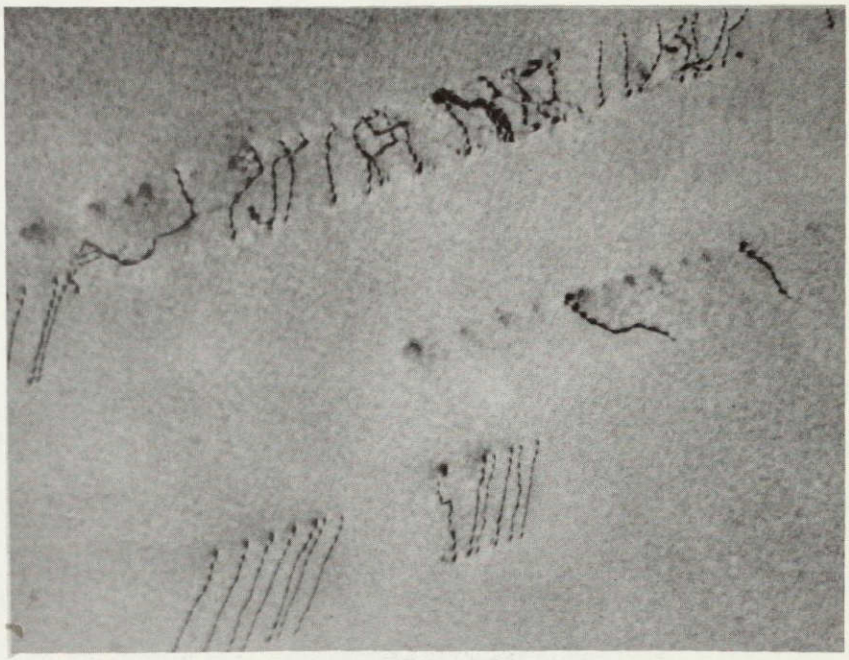

Fig. 38 - Dislocation Pairs on Active Prism Slip Plane in Ti-6Al-4V Alloy. Specimen Given 5% Plastic Strain. TEM (30,000 X)

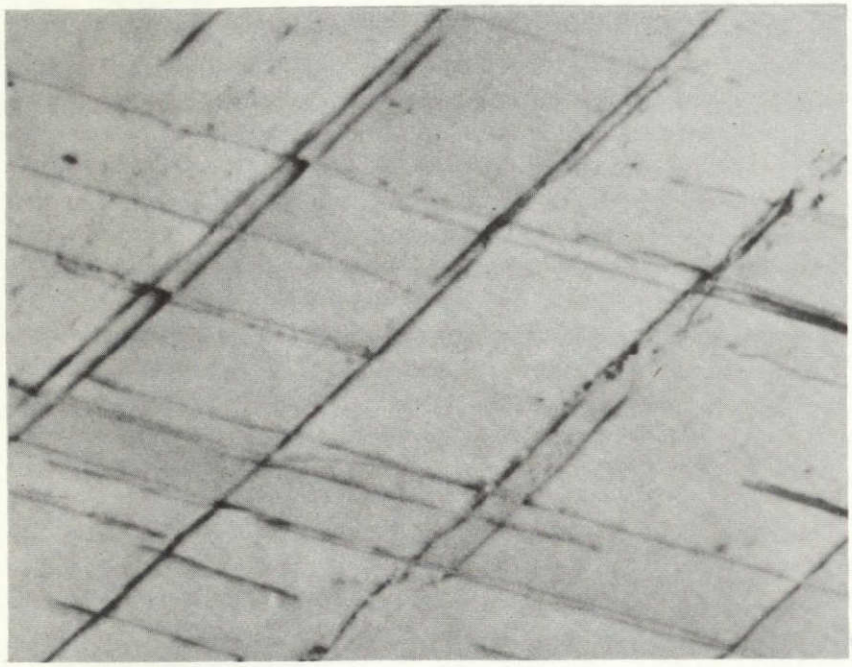

Fig. 39 - Prism Slip in Ti-6Al-4V. Specimen Given 10% Plastic Strain. TEM (105,000 X)

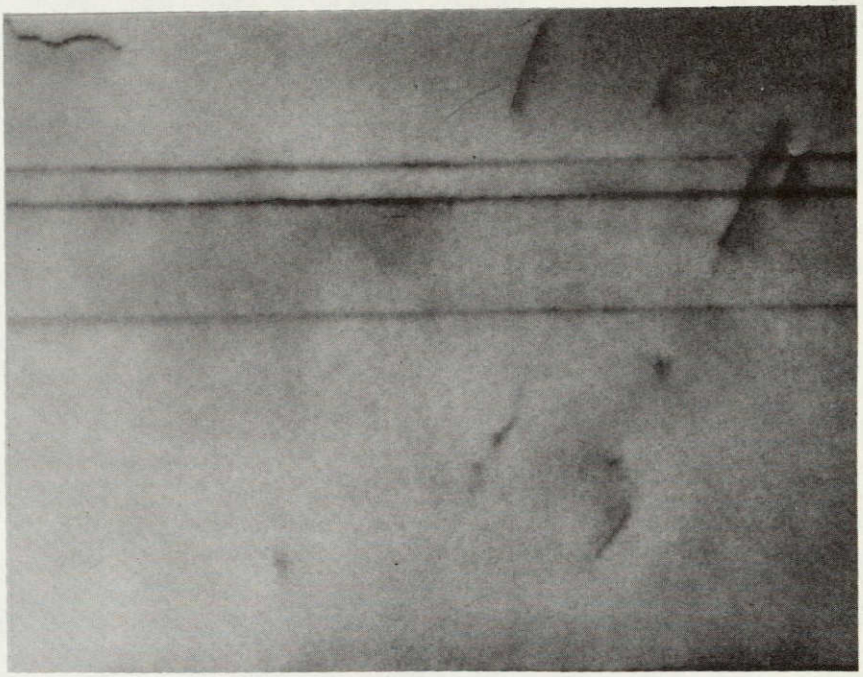

Fig. 40 - Basal Slip in Ti-6Al-4V Specimen Strained 5%.
TEM (40,000 X)

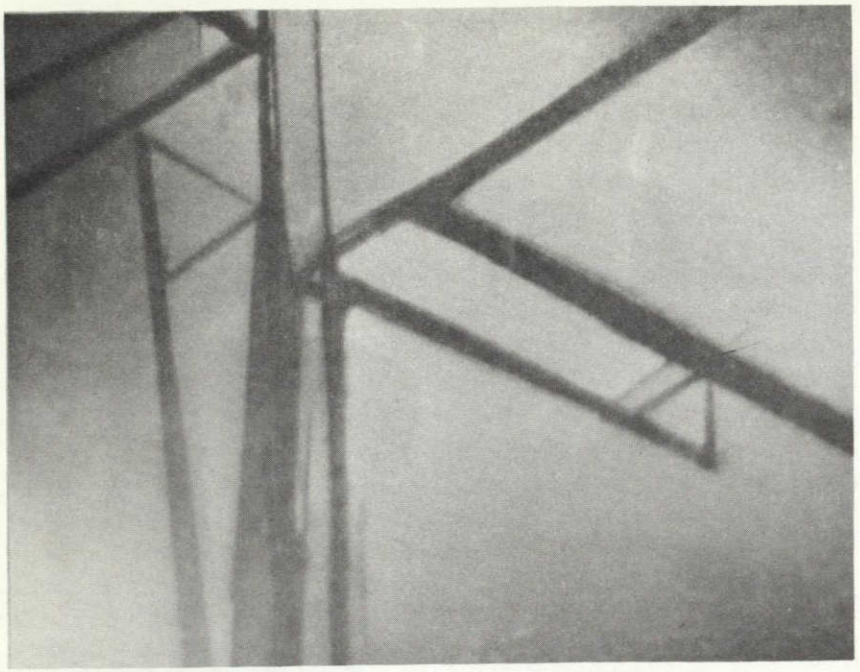

a

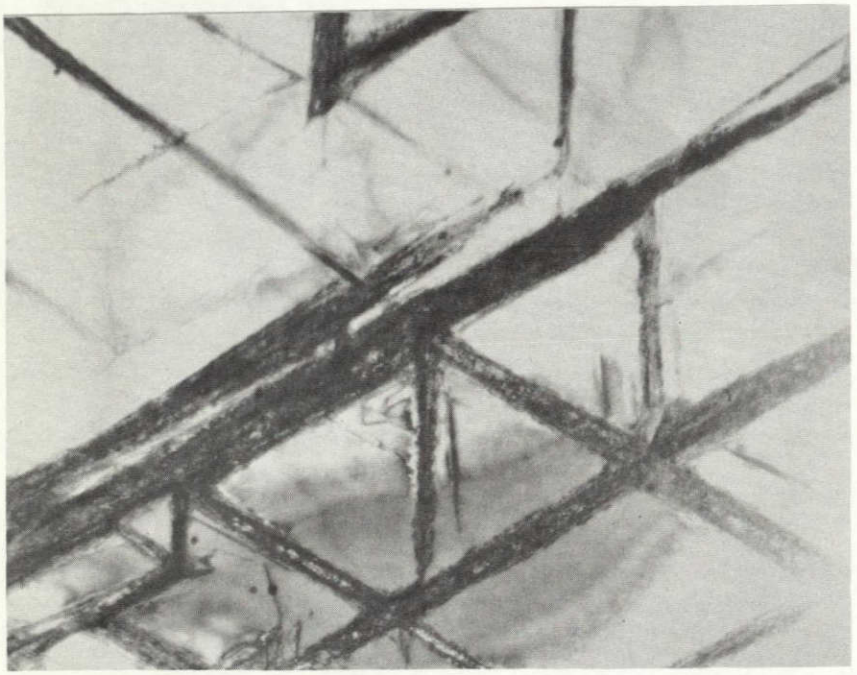

b

Fig. 41 - Spontaneous Hydrides on Prism Planes. Both Charged at -850 mV for One Hour. TEM a) (20,000 X) b) (28,000 X)

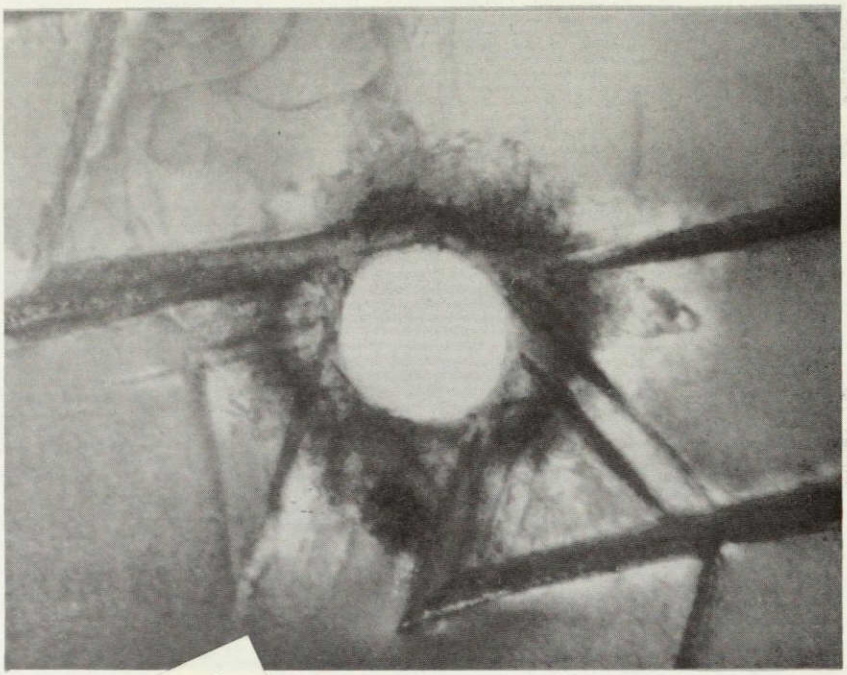

a

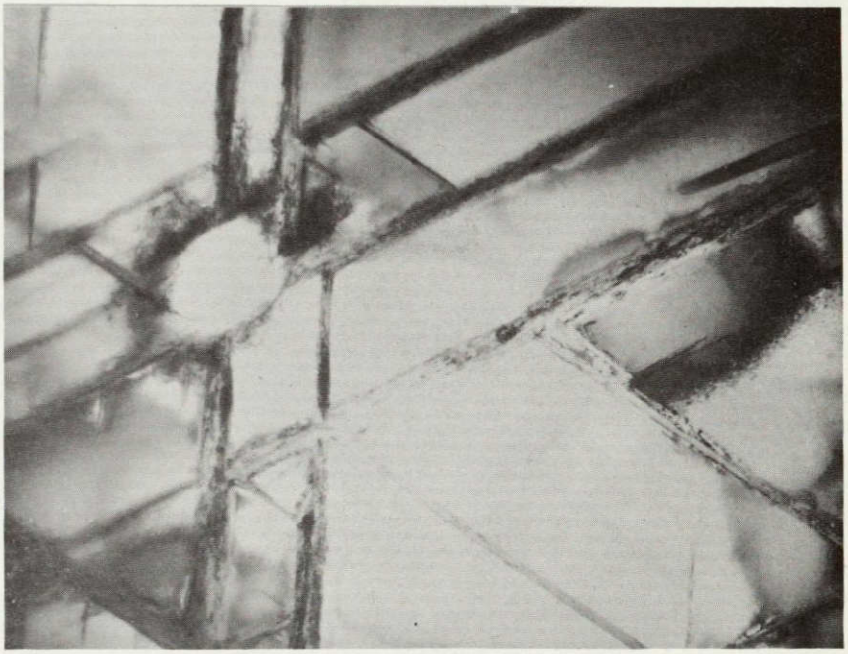

b

Fig. 42 - Spontaneous Hydrides about Beta Particles after Charging at -850 mV for One Hour. TEM a) (16,000 X) b) (18,000 X)

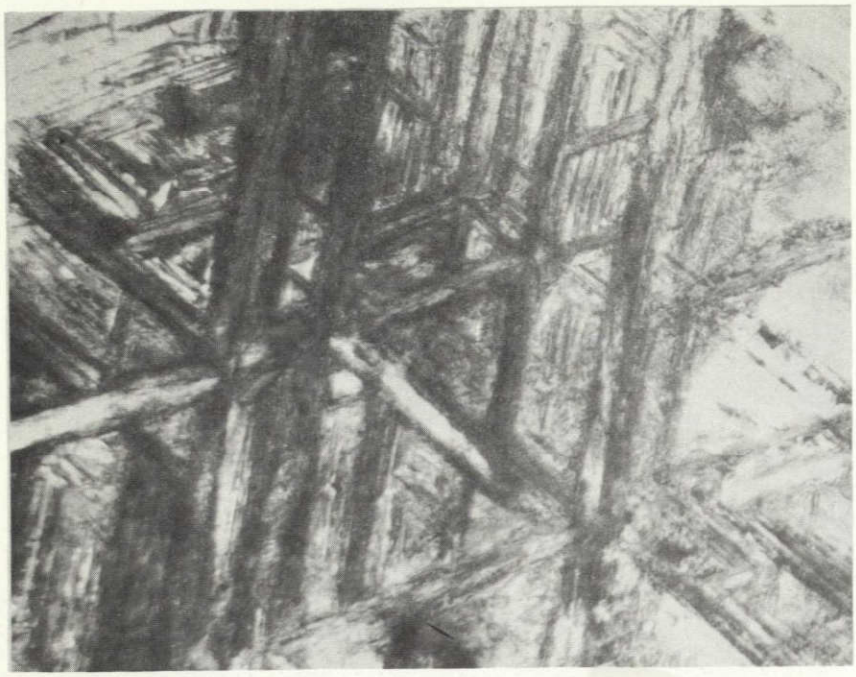

a

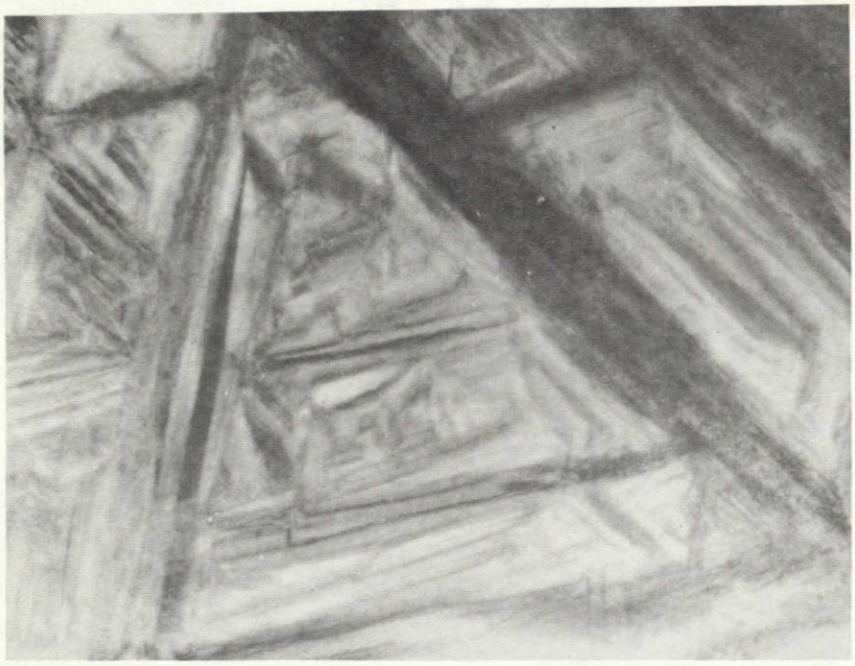

b

Fig. 43 - Basketweave Appearance of Hydrides.
a. Charged at -1500 mV for $\frac{1}{2}$ Hour. (28,000 X)
b. Charged at -1042 mV for $\frac{1}{2}$ Hour. (34,000 X)

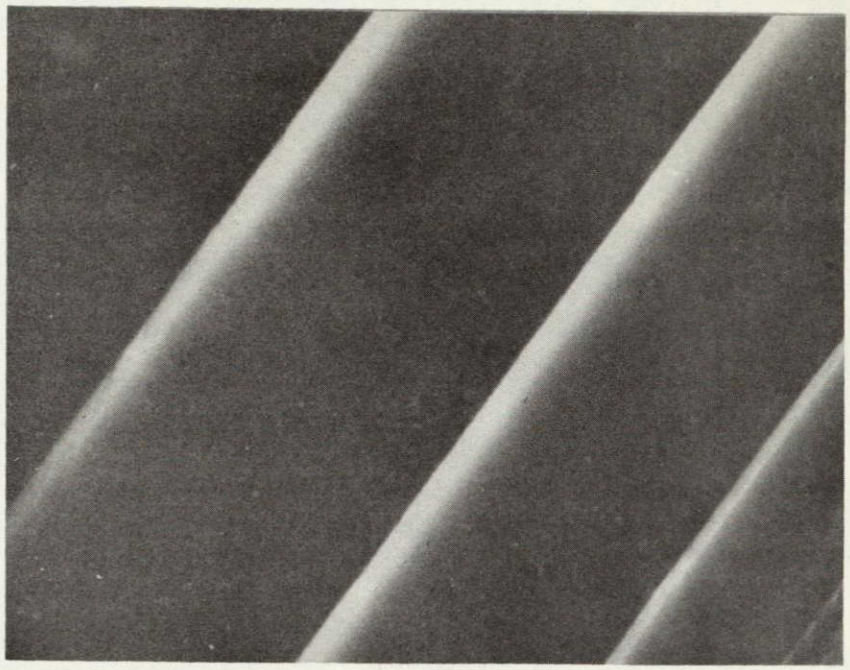

Fig. 44 - Spontaneous Hydrides in Dark Field Using $(\bar{1}1\bar{1})_\gamma$ Reflection. TEM (105,000 X)

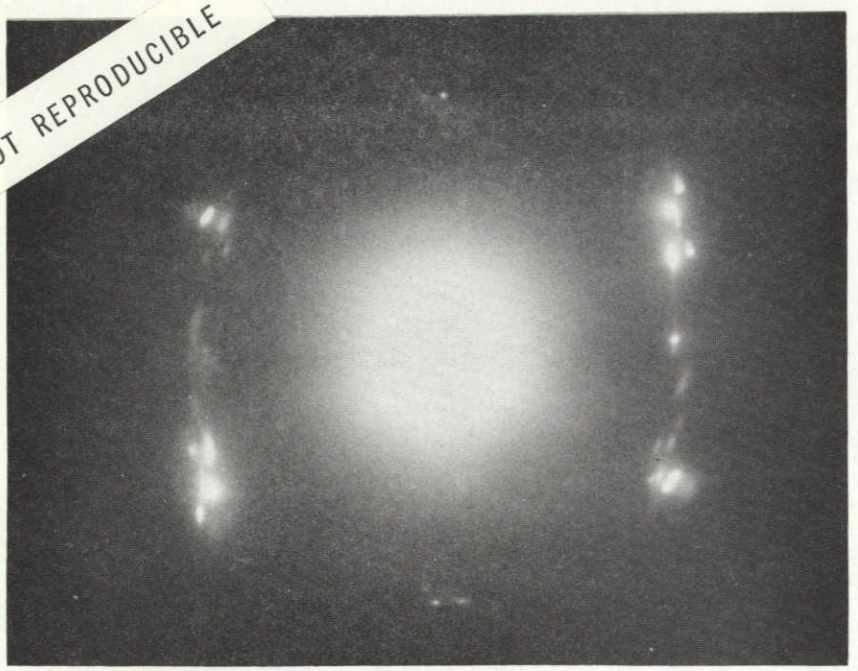

a

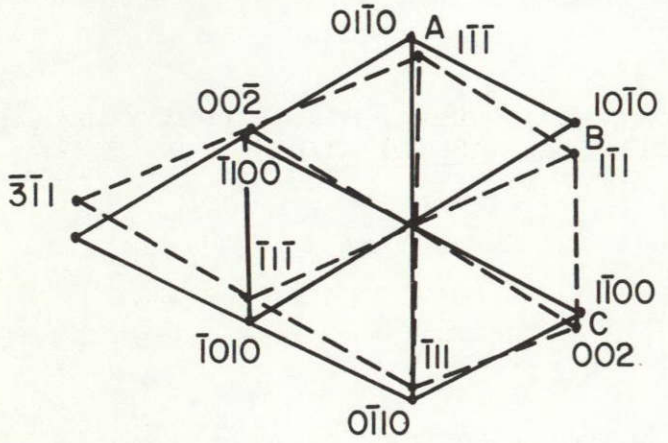

b

Fig. 45 - a. Diffraction Pattern From Hydrides Shown in Fig. 44.
b. Indexed Pattern Showing Habit Plane Trace.

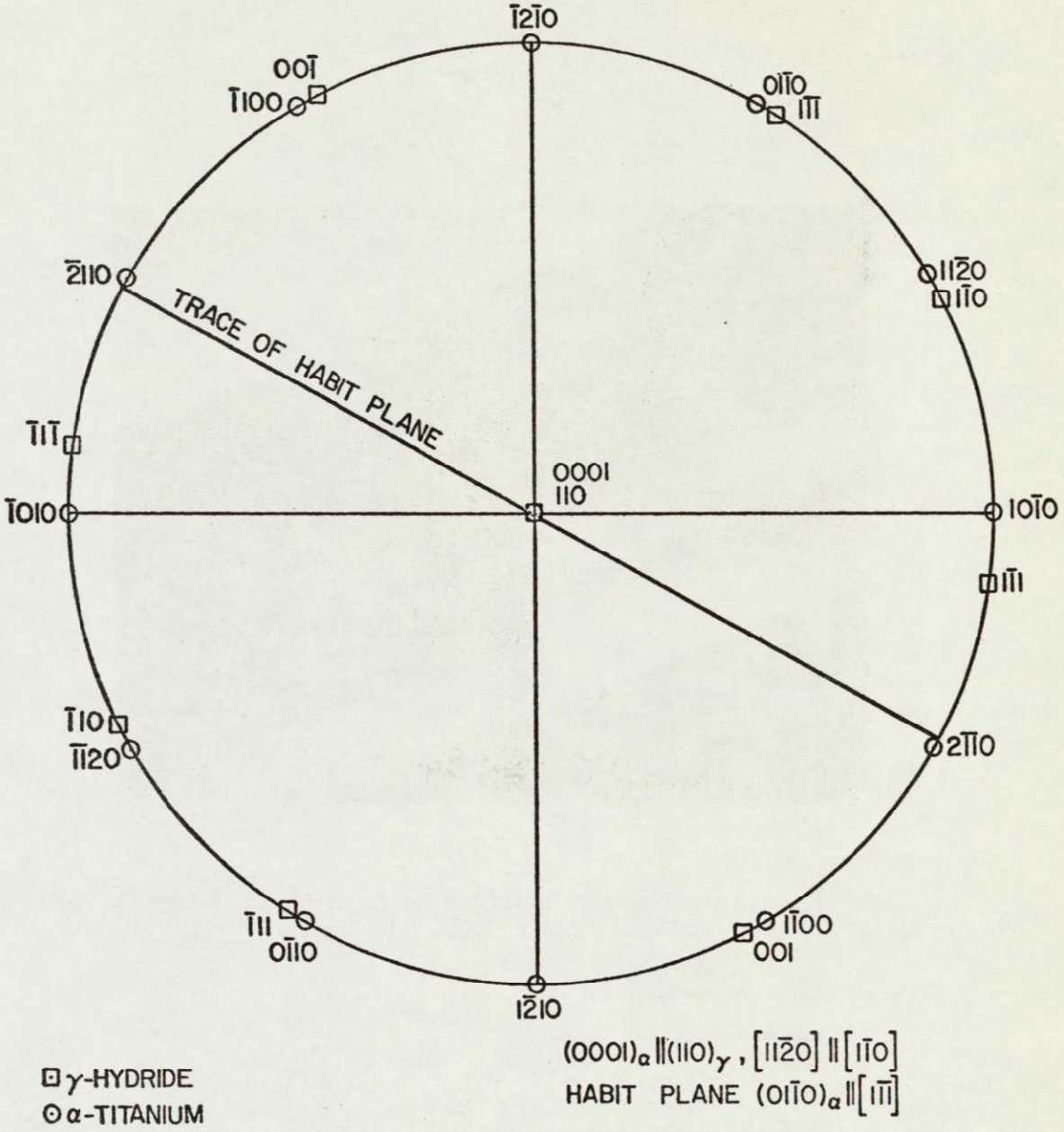

Fig. 46 - Trace Analysis Solution for Figs. 44 and 45

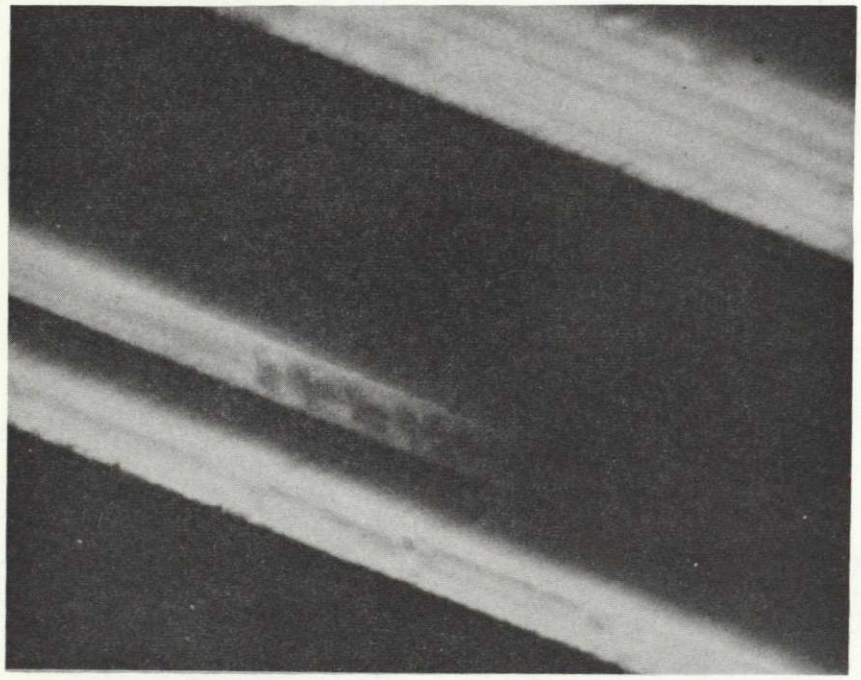

Fig. 47 - Strain-induced Hydrides in Dark Field Using $(\overline{1}10)_\gamma$ Reflection. TEM (60,000 X)

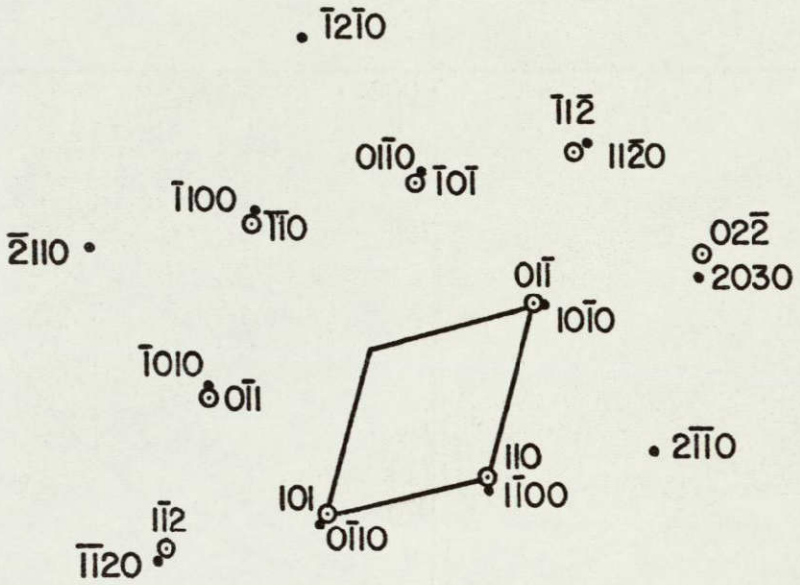

Fig. 48 - Indexed Diffraction Pattern Obtained from Hydrides in Fig. 47

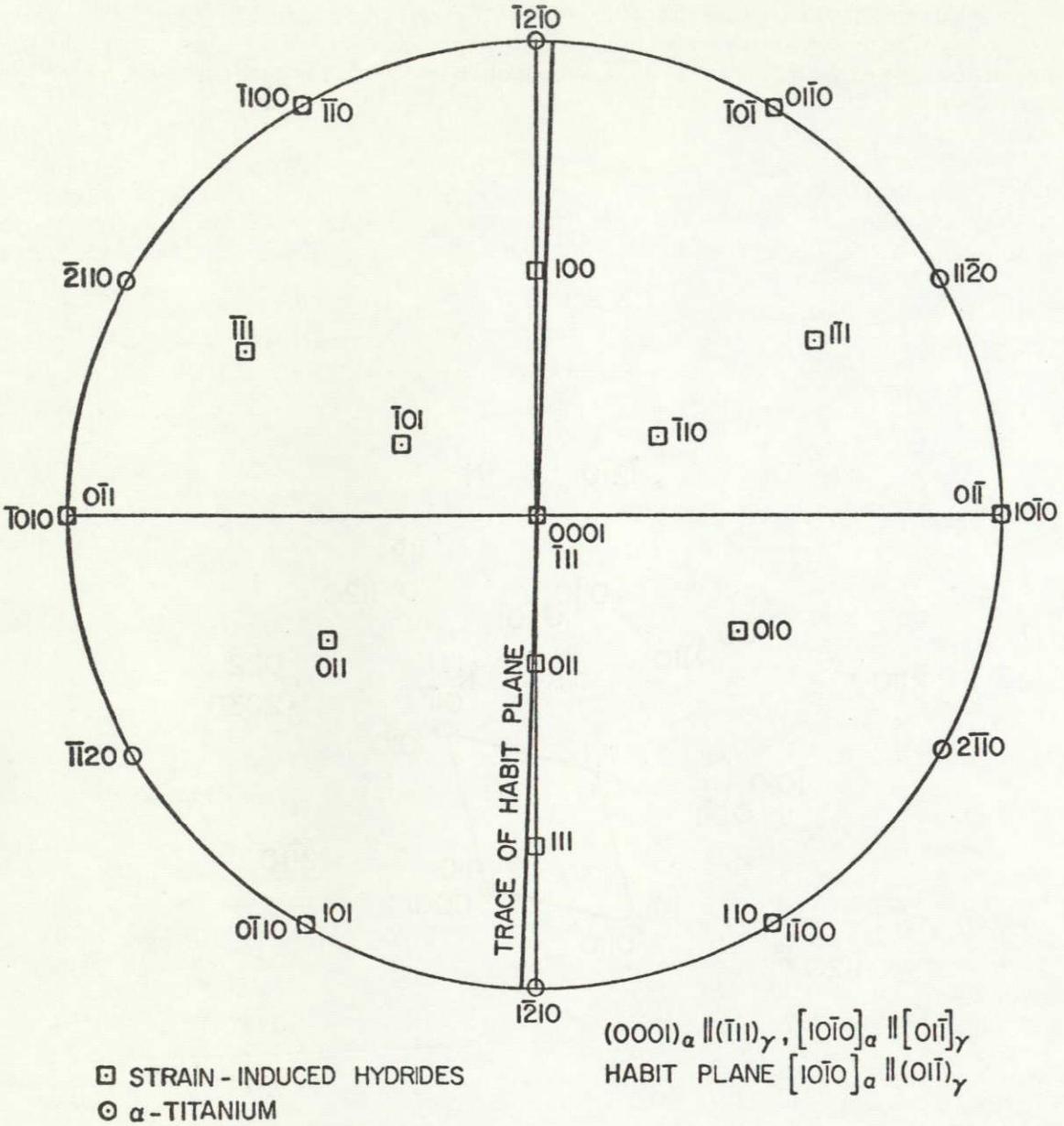

Fig. 49 - Trace Analysis Solution for Figs. 47 and 48

"Strain induced hydrides" were observed in both strained and unstrained specimens; however, their occurrence was much greater in the strained specimens. It is quite improbable that the strain induced hydrides which were observed in unstrained specimens were precipitated during foil preparation or subsequent handling. Rather, it is believed they were precipitated as a result of the lattice strains introduced at long charging times. Extreme care was taken to avoid straining the foil specimens and, in addition, there are several observations which tend to support the conclusion that they were not precipitated during handling:

1. These hydrides were generally thicker than the hydrides in strained specimens. This is understandable since these hydrides are only found in unstrained specimens with very high hydrogen concentrations.

2. These hydrides formed on one set of planes within one grain and were never coexistent with spontaneous hydrides in the same grain. These hydrides always formed along the entire length of each habit plane in each grain. Figures 50 and 51 illustrate these observations.

3. These hydrides were more stable in the electron beam than the thinner strain-induced hydrides.

4. Thin sheet specimens (0.001 in.) were deformed quite noticeably after charging to high hydrogen levels which could account for the necessary strain.

"Strain induced hydrides" formed in strained specimens are identical in appearance to the above hydrides and have the same habit planes and lattice constant. The only difference appears to be their plate thickness which is explainable on the basis of the hydrogen concentration involved and their relative stabilities in the electron beam which is probably due to this difference in plate thickness. The instability of the thinner strain-induced hydride makes its investigation extremely difficult. Figure 52 illustrates the character of this instability. The hydrides appear to dissolve by a ledge type mechanism. In a condensed beam for normal operation at 100 kV these hydrides dissolve extremely rapidly and one is afforded only a fleeting glimpse before they have disappeared. At lower accelerating voltages using a diverged beam and cold trap the dissolution process is slowed but any lengthy investigation is extremely difficult.

Figure 53 is a high magnification electron micrograph illustrating the appearance of strain induced hydrides inclined to the foil surface. The displacement fringe contrast seen in this figure is typical for these very thin hydride plates. Figures 54 and 55 illustrate the observation that these strain-induced hydrides in specimens with lower hydrogen contents do not necessarily extend across the entire length of the slip plane. In the bottom portion of Fig. 55 slip steps at the grain boundary are evident where the slip planes containing the hydrides intersect the grain boundary. This supports the general observation that the strain-induced hydrides only form on the active slip planes.

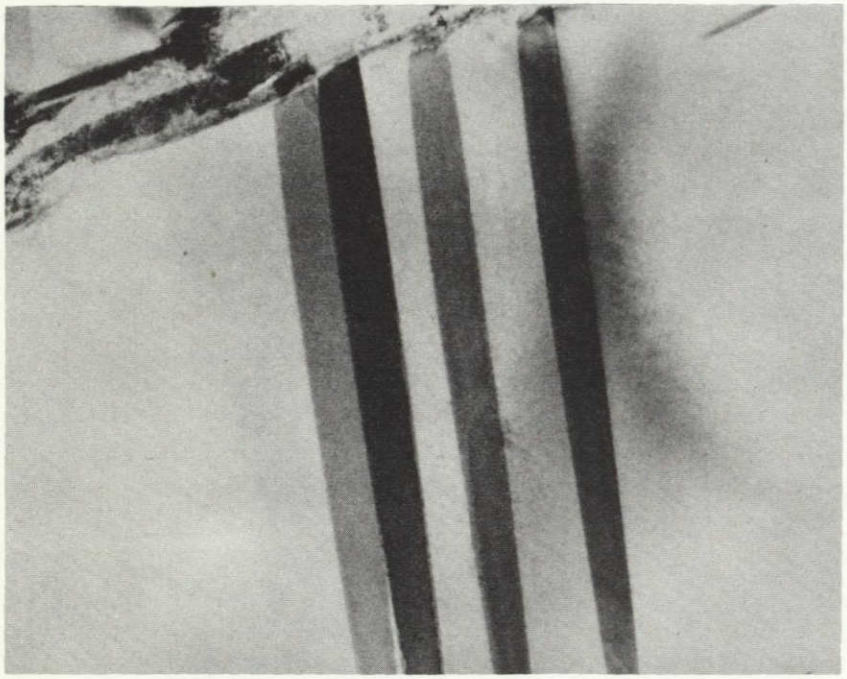

Fig. 50 - Strain-Induced Hydrides in Specimen Charged for one Hour at -850 mV in 5N HCl. TEM (24,000 X)

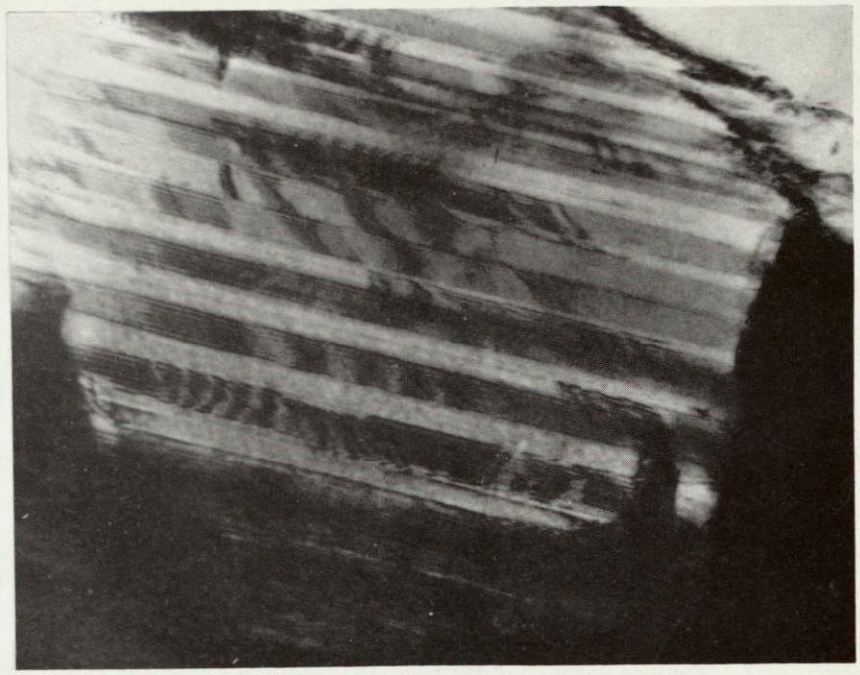

Fig. 51 - Strain-induced Hydrides in Specimen Charged One Hour at -850 mV in 5N HCl. TEM (28,000 X)

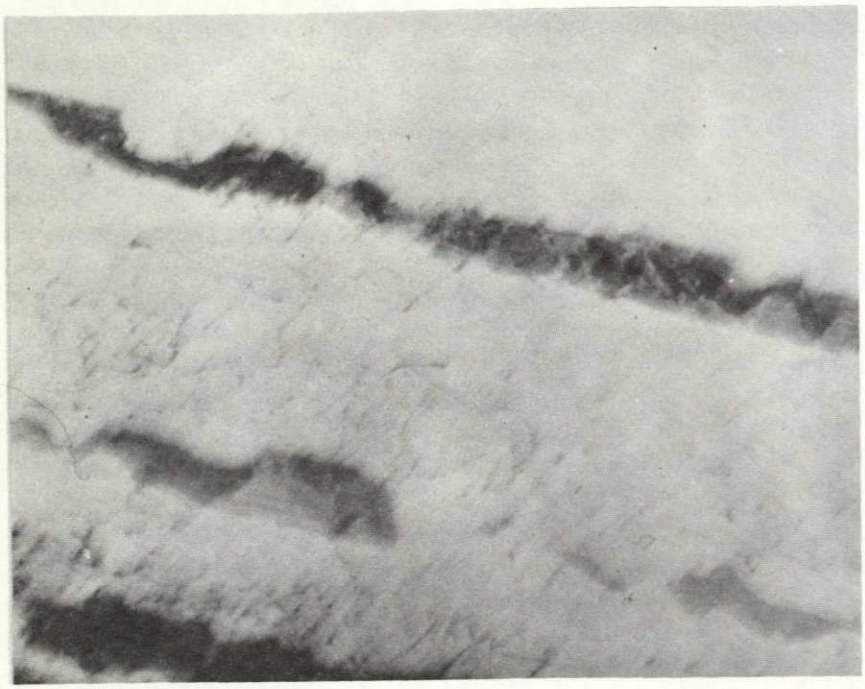

Fig. 52 - Strain-induced Hydrides During Dissolution in Electron Beam. Specimen Charged $\frac{1}{2}$ Hour at -850 mV and Strained 5%. TEM (60,000 X)
Note: Poor image quality due to inability to focus at 60 kV. Low accelerating voltage was used to reduce effect of beam heating.

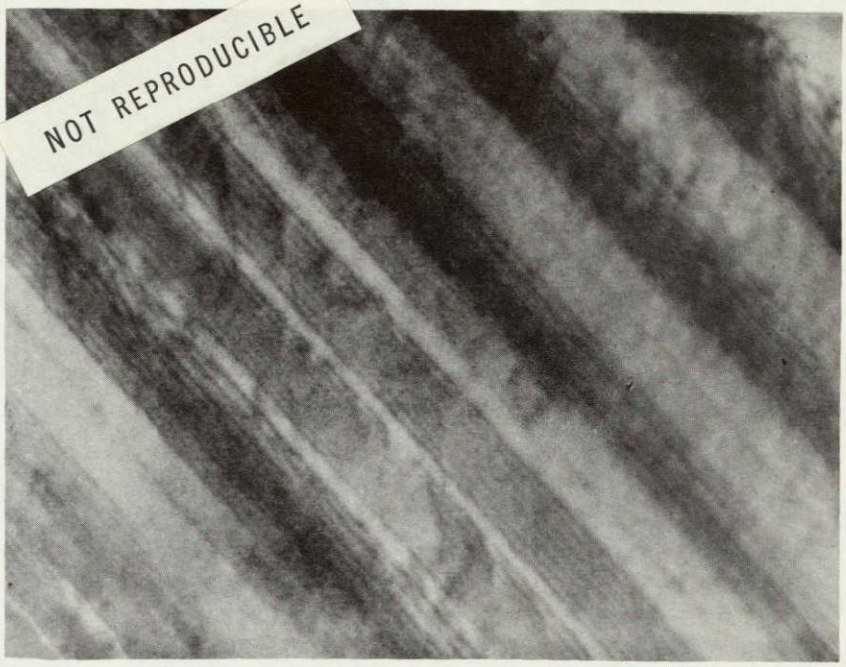

Fig. 53 - Strain-induced Hydrides Showing Contrast Effects and Interface Dislocations. Specimen Charged at -850 mV for One Hour in 5N HCl and Deformed 5% in Tension. TEM (72,000 X)

Fig. 54 - Strain-Induced Hydrides in Specimen Charged at -850 mV for One Hour and Deformed 5% in Tension. TEM (16,000 X)

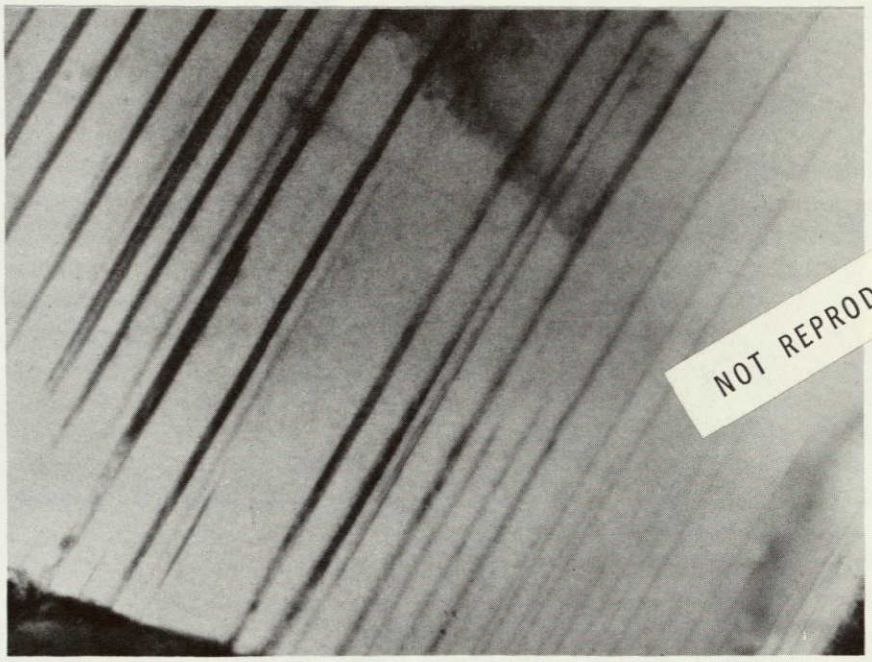

Fig. 55 - Strain-Induced Hydrides Lying on Active Slip Planes. Specimen Charged at -850 mV for One Hour and Deformed 5% in Tension. TEM (24,000 X)

V. DISCUSSION

The results of the present investigation may be broken into two parts; those results which apply basically to the initiation phase and those which apply to the propagation phase of stress-corrosion cracking. An attempt is made in this discussion to define these two separate processes and discuss models for each. It would of course be difficult to separate these two processes in an actual stress-corrosion system as it would be difficult to determine when initiation was complete and propagation begins.

Although this investigation was not primarily concerned with electrochemical measurements, it would be impossible to discuss any mechanism without considering the electrochemical aspects. The mere fact that this investigation was conducted in the negative potential regions believed to cause embrittlement is based upon an electrochemical mechanism. The results of this investigation are primarily qualitative owing to the nature of the problem.

INITIATION OF SCC

The initiation phase of stress-corrosion cracking may be defined as, "The process occurring on the surface of a metal which, under the influence of stress establishes the conditions necessary for the formation of an active stress-corrosion crack."

Thus, from this definition, it is apparent that initiation cannot occur without a resulting propagation. The opposite, of course, is not true since it is common practice in many experimental procedures to notch and pre-crack specimens, thereby eliminating initiation in order to more readily study the propagation processes.

Results reported in this investigation (Fig. 13) demonstrate that the load at failure in three-point bend specimens in 0.6M KBr is electrochemically dependent. Other workers[39,67] have observed that the propagation velocity is linearly related to the potential such that as the potential increases, the crack velocity increases (Fig. 7). Hence, propagation can proceed in pre-existing cracks at potentials above the susceptible region in Fig. 7, but not below this region. Thus, it appears that the SCC region in Fig. 13 is a measure of susceptibility to initiation. This region of SCC initiation is in the cathodic potential range between approximately -250 mV and -900 mV (SCE). Propagation will still occur at potentials above -250 mV but will not occur at potentials below -900 mV.

The model proposed for initiation is a pitting mechanism which requires the local breakdown of passivity perhaps by slip step emergence or rupture of the passive film. The repassiviation kinetics will then determine the susceptibility. This is similiar to the model suggested

by Scully.[51] If repassiviation is rapid, the pitting is negligible but, if repassivation is slow or incomplete, pitting will occur owing to the active nature of unpassivated titanium. Once a pit is established, repassivation does not occur in the pit and the mechanism becomes autocatalytic.

The pitting mechanism is believed to be related to the chloride ion. At potentials below approximately -1140 mV (SCE) the formation of titanium chloride ($TiCl_3$) becomes impossible. This is seen on the equilibrium potential-pH diagram shown in Fig. 56. Above this potential "chloride-ion attack" may occur. That initiation is prevented in the potential range above -250 mV is probably due to the rate of repassivation which is high enough to prevent the establishment of localized pitting. The role of the stress in this model is to supply "fresh" metal to the environment and perhaps act to localize the pitting attack to certain preferred directions.

Once a pit has been established it acts as a stress raiser which localizes the stresses. A pit may link up and establish a pseudocrack. The electrochemical processes within the crack establish high hydrogen and chloride ion concentrations. These conditions of high stress intensity at the crack tip, high Cl^-, high H^+ and low O_2 are all necessary for propagation to begin.

The results of this investigation in acidic environments indicate that the Ti-6Al-4V alloy does pit at cathodic potentials. This same alloy, given this same treatment in the unstressed condition in a 3-1/2% NaCl environment shows no pitting tendencies. It therefore appears necessary that local cells must be established through the combined action of stress and corrosion. The mechanism is schematically illustrated in Fig. 57. In 57a the protective film (TiO_2) is ruptured by an emergent slip step. If the repassivating agent H_2O or OH^- for example, is present in sufficient quantities, the surface becomes repassivated rapidly as in Fig. 57b. If however, partial repassivation has sufficiently reduced the concentration of the passivating agent, the unpassivated surface remains active. Anodic dissolution or chloride ion attack establishes a layer which essentially blocks the passivating agents. The presence of the Cl^- ions is balanced by the migration of H^+ ions into this region. The titanium chloride formed in the environment or, by the chloride ion attack mechanism on the surface, hydrolyzes and in so doing further prevents the water molecules from gaining access to the bare surface. This is shown in Fig. 57c. Scully[51] refers to the rate of repassivation as envisioned in the above discussion to be "the critical step in seawater stress-corrosion".

PROPAGATION OF SCC

The propagation phase of stress corrosion cracking may be defined as slow crack growth resulting from the combined action of a corrosion

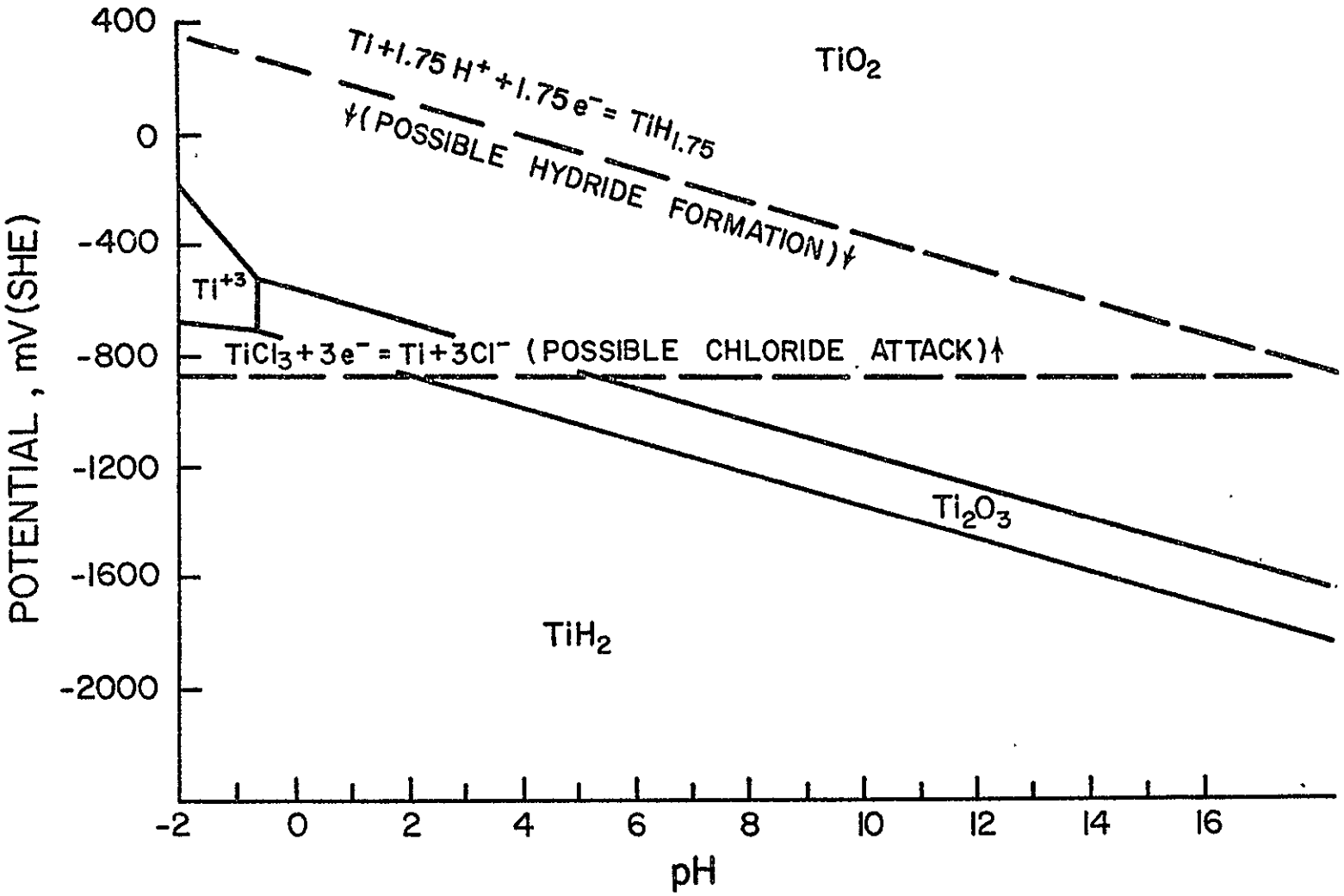

Fig. 56 - Potential - pH Diagram for Titanium Which Includes a Stable Hydride Phase

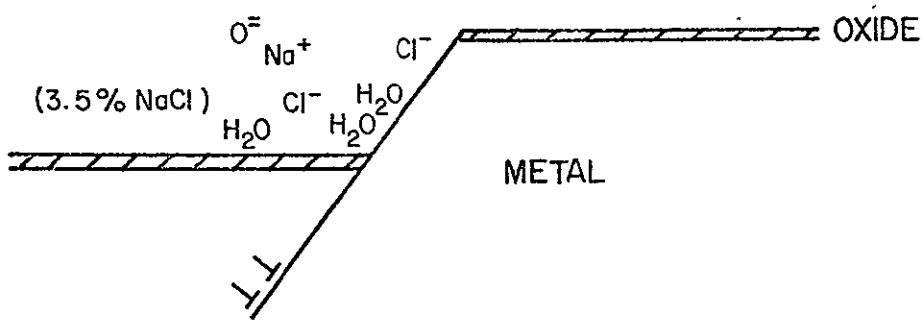

a

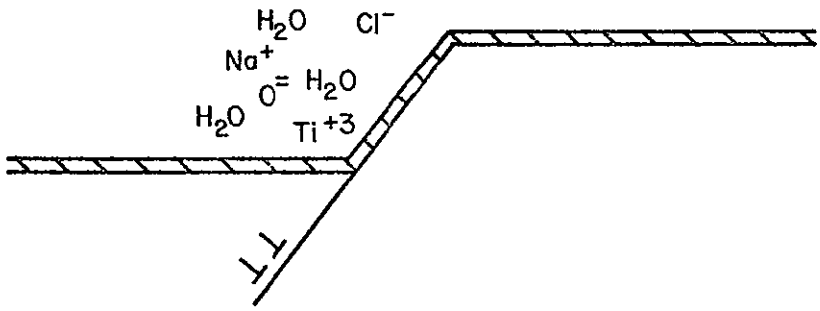

b

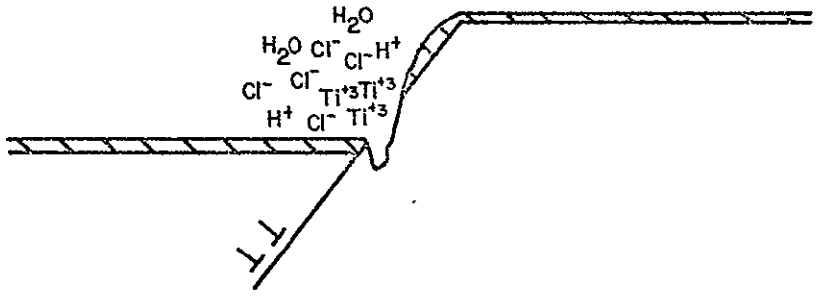

c

Fig. 57 - Model for SCC Initiation
(a) Emergent Slip Step
(b) Complete Rapid Repassivation
(c) Partial Repassivation Leading to a Pitting Mechanism

process and a tensile stress. This is a rather classical definition of stress-corrosion propagation. The necessity of a corrosion process does not necessitate that the crack propagate by anodic dissolution, but rather that the corrosion process be an integral part of the mechanism. The corrosion process could, for example, merely act indirectly in that it would supply the active species responsible for the cracking process.

The model proposed in this investigation assumes hydrogen to be the species responsible for stress-corrosion propagation. It would, of course, be very difficult to speculate as to the exact processes occurring at an active crack tip since we are unable to observe or even measure these processes. Therefore, any model must be based upon observations which are made away from this region of interest. The present model assumes that an active corrosion process is occurring at the crack tip in an acidic environment. This corrosion process includes both anodic and cathodic reactions. Whether or not these two separate processes are segregated in this crack tip region is a matter of speculation and will be discussed in more detail later. It is assumed that the cathodic reaction is the reduction of hydrogen ions present in the crack from any or all of several sources. The hydrogen ions can originate from the instability of water at the active potentials in the crack tip region, the hydrolysis of $TiCl_x$ compounds, which may result from the anodic process, or possibly from ion transport of the positive hydrogen ion toward the negative electrode. The fact that the crack is acidic was determined by Brown.[69] His procedure measured an average bulk pH for the crack of approximately pH 1.7. It is believed that in the immediate crack tip region the pH is even lower. This is the basis for the 5N HCl environment used in this investigation.

That a stress corrosion crack is also a crevice leads to the application of the better understood crevice corrosion mechanism to the crack tip region. There are some important differences, however, such as the highly strained metal at the crack tip and that "fresh surfaces" are being continually generated. In addition, the environment is not stagnant as in a crevice but experiences turbulence from the sucking action of the opening crack.

Crevice corrosion and, indeed, stress corrosion involve the establishment of an active corrosion process within a confined volume. The mechanism believed [70] to be responsible for crevice corrosion is simply the depletion of oxygen within the crevice by the reduction reaction

$$O_2 + 2H_2O + 4e^- \rightarrow 4OH^-.$$

Once the oxygen, which has a low solubility in aqueous solutions, has been removed, the conditions are established for the crevice to act as the anode and the exterior passive surfaces to act as the cathode. Thus, within the crevice the anodic reaction,

$$Ti \rightarrow Ti^{+x} + xe^- \quad (x = +3 \text{ or } +4)$$

is occurring. Since there is a concentration of metal ions within the crevice, the negative chloride ions migrate into the region to balance the charge. These chloride ions react with the metal ions to form metal chlorides which hydrolyze according to the reaction.

$$TiCl_x + XH_2O \rightarrow Ti(OH)_x + xH^+ + XCl^-$$

This hydrolysis reaction produces an insoluble hydroxide and a free acid. This then results in a lowering of the pH and an increase in chloride ion concentration, both of which tend to increase the rate of metal dissolution by destroying the oxide or passive film on the metal within the crevice.

The potential at the crack tip would be expected to fall in the region between -600 mV and -1000 mV (SCE) depending upon the pH[71]. Also, this potential is independent of any applied potential since it is determined solely by the electrochemical processes which occur in this region in the absence of any passivating species. T. R. Beck[39] has measured the potential on freshly generated surfaces of Ti-8-1-1 to be approximately -850 mV (SCE) at pH 1 and -800 mV (SCE) at pH 0.

Within the crevice or crack, macro cells are established such that the crack tip region is active with respect to the walls of the crack at some distance behind the apex of the crack. Griess[71] has observed hydrogen bubbles escaping from the edges of crevice specimens which would indicate that hydrogen ions are being reduced within the active region. The results of Griess's investigation indicate that the activity of the hydrogen ion is increased by increased chloride ion concentrations. Also, he indicates that it is the activity of the hydrogen ion which determines the rate of attack in a crevice.

The present model assumes the bulk of the hydrogen ion reduction to occur in the active regions at or near the crack tip. The reduction process, involving the adsorption of hydrogen atoms as a result of the discharge reaction, establishes a coverage of the cathodic reaction sites by hydrogen. This is, of course, a dynamic system and the anodic and cathodic sites are moving with the crack. Hydrogen atoms are assumed to either absorb and diffuse to the crack tip region under the influence of concentration, stress and electric field gradients and/or migrate by surface diffusion in the electric field down the crack wall. Either case will yield a continuous flux of hydrogen atoms toward the region of interest.

The hydrogen atoms, present in sufficient concentrations, will precipitate on the active prism slip planes, thereby preventing plastic relaxation around the crack tip. If plastic relaxation is prevented, the metal will act as a brittle material. Griffiths'[73] criterion for crack propagation in a brittle material is simply that the decrease in stored elastic strain energy must be greater than the increase in surface energy. These two energy terms may be given as:

Stored Elastic Strain Energy: $W_E = \frac{\pi\sigma^2 C^2}{E}$

and

Surface Energy: $W_S = 4C\gamma_S$

where

σ = nominal stress
C = crack length
E = elastic modulus
γ_S = surface energy (work done to create new surface area)

The Griffith criterion can then be written as:

$$\frac{\partial W_E}{\partial C} \geq \frac{\partial W_S}{\partial C}$$

so that

$$\sigma = \sigma_F = \sqrt{\frac{2E\gamma_S}{\pi C}}$$

where σ_F is the minimum nominal stress for brittle fracture. If, however, we have a material which will undergo plastic deformation (assuming the yield stress is below σ_F) the stored elastic strain energy cannot by itself exceed the value required for propagation. If localized plastic deformation occurs then a certain amount of plastic work γ_P is expended during propagation. Thus, the total work done in extending the crack is increased from γ_S to $(\gamma_S+\gamma_P)$. Griffith's criterion is then modified such that

$$\sigma_F = \sqrt{\frac{2E}{\pi C}\ (\gamma_S+\gamma_P)}$$

It can be seen then that the more plastic deformation that occurs the greater will be the nominal stress for fracture and hence, the tougher the material. On the other hand, a "tough" material may be rendered "brittle" by prevention of localized plastic deformation. It is proposed that the hydrides act in this manner by precipitating on the active slip planes.

The above arguments, it would appear, would hold for a brittle or cleavage type fracture which normally occurs in brittle materials at velocities much greater than those measured for stress-corrosion cracking. It does not appear likely, therefore, that this mechanism explains continuous SCC crack growth. However, stress-corrosion cracking is observed[89] to propagate discontinuously. It is possible, therefore, that propagation is by a cleavage mechanism for a short distance until the crack is stopped by plastic relaxation after it has extended past the region where the strain-induced hydrides have precipitated. This plastic relaxation

would account for the small amount of plastic flow commonly observed on fracture surfaces. Blunting of the crack should occur when it is stopped by the action of the plastic deformation. Reinitiation of the stopped crack could occur by the combined action of electrochemical sharpening of the crack tip and the precipitation of the strain-induced hydrides. The highly strained metal at the crack tip would tend to undergo anodic dissolution much more rapidly than the unstrained metal. As the root radius (ρ) of the crack decreases, the tensile stress at the crack tip increases according to the following relationship:[74]

$$\sigma_{max} = 2\sigma\sqrt{\frac{C}{\rho}}$$

In addition, hydrogen which diffuses to the highly strained plastic region about the crack tip precipitates on the active slip planes. By limiting plastic deformation and sharpening the crack tip the conditions for cleavage will be established and the crack will extend itself until it is again stopped by plastic relaxation.

From the vacuum fusion analyses (Fig. 17) it appears that titanium absorbs hydrogen rapidly. The analyses presented in Fig. 17 were not equilibrium values but, rather, the hydrogen content in 0.002-inch sheet specimens after exposure at the given potentials for various lengths of time. The specimens would contain concentration gradients from each surface. Hence, the actual rates of absorption are much larger than may be inferred from Fig. 17. For example, the initial rate of hydrogen pickup for this 2-mil specimen at -850 mV is the initial slope of the curve in Fig. 17. This value is approximately 100 ppm/minute. However, it is only a very thin surface layer which is experiencing this increase in hydrogen concentration. As an approximation, using the relationship

$$X_o = \sqrt{\pi D t}$$

We can determine X_o which is an estimate of the depth of penetration, where D is the diffusion coefficient at room temperature in alpha titanium (2×10^{-11} cm^2/s) and t is the time in seconds. If one minute is taken as the time of interest, X_o is determined to be approximately 2×10^{-5} inches. Hence, almost all of the hydrogen in this case occupies 2% of the volume or 0.04 mil since both surfaces of the sheet must be included. Extending this line of reasoning, the rate of hydrogen absorption in this 0.04-mil surface layer should be in the order of 100 ppm/s. This, of course, is still not an equilibrium figure since a concentration gradient still exists. Also, this argument has not considered the very thin surface hydride layer which exists and could account for this rather high value of 100 ppm/s. Nevertheless, this argument does demonstrate that titanium will absorb hydrogen at extremely high rates in acid environments at the potentials assumed to exist in the crack tip region.

The increase in current noted as a function of time at a given potential (Fig. 18) probably reflects the formation of the hydride layer on the surface. Otsuka[32] has studied this surface hydride formation in hydrochloric acid environments and has found that it is passivating even in severely corrosive acids. The effect of this hydride may be to increase the hydrogen overpotential or to decrease the overpotential for the anodic reaction. There is a definite time lapse before formation of this hydride layer is detectable from the recorded currents. This lapse was normally from several minutes up to fifteen minutes. The surface hydride is, therefore, probably not formed on the active surface at the crack tip since the crack is moving fast enough to outrun its formation. It does, however, undoubtedly form on the crack walls behind the crack tip region.

The neodymium hydrogen detector method used in this investigation has demonstrated that the hydrogen enters the alpha grains and is evenly distributed throughout each grain. The apparent difference in concentration from one grain to the next is either due to an orientation effect, which is doubtful owing to the strong texturing tendencies of these specimens, or to the presence of some protective passive film on some of the grains. This could possibly be the hydride layer expected to form on titanium at these potentials in this acidic environment.

That hydrogen segregation at the alpha-beta and alpha-alpha interfaces and in the beta phase was difficult to detect except at high hydrogen concentrations (Fig. 22) is understandable from an energy standpoint. Concentrations of hydrogen in these regions exist but the energy of the hydrogen atoms is also much lower owing to the easy accommodation of the hydrogen atoms in these locations. Hence, the small activation energy (300°F) was insufficient to drive any appreciable amount of hydrogen out except from the beta phase at high concentrations as shown in Fig. 22.

In the sequence of Figs. 20, 21, and 22, the density of the NdH_2 reaction sites increases from Fig. 20 to Fig. 21, as would be expected, but in Fig. 22 the only reaction sites visible are those about the beta phase. Somewhere between Fig. 21 and Fig. 22 the hydride phase precipitated which tied up the hydrogen and accounts for the low density of reaction sites on the alpha grains. It appears that once the gamma phase precipitates, it accounts for all the available hydrogen within each alpha grain.

That the Nd detector method showed larger hydrogen concentrations in the notch tip region of the double notch specimens indicates that this region is absorbing hydrogen faster than the bulk. The Nd method, understandably, gives relative concentrations as discerned by light density and in these cases this difference was subtle. There was no interface between the lighter and darker areas. Also, since the size of the plastic zone is unknown, it was impossible to determine whether the hydrogen absorbed faster in the plastic or elastic regions. The observation of hydrides in the tip regions before they are found in the bulk was determined on specimens loaded to 80% of the fracture stress and charged for

one hour at -850 mV. This confirms the observation that hydrogen is picked up faster at the notch tip region.

That hydrogen is absorbed faster on a mechanically polished surface than on an untreated surface or an electropolished surface is probably due to the plastic deformation introduced during polishing. This is directly applicable to the walls of a crack which have undergone plastic deformation. Also, that hydrogen segregates to the regions of tension illustrates that hydrogen in an SCC specimen will tend to migrate to the crack tip region. This is, of course, expected for the hydrogen atom which expands the lattice.

The nature of the surface attack shown in Figs. 23 through 29 is quite interesting. Figures 23 and 24 illustrate the attack of the beta phase on unstressed specimens. This localized attack is quite severe. It is believed that the alpha grains were protected from anodic attack by the surface hydride layer which forms on them but the beta was not. This established a large cathode to anode ratio which is responsible for the severity of this attack. That some of the alpha grains were attacked, see Fig. 25, is again probably due to differences in the surface hydride from one grain to another. This effect is also believed responsible for the differences in hydrogen concentration from one grain to the next as observed in the neodymium detector method. The attack of the alpha grain in Fig. 25 appears to be pitting. Figure 26 shows the attack at -500 mV for one hour which appears less severe in the beta phase. Attack of the alpha appears uniform on each grain and several small pits are visible on the surface. This same type of attack is observed in Fig. 27 for a specimen held at its corrosion potential for 10 hours. Again, the differences in the protectiveness of the thin surface hydride layer is believed responsible for the preferential attack of certain grains. The application of a large cathodic potential, -1500 mV (SCE), results in a more uniform attack over the entire surface (Fig. 28).

Figure 29 illustrates the attack on a specimen stressed to approximately its yield stress and charged at -742 mV for two hours. The attack has changed from the beta phase to the alpha-beta interface. In this case, the surface hydride was apparently unable to passivate the alpha grains in the vicinity of the beta grains. The beta grains would be expected to be noble with respect to the alpha owing to the high concentration of vanadium in the case of Ti-6Al-4V. The breakdown of the passivating layer could be attributable to rupturing perhaps by slip step emergence. That the attack was concentrated at the alpha-beta interface in the alpha is most readily explained by the close proximity of these sites to the cathodes (the beta phase). This attack is quite different and more rapid than was observed on unstrained specimens. The attack appears crystallographic in nature and from the shape of the pits and known texture of this sheet material it appears to have proceeded in a direction perpendicular to the basal plane.

These observations might be extended to the behavior expected at a crack tip. A surface hydride would not be expected at the active crack tip so the anodic dissolution reaction would be expected to proceed along reactive paths such as the alpha-beta interfaces or the alpha-alpha interfaces. This would lead to an intergranular failure. Stress-corrosion cracking in alpha-beta alloys in aqueous environments is, however, transgranular. This dissolution along reactive paths could be responsible for branching. It is doubtful, however, that anodic dissolution could occur at the velocities required to account for branching. In this regard, it would be difficult to account for any anodic process being entirely responsible for propagation at the velocities observed. It is, however, believed that the anodic reaction plays an important roll by sharpening the crack tip and supplying $TiCl_x$ for hydrolysis.

The precipitation of the FCC spontaneous hydride occurs principally on the prism planes. The heterogeneous precipitation of this hydride occurs at the alpha-beta interfaces and, to a lesser degree, at the alpha-alpha interfaces. These sites correspond to the regions of highest hydrogen concentration. Once nucleation occurs, growth is rapid until the available hydrogen is consumed. Growth is diffusion controlled perhaps by a ledge mechanism. The orientation relationship reported in this investigation for the spontaneous hydride in the Ti-6Al-4V alloy is in agreement with the orientation relationship reported for this phase in the Ti-8Al-1Mo-IV alloy by other workers.[16,26] These hydrides appear quite similiar in these two alloys. These are not the hydrides believed responsible for either stress-corrosion cracking or slow-strain-rate embrittlement. They could, however, be responsible for impact embrittlement.

The strain-induced hydrides also precipitate on the $(10\bar{1}0)$ prism planes; however, their lattice is determined to be BCC. These hydrides are not the equilibrium gamma hydride. According to Boyd,[25] they are intermediate precipitates that have a lower activation energy for nucleation than the gamma phase. These hydrides appear to nucleate on sites on the active slip planes. Boyd[25] postulates these hydrides nucleate at glide dislocations and that diffusion is fast enough to allow this phase to grow during deformation at strain rates comparible with those ahead of a moving crack tip. These hydrides appear to dissolve by a ledge mechanism on heating in the electron beam (see Fig. 52) which would support the idea that these precipitates grow by a ledge mechanism.

These are the hydrides believed responsible for slow-strain-rate embrittlement and stress-corrosion cracking. The exact mechanism for this embrittlement is not understood. The present model suggests that the precipitation of the hydride prevents or retards relaxation about the crack tip which, combined with anodic dissolution at the crack tip leads to an increase in stress intensity at the apex of the crack. The stresses at the apex are built up until the critical normal stress is exceeded and cleavage occurs.

This model necessitates that slip be coplanar. This, perhaps, explains the general observation that lower aluminum alloys of titanium, which exhibit cellular dislocation arrays, do not exhibit stress-corrosion-cracking. The alloys containing greater than 5 wt.% aluminum exhibit both coplanar slip and stress-corrosion-cracking. The Ti-6Al-4V alloy examined in this investigation exhibited both cellular and coplanar dislocation arrays. This alloy is generally more resistant to SCC than the higher aluminum Ti-8Al-1Mo-1V alloy which exhibits primarily coplanar slip.

The model presented here is consistent with most of the significant observations concerning stress-corrosion cracking of titanium alloys in aqueous environments. These are presented below:

1. That cracking is specific to certain anions (Cl^-, Br^- I^-) is explainable if we consider the hydrolysis reaction of the metal salt as the supply of hydrogen ions in the crack tip region. Another possible contribution of the chloride ion is as a cathodic poisoner which increases the rate of hydrogen absorbtion.

2. That the crack velocity increases with potential as shown in Fig. 6 may be explainable either from the fact that the rate of formation of titanium chloride is increased or that the magnitude of the electric field is increased which could increase the rate of hydrogen diffusion to the crack tip. That the crack velocity stops at potentials below approximately -900 mV (SCE) can be explained by the fact that this potential is close to the reversible potential for titanium chloride formation.

3. That cracking does not generally occur in beta alloys and does not propagate through beta grains in alpha-beta alloys is explained by the much larger solubility for hydrogen in the beta phase.

4. The fact that the fractures appear to be a cleavage mechanism is explained. The fractures do not generally show signs of an anodic reaction which would be expected if the crack propagated entirely by anodic dissolution.

5. The conditions of hydrogen concentration and strain-rates which were demonstrated by Boyd[25] to be responsible for strain-induced hydrides correspond to the conditions known to give slow-strain-rate hydrogen embrittlement and these strain-rates appear to be close to those predicted in the vicinity of an advancing stress corrosion crack.

6. The necessity for coplanar slip as discussed previously.

7. That the fracture plane is $(10\bar{1}8)$ or $(10\bar{1}7)$ in Ti-8-1-1 is perhaps explainable from the application of Stroh's theory[63] as discussed by Mauney and Starke.[62] More likely, Blackburn[45] reports that the cleavage fracture planes of Ti-8Al in air are these exact planes. This would support the observation that fracture is cleavage. It would be difficult for an anodic dissolution mechanism alone to account for this unusual fracture plane.

8. That the stress intensity factor K_{Ic} for fracture in air Ti-8-1-1 is lowered approximately to the value for stress-corrosion fracture, K_{Iscc} as the interstitial hydrogen content is increased[75] is consistent with this model.

9. That hydrides are found to form in susceptible alloys in environments that cause SCC but not in environments that do not[59] is almost a verification of the proposed model.

10. That hydrogen is always adsorbed when Ti is actively corroding in an acidic environment[32] is important to this model.

11. That hydrogen diffuses in an electric field to the negative electrode[76] and in a stress gradient to the regions of high elastic strains can help explain the migration of hydrogen to the crack tip region.

12. That the microstructure determines an alloys susceptibility is explainable on the basis of this model.[54] For instance, mictostructures with coarse platelets are most susceptible and fine platelets and alpha dispersions are not[54] so susceptible. The coarse platelets would contain fewer grain boundaries, for example, which would slow or stop a crack and act as preferential sites for hydrogen segregation. Also, from an initiation standpoint, the larger grains would tend to result in larger slip steps which would be more difficult to passivate and, hence, render the alloy more susceptible to scc.

13. That the fracture may propagate discontinuously would support this model. The macroscopic crack front is observed[39] to propagate discontinuously but it has not been determined conclusively how the microscopic cracks progress.

It therefore appears that this model can account for the observed behavior of stress-corrosion cracking in alpha and alpha-beta alloys. There is, however, one breakdown in this model which has prevented the unanimous approval of other hydrogen and/or hydride models. This is the concern that the crack which propagates at velocities of 10^{-3} to 10^{-2} cm/s will outrun the ability for the hydrogen to diffuse to the crack tip region. This concern is based upon the assumption that cracking is continuous and upon the assumption that the electrodes are separated such that the cathode is approximately one micron behind the crack tip. The assumption of discrete electrodes is unfounded.

There is no information available on the diffusion of hydrogen in titanium alloys under the conditions which exist in the vicinity of a crack tip. Using the diffusion coefficient obtained by Wasilewski and Kehl[33] for hydrogen in relatively pure alpha titanium, it is apparent that the hydrogen cannot keep up with the propagating crack. The diffusion coefficient needed to keep up with the crack would need to be two to three orders of magnitude larger (10^{-8} to 10^{-9} cm^2/s). This, of course, assumes the crack to propagate continuously. If the crack propagation is, in fact, discontinuous, then the value of 10^{-11} cm^2/s could perhaps be sufficient. Also, the gradients of concentration, stress, and electrical potential not to mention that the metal has undergone plastic deformation can all contribute to the diffusion coefficient. The magnitude of these effects is speculative, but it is not inconceivable that it could be as much as the two or three orders of magnitude required.

The possibility exists that surface diffusion down the crack walls could contribute to the hydrogen pick-up at the crack tip. Values for hydrogen surface diffusion on titanium do not exist. It is commonly believed that surface diffusion occurs much more readily than diffusion through the metal lattice, but some recent work by Satterfield and Iino[77] and Wortman et al.[78] indicates that this may not be the case. Their work indicates that the activation energy for hydrogen diffusion on nickel is larger than expected and the diffusion coefficient for surface diffusion (4×10^{-8} cm^2/s) is close to the diffusion coefficient for hydrogen in nickel (4.5×10^{-9} cm^2/s).

On the other hand, Rideal and Sweett[79] have calculated that the activation energy for surface diffusion of hydrogen on nickel is from 3.5 to 1 kcal/g atom depending upon the coverage. These activation energies are at least 50% lower than those reported by Satterfeld and Iino[77] and Wortman et al.[78] These widely varying results indicate that it would not be appropriate to try to apply the results from other systems to this particular problem. Therefore, in order to evaluate this possibility the activation energy for hydrogen on titanium will need to be determined.

VI. CONCLUSIONS

The conclusions resulting from this investigation are summarized below.

1. Initiation is an electrochemically dependent process. The potential region for SCC susceptibility lies between -250 mV and -900 mV (SCE).

2. Ti-6Al-4V pits at cathodic potentials in a 5N HCl environment. Application of stress changes the mode of attack from the beta phase to the alpha at the alpha-beta interface.

3. Titanium picks up hydrogen very rapidly at the potential and in the environment assumed at the crack tip.

4. Hydrogen is absorbed more rapidly on polished surfaces and in more highly stressed regions.

5. Hydrogen charged at room temperature is evenly distributed in the surface of each individual grain as contrasted to elevated temperature charging where the hydrogen partitions to the beta phase.

6. The FCC spontaneous hydrides nucleate at the alpha-beta and alpha-alpha interfaces. There is apparently a large supersaturation required for nucleation and once this driving force is exceeded, growth is rapid and consumes nearly all of the available hydrogen.

7. The habit plane relationship for the FCC hydride was determined to be $(01\bar{1}0)_\alpha \parallel (1\bar{1}\bar{1})_\gamma$. The orientation relationship is $(0001)_\alpha \parallel (110)_\gamma$, $[11\bar{2}0]_\alpha \parallel [1\bar{1}0]_\gamma$. These relationships agree with those determined for the Ti-8Al-1Mo-1V alloy.

8. The BCC strain-induced hydrides are precipitated on the active slip planes. These hydrides are much thinner than the FCC hydrides and are very unstable.

9. The habit plane relationship for this BCC hydride was determined to be $(10\bar{1}0)_\alpha \parallel (01\bar{1})_\gamma$ and the orientation relationship is $(0001)_\alpha \parallel (\bar{1}11)_\gamma$, $[10\bar{1}0]_\alpha \parallel [0\bar{1}\bar{1}]_\gamma$.

10. The strain-induced hydrides appear to grow by a ledge mechanism.

11. Annealed Ti-6Al-4V exhibits both coplanar and cellular dislocation arrays. The coplanar slip occurs primarily on the prism planes but some basal slip was observed.

12. The mechanism believed responsible for SCC initiation is a pitting mechanism which occurs by chloride ion attack.

13. The mechanism believed responsible for SCC propagation involves the precipitation of the BCC hydride on the active slip systems which prevents relaxation which, combined with the anodic reaction at the crack tip, builds up the stresses at the crack tip until the critical normal stress is exceeded and cleavage fracture occurs.

VII. PROPOSED FUTURE WORK

Inasmuch as the present investigation is only one part of a continuing research project the author feels a responsibility to propose future research for those who follow. These proposals are based primarily upon the research contained in this investigation in the hope they will further clarify the results of this investigation and hopefully verify the proposed models.

These proposals are:

1. Future research should be performed on the Ti-8Al-1Mo-1V alloy which is better documented.

2. The initiation processes should be studied. It is proposed that the scanning electron microscope be used for a thorough investigation into this process on the Ti-8-1-1 alloy in sea water and methanol environments.

3. Diffusion data for hydrogen in an alpha alloy, such as Ti-8Al, should be obtained. It would also be informative to study the diffusion of hydrogen under the influence of strain gradients and electric fields.

4. Future hydrogen charging should be done from the gas phase so that the hydrogen content of the specimen is known and such that concentration gradients do not exist. The present investigation ran into great difficulties in mechanical testing which was attributable to a brittle surface layer. Low temperature annealing in vacuum removed this gradient but also removed most of the hydrogen.

5. Fracture mechanics should be used to study propagation. Use of a double cantilever beam specimen with a constant stress intensity would allow propagation activation energy studies to be made. Crack velocities as a function of potential and environment combined with the activation energies would be quite informative. The effects of microstructure, environment, potential and stress intensity as they relate to crack velocities could then be studied independently.

APPENDIX A

METALLOGRAPHIC POLISHING TECHNIQUES FOR TITANIUM

The following polishing procedure was determined to be the most satisfactory for the Ti-6Al-4V alloy used in this investigation.

1. Wet grind on silicon carbide paper to 600 grit.

2. Etch and regrind on the 600 grit paper twice.

3. Polish on silk wheel using 6μ diamond paste.

4. Etch and repolish.

5. Final polish on AB microcloth (Buehler Ltd.) using gamma alumina powder and a solution of 1% HF.

6. Etch and repolish.

There are many etchants available; however, for the above polishing procedures, a 20% HNO_3, 20% HF and 60% glycerin mixture is recommended. This is an unstable mixture and cannot be stored for periods exceeding 12 hours. Another etch which has been found quite satisfactory, especially for revealing the hydride plates, is a mixture of 3-1/2 parts HNO_3, 1-1/2 parts HF and 95 parts water by volume.

APPENDIX B

THE WINDOW TECHNIQUE

The "window" technique used for foil preparation is illustrated in Fig. 58. Figure 58a shows the specimen at the start of polishing. Figure 58b shows the same specimen after some time. Perforation and most rapid thinning generally occurs near the top first. Some perforations may also occur along the lacquer-metal interface. At this stage the specimen is removed, turned upside down, and relacquered to cover the edge perforations. The specimen is then polished until sufficient thin areas are obtained as shown in Fig. 58c. The specimen is then removed quickly and immersed in methyl alcohol in a petri dish. The specimen are cut under the methanol using a sharp surgical blade.

There are several precautions which must be observed in the above procedure. First, the specimen must be allowed to reach the temperature of the electrolyte (-30°C) before electropolishing begins. If this is not observed the "dreaded blue grot" (a blue surface film) will appear and ruin the specimen. Also, the foil specimens must not be exposed to air for very long for they will become contaminated. Storage of specimens is best accomplished in vacuum or under ethyl alcohol.

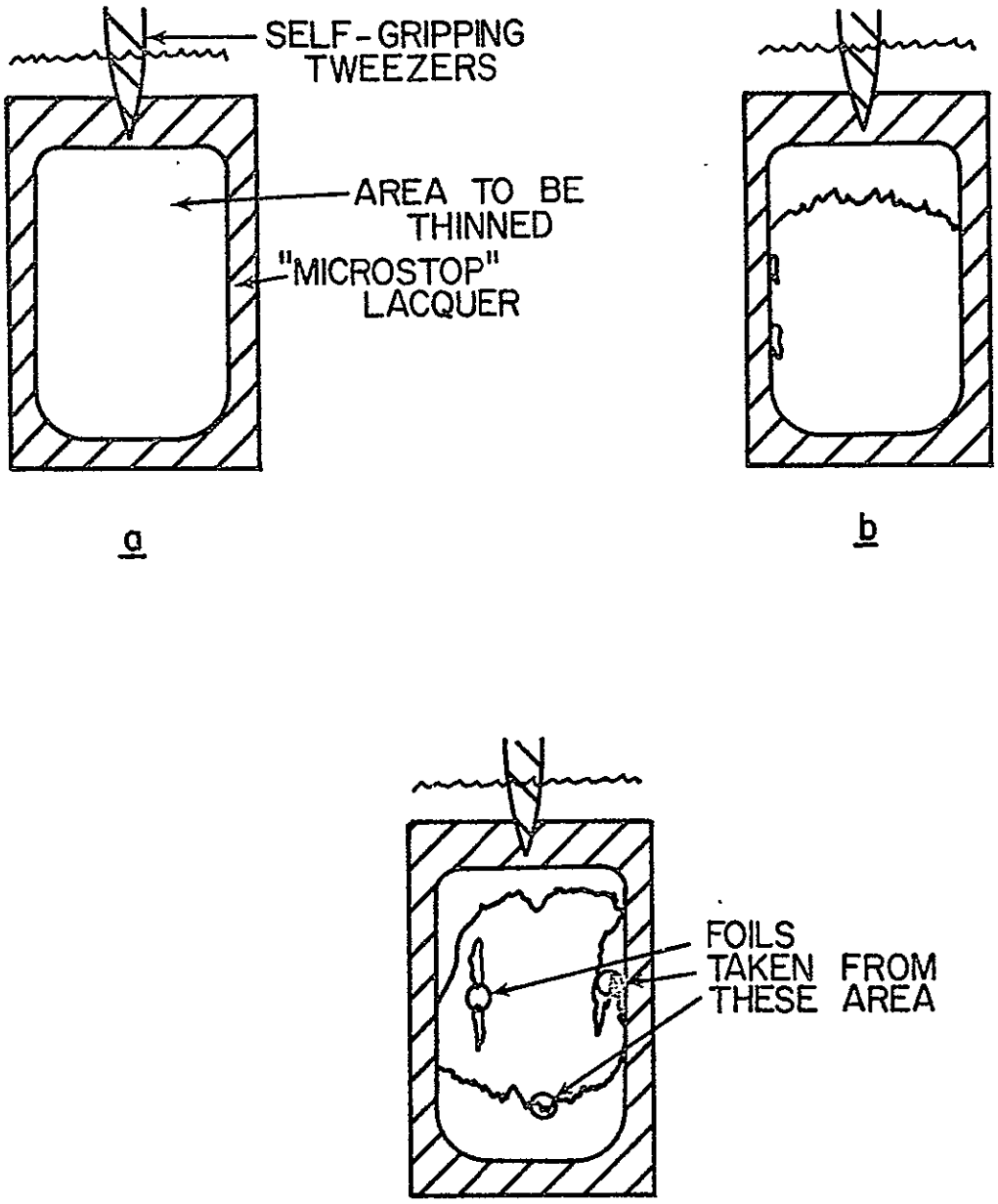

Fig. 58 - The "Window" Electropolishing Technique

REFERENCES

1. Kirschfeld, L. and Severts A., Titan and Wasserstoff, Vol. 145: 227, 1929.

2. Dushman, S., Scientific Foundations of Vacuum Technique, John Wiley (New York) 1950.

3. McQuillan, A. D., Proc. Roy. Soc., A204, p. 309, 1950.

4. McQuillan, A. D., J. Inst. Metals, Vol. 78, p. 249, 1950.

5. McQuillan, A. D., J. Inst. Metals, Vol. 79, p. 371, 1951.

6. McQuillan, A. D., J. Inst. Metals, Vol. 80, p. 1355, 1951.

7. Cotterill, P., "The Hydrogen Embrittlement of Metals," Progress in Matl's Sci., Vol. 9, Pergamon Press Ltd., 1961.

8. Livanov, V. A., Bukhanova, A. A. and Kolachev, B. A., Hydrogen in Titanium 1962, Daniel Davey and Co., Inc., New York.

9. Gibb, T. R. P. and Kruschwitz, H. W., J. Amer. Chem. Soc. 72, p. 5365, 1950.

10. Lenning, G. A., Craighead, C. M. and Jaffee, R. I., "Hydrogen Contamination in Descaling and Acid Pickling of Titanium," Trans. AIME 200, p. 367, 1954.

11. Koster, Bangert and Ewert, Z. Metallkunde, No. 8, 1956.

12. McQuillan, A. D., Metallurgy of Titanium, Sept. 1956, New York.

13. Lenning, G. A., Berger, L. W. and Jaffee, R. I., "The Effect of Hydrogen on Mechanical Properties of Titanium and Titanium Alloys," Fourth Summary Report from Battelle Memorial Institute to Watertown Arsenal Laboratory, Contract No. DAI-33-019-505-ORD-(P)-1. July 31, 1955.

14. Lenning, G. A., Spretnak, J. W., and Jaffee, R. I., "Effect of Hydrogen on Alpha Titanium Alloys," Trans. AIME, Oct. 1956.

15. Berger, L. W., Williams, D. N. and Jaffee, R. I., "Effect of Hydrogen on the Mechanical Properties of Titanium-Aluminum Alloys," Report from Battelle Memorial Institute to Watertown Arsenal Laboratory, Contract No. DA-33-019-505-ORD-7, April 30, 1957.

16. Sanderson, G. and Scully, J. C., "Hydride Formation in Thin Foils of Dilute Titanium Aluminum Alloys," Trans. AIME, Vol. 239, Dec. 1967.

17. Boyd, J. D., Haynie, F. H., Boyd, W. K., Wood, R. A., Williams, D. N. and Jaffee, R. I., "The Effect of Composition on the Mechanism of Stress-Corrosion Cracking of Titanium Alloys in N_2O_4 and Aqueous and Hot-Salt Environments," Fifth Quarterly Progress Report from Battelle Memorial Institute to the National Aeronautics and Space Administration, Contract No. NASr-100 (09), February 29, 1968.

18. Hagg, G., Z. Physik. Chem., Vol. B12, p. 33, 1931.

19. Margolin, H. and Porfisch, H., Trans. AIME, 242, p. 1901, 1968.

20. Lenning, G. A., Craighead, C. M. and Jaffee, R. I., Trans. AIME 200, p. 367, 1954.

21. Hagg, G., J. Phys. Chem., Vol. II:433, 1930.

22. Yakel, H. L., Acta Cryst., Vol. 11, p. 46-51, 1958.

23. Sidhu, S. S. et al., Acta Cryst. 9, 1956.

24. Jaffee, R. I., J. Metals 87, p. 861, 1956.

25. Boyd, J. D., "Precipitation of Hydrides in Titanium Alloys," Trans. ASM, Vol. 62, 1969.

26. Boyd, J. D., Moreland, P. J., Boyd, W. K., Wood, R. A., Williams, D. N. and Jaffee, R. I., "The Effect of Composition on the Mechanism of Stress-Corrosion Cracking of Titanium Alloys in N_2O_4 and Aqueous and Hot-Salt Environment, "Battelle Memorial Institute to NASA, Contract No. NASr-100-(09), August 26, 1969.

27. Louthan, M. R., Jr., "Stress Orientation of Titanium Hydride in Titanium," Trans. AIME, Vol. 227, Oct. 1963.

28. Keeler, J. H. and Geiler, A. H., "Preferred Orientation in Rolled and Annealed Titanium," Trans. AIME, Vol. 206, 1956.

29. McGreen, J. and Genshaw, M. A., "The Electrochemical Introduction of Hydrogen into Metals," Proceedings of the Conference on Fundamental Aspects of Stress Corrosion Cracking, Sept. 11-15, 1967, The Ohio State University, NACE, 1969.

30. Gulbransen, E. A. and Andrew, K. F., "Mechanism of the Reaction of Hydrogen with Zirconium," J. Electrochem. Soc., Vol. 101, No. 7, July, 1954.

31. Ogawa, S. and Wantanabe, D., "Electron Diffraction on Titanium Attacked by Various Acids," Science Reports of the Research Institute, Tohoku University, Vol. 7A, 1955.

32. Otsuka, R., "Studies on the Corrosion of Titanium," Scientific Papers, Inst. Phys. and Chem. Res. 54, 97 1960.

33. Wasilewski, R. J. and Kehl, G. L., "Diffusion of Hydrogen in Titanium," Metallurgia XI, 50, 301, Nov. 1954.

34. Li, J. C. M., Oriani, R. A. and Darken, L. S, Z. Physik. Chem. (N.F.) 49, 271, 1966.

35. Troiano, A. R., Trans. ASM 52,54, 1960.

36. Berger, L. W., Williams, D. N. and Jaffee, R. I., "The Effect of Hydrogen on the Mechanical Properties of Titanium-Aluminum Alloys," Report from Battelle Memorial Institute to Watertown Arsenal Laboratory, Contract No. DA-33-019-505-ORD-7, April 30, 1957.

37. Williams, D. N., "Hydrogen in Titanium Alloys," TML Report No. 100, May 16, 1958.

38. Jaffee, R. I. and Maykuth, D. J., "Survey of Delayed Cracking in Formed Titanium Parts," TML Report No. 7, June 20, 1955.

39. Beck, T. R., "Electrochemical Aspects of Titanium Stress Corrosion Cracking," Proceedings of Conference - Fundamental Aspects of Stress Corrosion Cracking, held at The Ohio State University, Sept. 11-15, 1967, N.A.C.E., Houston, 1969.

40. Fontana, M. G. et al., "Corrosion Cracking of Metallic Materials," Technical Report AFML-69-16, The Ohio State University to Air Force Materials Laboratory, Wright-Patterson Air Force Base, Ohio, February 1969.

41. Brown, B. F. et al., "Marine Corrosion Studies," Third Interim Progress Report, NRL Memorandum Report 1634, July, 1965.

42. Feige, N. G. and Murphy, T. J., "Environmental Effects on Titanium Alloys," TMCA Second Annual Conference, April, 1966.

43. Churchman, A. T., "The Slip Modes of Titanium and the Effect of Purity on Their Occurrence during Tensile Deformation of Single Crystals," Proc. Roy. Soc. A226, 1954.

44. Blackburn, M. J., "Relationship of Microstructure to Some Mechanical Properties of Ti-8Al-1V-1Mo," Trans. ASM, Vol. 59, 1966.

45. Blackburn, M. J. and Williams J. C., "Metallurgical Aspects of Titanium Stress Corrosion Cracking," Proceedings of Conference-Fundamental Aspects of Stress Corrosion Cracking, held at The Ohio State University, Sept. 11-15, 1967, N.A.C.E., Houston, 1969.

46. Brown, B. F. et al., "Marine Corrosion Studies," Third Interim Report of Progress, NRL Memorandum Report 1634, July, 1965.

47. "A Study of the Stress Corrosion Cracking of Titanium Alloys in Sea Water with Emphasis on the Ti-6Al-4V and Ti-8Al-1Mo-1V Alloys," Research Report No. R471, Project No. 93002, Reactive Metals, Inc., Oct. 18, 1965.

48. Peterson, M. H., Brown, B. F., Newbegin, R. L. and Groover, R. E., Corrosion 23, 142, 1967.

49. Jackson, J. D. and Boyd, W. K. "Stress-Corrosion and Accelerated Crack-Propagation Behavior of Titanium and Titanium Alloys," DMIC Technical Note, Battelle Memorial Institute, Feb. 1, 1966.

50. Seagle, S. R., Seeley, R. R. and Hall, G. S., "The Influence of Composition and Heat Treatment on the Aqueous Stress Corrosion of Titanium," Research and Development Report 492, Reactive Metals, Inc., March 15, 1967.

51. Scully, J. C., "Kinetic Features of Stress Corrosion Cracking," Corrosion Science Vol. 7, 1967.

52. Bomberger, H. B., "The Corrosion Resistance of Titanium," RMI TR D-15, Reactive Metals, Inc., March 28, 1966.

53. Hose, D. G., "Effects of Vacuum and Inert Atmosphere Heat Treatment on the Stress-Corrosion-Cracking Resistance of Several Titanium Alloys," Presented at Advanced Research Projects Agency Review, Lehigh University, August 1-2, 1966.

54. Lane, I. R., Cavallero, J. L. and Morton, A.G.S., "Fracture Behavior of Titanium in the Marine Environment," MEL R&D Phase Report 231/65, U.S. Navy Marine Engineering Laboratory, Annapolis, Maryland 1965.

55. Rideout, S. D., Louthan, M. R. and Selby, C. L., "Basic Mechanisms of Stress Corrosion Cracking of Titanium," presented at Fifth Pacific Area National Meeting of ASTM, Seattle, Washington, October 31-November 5, 1965.

56. Sanderson, G., Powell, D. T. and Scully, J. C., "Metallographic Studies of the Stress Corrosion Cracking of Titanium Alloys in Aqueous Chloride Solutions, "Pr ceeding of Conference on Fundamental Aspects of Stress Corrosion Cracking held at The Ohio State University, Sept. 11-15, 1967, N.A.C.E., Huston, 1969.

57. Mackay, T. L., Gilpin, C. B. and Tiner, N. A., "Stress Corrosion Cracking of Titanium Alloys at Ambient Temperature in Aqueous Solutions," Quarterly Progress Report SM-49105-Q2, Missile and Space Systems Division, Astropower Laboratory, Jan. 1967.

58. Mackay, T. L., Gilpin, C. B. and Tiner, N. A., "Stress Corrosion Cracking of Titanium Alloys at Ambient Temperature in Aqueous Solutions," Quarterly Progress Report SM-49105-Q3, Missile and Space Systems Division, Astropower Laboratory, April, 1967.

59. Sanderson, G. and Scully, J. C., "Hydride Formation in Corroded Titanium Alloys," Corrosion Science Vol. 6, 1966.

60. Boyd, J. D. et al., "The Effect of Composition on the Mechanism of Stress-Corrosion Cracking of Titanium Alloys in N_2O_4, and Aqueous and Hot-Salt Environments," Fourth Quarterly Progress Report, NASA Contract No. NASr-100 (09), Feb. 29, 1968.

61. Tiller, W. A. and Schrieffer, R., "A Hydrogen Pump for Stress Corrosion Cracking," Scripta Metallurgica, Vol. 4, 1970.

62. Mauney, D. A. and Starke, E. A. Jr., "Technical Note: Explanation of The Cleavage Plane in Stress Corrosion Cracking of Alpha Phase Titanium-Aluminum Alloys," Corrosion, Vol. 25, No. 4, April, 1969.

63. Stroh, A. N., Journal of Applied Physics 6, 1957.

64. Toy, S. M. and Phillips, A., "Hydrogen Emanation and Distribution in Metals and Alloys," Corrosion, Vol. 26, No. 7, July, 1970.

65. Byars, E. F. and Snyder, R. D., "Engineering Mechanics of Deformable Bodies," International Text Book Company, Scranton, Pa.

66. Williams, D. N., Written discussion, Trans ASM, Vol. 50, 453, 1958.

67. Hickman, B. S., Williams, J. C. and Marcus, H. L., "Transgranular and Intergranular Stress Corrosion Cracking of Titanium Alloys," Reprint submitted to International Interfaces Conference, April 14, 1969.

68. May, R. C., Private communication.

69. Brown, B. F., Fujii C. T. and Dahlberg, E. P., J. Electrochemical Society 116, 218, 1969.

70. Rosenfeld, I. L. and Marshakov, I. K., Corrosion 20, 4, 115t-125t, 1964.

71. Beck, F. H., "Stress Corrosion Cracking of Titanium Alloys," The Ohio State University Research Foundation Report 2267-2 July 11, 1967.

72. Griess, J. C., "Crevice Corrosion of Ti in Aqueous Salt Solutions," Corrosion, Vol. 24, 1968.

73. Griffith, A. A., Proceedings of International Congress of Applied Mechanics, 55 (1924).

74. Tetelman, A. S. and McEvily, A. J., Jr, Fracture of Structural Materials, John Wiley & Sons, N.Y. (1967).

75. Scully, J. C., (private communication from Sandox and Newbegin, R. L.) "The Stress Corrosion Cracking of Alpha Titanium Alloys at Room Temperature," The Science Technology and Application of Titanium, R. Jaffee and N. Promisel, editors, Pergamon Press, New York, 1970.

76. Livanov, V. A., Kolachev, B. A. and Bukanova, A. A., "Hydrogen Embrittlement of Titanium and Its Alloys," The Science Technology and Application of Titanium, R. Jaffee and N. Promisel, editors, Pergamon Press, New York, 1970.

77. Satterfeld, C. H. N. and Iino, H., Ind. Eng. Chem., Vol 7, No. 2, 1968.

78. Wortman, R., Gomer R. and Lundy, R., Journal of Chemical Physics 27, 1957.

79. Rideal and Sweett, Proc. Roy. Soc. A257, 291, 1960.